Structural Behaviour of Conventional and FRP- Reinforced Concrete Deep Beams

Fawzi Ali Latosh

A Thesis

in

The Department

Of

Building, Civil, and Environmental Engineering

Presented in Partial Fulfillment of the Requirements

For the Degree of

Doctor of Philosophy (Building, Civil, and Environmental Engineering) at

Concordia University

Montréal, Québec, Canada

February 2014

CONCORDIA UNIVERSITY

SCHOOL OF GRADUATE STUDIES

This is to certify that the thesis prepared

By: **Fawzi Ali Latosh**

Entitled: **Structural Behaviour of Conventional and FRP- Reinforced Concrete Deep Beams** and submitted in partial fulfillment of the requirements for the degree of

DOCTOR OF PHILOSOPHY (Civil Engineering)

Complies with the regulations of the University and meets the accepted standards with respect to originality and quality.

Signed by the final examining committee:

_____Chair
Dr. Brigitte Jaumard

_____External Examiner
Dr. Dagmar Svecova

_____External to Program
Dr. M. Packirisamy

_____Examiner
Dr. K. Galal

_____Examiner
Dr. L. Lin

_____Thesis Supervisor
Dr. A. Bagchi

Approved by_____
Dr. M. Elektorowicz, Graduate Program Director

February 27, 2014_____
Dr. Christopher Trueman,
Dean of Faculty of Engineering & Computer Science

ABSTRACT

Structural Behaviour of Conventional and FRP- Reinforced Concrete Deep Beams

Fawzi Ali Latosh, Ph.D.

Concordia University, 2014

Many structural applications such as pile caps, girders, foundation walls and offshore structures include the use of reinforced concrete deep beams as structural elements. The structural behaviour of deep beams is affected by its span to depth ratio, type of loading, reinforcement ratio in vertical and horizontal directions, concrete strength, and type of cross section. Since the traditional beam theory is not applicable for designing deep beams, the strut and tie model (STM) was developed earlier as a rational method for estimating the capacity of a reinforced concrete deep beam and accepted in the current codes and standards for the design of such beams. While for designing a conventional (i.e. steel reinforced) concrete deep beams STM has been available in different codes and standards, for FRP-reinforced concrete deep beams such provisions are not available in most codes and standards. Only in the recent edition of the relevant Canadian standard (i.e., CAN/CSA S-806-12) which came out much later than the commencement of the present research, an STM approach has been provided, which is primarily based on that of conventional deep beams with some adjustments by using FRP reinforcement's properties to calculate the tie capacity. One of the reasons for the lack of standards or code provisions for such systems in other codes (e.g., ACI and Eurocode) is perhaps the lack of adequate experimental data available on the performance of such beams. As the use of FRP reinforced concrete structures is increasing, there is a need to the

development of a design method for FRP-reinforced concrete deep beams, which could be similar to the existing STM method available for the conventional deep beams, similar to the approach taken by the Canadian standard. But, such provisions must be validated and/or modified appropriately and calibrated with experimental studies.

The objectives of the present research are to: (1) Identify the critical parameters governing the behaviour of conventional concrete deep beams; (2) Develop a design procedure for FRP reinforced concrete deep beams; (3) Study the critical factors in FRP-reinforced concrete deep beams and evaluate the proposed design procedure using numerical and experimental tests; and (4) Evaluate the STM procedure outlined in the CSA-S806-12[2012] for designing FRP reinforced deep beams. The current design provisions for conventional concrete deep beams as provided in the following three prominent standards that use the strut–and-tie model have been extensively reviewed: ACI 318-08, Eurocode EN 1992-1-1-2004(E) and Canadian code CSA A23-3-04. The influence of different variables on the ultimate strength of deep beam estimated using STM provisions in the codes are studied. A large database of available experimental studies on conventional deep beams has been created. The ultimate load capacity and failure pattern for each sample in the database have been evaluated using the STM models provided in the above three standards, and compared with the experimental results and critical parameters that have been identified. The results of the preliminary study show that the use of Strut and Tie model are generally appropriate method for beams with shear-span to depth ratio less than or equal to two. Also the study confirmed that both the shear span-to-depth ratio and the amount of shear web reinforcement have

the most significant effect on the behaviour of deep beams and on the codes predictions of the ultimate strength of deep beams.

Based on the review of the STM models available for the conventional deep beams as provided in the current standards, a similar model has been developed here to design FRP-reinforced deep beams. Using the proposed method, a set of FRP-reinforced deep beam has been designed and constructed. An experimental program has been carried out to test these beams to study the applicability of the proposed method and effect of the critical design parameters. Nine FRP reinforced concrete deep beams were divided into three groups, based on their shear span-to-depth ratio (*a/d*), and tested under a single concentrated load to investigate their behaviour and strength. The test variables were the shear span-to-depth ratio and the quantity of web shear reinforcement. The behaviour of deep beams is indicated by their shear strength capacity, mid span deflection, strain at the FRP longitudinal and web reinforcement, crack propagation, and type of failure. A new equation is presented in this study to calculate the contribution of the FRP web reinforcement to the ultimate shear capacity of FRP-reinforced concrete deep beams. As a new version of the CSA standard is available now which provides STM procedure for FRP-reinforced deep beams, the test results have been compared to predictions based on the current CSA design procedure.

This investigation reveals that the Strut and Tie model procedure in the CSA-S806-12 code provides a conservative and convenient design procedure for FRP-reinforced concrete deep beams. However, there are some areas where the code provisions can be improved and some inconsistencies in the way the strut capacity is determined can be removed. In addition, the shear design procedures of the ACI 440.1R-06 Code and of the

modified Strut and Tie model (STM) from Appendix A of the ACI 318-08 Code were compared based on their test results and a modified STM procedure based on ACI 318-08 provision has been proposed for the adoption to ACI 440. This investigation reveals that adopting the procedure in the ACI 318-08 Code and taking into consideration the properties of FRP reinforcement provides a conservative and rational design procedure for FRP reinforced concrete deep beams.

ACKNOWLEDGEMENTS

This thesis is dedicated to the soul of my father, to my beloved Mother, my brother, my Wife, and my children, for care and support all the time. I would like to thank my supervisor, Dr. Ashutosh Bagchi, for his kind instructions, continuous guidance and encouragement he has provided throughout my time as his student. I would also like to thank Dr.Khaled Galal for his cooperation. Many thanks to the structural laboratory staff, especially for the help from Jaime Yeargans, Brian Cooper. Many thanks are due to my colleagues Dr.Arash Rahmatian and Mr. Hany Seif Eldin and Mr. Ram Adhikari for their support and valuable advice. Also, big thanks to the entire civil engineering faculty staff for an amazing five years.

Also I wish to express my gratitude and sincere appreciation to the Libyan Government for the scholarship provided to me to pursue graduate study at Concordia. The support of the Natural sciences and Engineering research Council of Canada (NSERC) is gratefully acknowledged. The authors would also like to thank Pultral Inc., Quebec for donating the FRP materials required for the research.

TABLE OF CONTENTS

LIST OF FIGURES

LIST OF TABLES

LIST OF SYMBOLS

a	Shear span, equal to distance from center of concentrated load to either: (a) face of support for continuous or cantilevered members, or (b) center of support for simply supported members
α_i	Angle between the axis of a strut and the bars in the i-th layer of reinforcement crossing that strut
A_c	Area of concrete section resisting shear transfer
$A_{sd\ b\ min}$	Cross sectional area
A_{cs}	Cross-sectional area at one end of a strut in a strut-and-tie model, taken perpendicular to the axis of the strut
A_{fv}	Amount of FRP shear reinforcement within spacing s
A_{nz}	Area of a face of a nodal zone or a section through a nodal zone
A_{st}	Total area of nonprestressed longitudinal reinforcement (bars or steel shapes)
A_{tf}	Area of FRP reinforcement in tension tie
A_{tp}	Area of prestressing steel in a tie
b	Width of compression face of member
b_w	Web width, or diameter of circular section
b_s	Width of strut
d	Distance from extreme compression fiber to centroid of longitudinal tension reinforcement
$f`_c$	Specified compressive strength of concrete
f_{cd}	Design value of concrete compressive strength
f_{ce}	Effective compressive strength of the concrete in a strut or a nodal zone
f_{ck}	Characteristic compressive cylinder strength of concrete at 28 days
f_{cu}	Limiting compressive stress in concrete strut

f_{fb}	Strength of bent portion of FRP bar
f_{fu}	Design tensile strength of FRP, considering reductions for service environment
f_{fv}	Tensile strength of FRP for shear design, taken as smallest of design tensile strength
f_{fu}	Strength of bent portion of FRP stirrups f_{fb}, or stress corresponding to $0.004E_f$
f_{se}	Effective stress in prestressing steel (after allowance for all prestress losses)
f_y	Specified yield strength of reinforcement
F_n	Nominal strength of a strut, tie, or nodal zone
F_{nn}	Nominal strength at face of a nodal zone
F_{ns}	Nominal strength of a strut
F_{nt}	Nominal strength of a tie
F_u	Factored force acting in a strut, tie, bearing area, or nodal zone in a strut-and-tie model
h	Overall thickness or height of member
k	Ratio of depth of neutral axis to reinforcement depth
K_1	Coefficient
K_2	Coefficient
K_3	Coefficient
l_n	length of clear span measured face-to-face of supports
S	Center-to-center spacing of items, such as longitudinal reinforcement, transverse reinforcement, prestressing tendons, wires, or anchors,
S_i	Center-to-center spacing of reinforcement in the i-th layer adjacent to the surface of the member
V_n	Nominal shear strength at section
V_c	Nominal shear strength provideby concrete
V_{calc}	Shear force at section calcoulated by code provisions

V_{Ed}	Design value of the applied shear force
V_{exp}	Mesurd shear force at section
V_f	Shear resistance provided by FRP stirrups
V_n	Mesurd shear force at section
V_n^{test}	Shear force at section calcoulated by code provisions
V_u	Factored shear force at section
w_s	Width of a strut perpendicular to the axis of the strut, mm
β	Coefficient
β_s	Factor to account for the effect of cracking and confining reinforcement on the effective compressive strength of the concrete in a strut
β_n	Factor to account for the effect of the anchorage of ties on the effective compressive strength of a nodal zone
Δf_p	Increase in stress in prestressing steel due to factored loads
ε_1	Principal tensile strain in cracked concrete due to factored loads
ε_s	Strain in reinforcement
ε_x	Longitudinal strain at mid-depth of the member due to factored loads
θ	Angle between axis of strut, compression diagonal, or compression field and the tension chord of the member
θ_s	Smallest angle between compressive strut and adjoining tensile ties
λ	Modification factor reflecting the reduced mechanical properties of lightweight concrete
γ_c	Partial factor for concrete
v	Strength reduction factor for concrete cracked in shear

$\sigma_{Rd,\ max}$	Maximum stress which can be applied at the edges of the node
ϕ	Resistance factor applied to a specified material
ϕ_c	Resistance factor for concrete
ϕ_s	Resistance factor for non-prestressed reinforced bars
v	Strength reduction factor for concrete cracked in shear

Chapter 1: Introduction

1.1. Introduction:

Many structural applications include the use of reinforced concrete deep beams e.g. pile caps, girders, foundation walls and offshore structures. The structural behaviour of deep beams is affected by its span to depth ratio, type of loading, reinforcement ratio (vertical and horizontal), concrete strength, and the type of cross section. As the variation in longitudinal strain is nonlinear over the depth of the cross section of the beam, the plane sections theory that applies to the design of simple beams cannot be used in designing deep beams. The Strut and Tie model (STM) has been adopted by the modern codes to design the deep beams in a more effective way. The STM provides a rational and acceptable theory for the design of deep beams which generally agrees well with the results of experimental studies. Michael et al. [2006] reported that the first application of STM was in the eighties in the Canadian Code [1984], followed by the Eurocode [1992] in applying the STM to design deep beams. The first appearance of the STM in the American Concrete Institute Code ACI 318 [2002] was at the end of the twentieth century. It should be noted that the implementation of the STM models as provided in the above-mentioned codes differ from each other. Some differences exist among the codes in the implementation of STM, particularly in determining the amount of web reinforcement and the shape of the struts.

Deep beams in many structural applications are exposed to the risk of corrosion or to severe environmental conditions that may result in shortening of their lifespans. Compared to conventional steel reinforcement, Fiber-Reinforced Polymer (FRP)

materials are stronger, lighter and free of corrosion problem. FRPs are therefore being used as an alternative to steel reinforcement in many structural applications, including deep beams. While, many studies have demonstrated the effectiveness of FRP bars in concrete structural elements, not many studies are available for concrete deep beams reinforced with FRP bars. The increasing use of this material in construction led to the development of standards for the design and construction of building components with Fiber-Reinforced Polymers.

The CAN/CSA-S806-02[2002], the ACI 440.1 R-06[2006] and the CAN/CSA-S806-12 [2012] standards provide requirements for the design and evaluation of building and building components reinforced (internally or externally) with FRPs. A design manual has been issued by the Canadian Network of Centres of Excellence on Intelligent Sensing for Innovative Structures (ISIS Canada Research Network [2007]) to provide guidelines and design equations that can be used for the design of FRP-reinforced concrete structures.

For designing normal (i.e. shallow) beams using any FRP standard, the relevant equations for steel reinforced concrete have been adopted and modified for FRP reinforcement. CAN/CSA-S806-02 Standard [2002], ACI 440.1 R-06[2006] and the ISIS design manual did not provide any procedure to design deep beams reinforced with FRP bars. Moreover, according to clause 8.6.6.4 of CAN/CSA-S806-02[2002] the strut and tie models was not permitted in the design of beams. The present research was motivated by the increasing use of FRP reinforcement in concrete structures and the lack of appropriate design provisions for FRP-reinforced concrete deep beams.

The newer edition of the Canadian Standard, CAN/CSA-S806-12[2012] does adopt the STM approach, originally developed for conventional (i.e. steel reinforced) deep beams, with some adjustments that account for the properties of FRP. However, these provisions are not adequately verified with experimental studies of FRP-reinforced concrete deep beams. Presently, a very limited number of experimental studies are available for FRP-RC deep beams. ACI 440.1 R-06 [2006] does not provide any design procedure for FRP-reinforced concrete deep beams as of yet. For designing conventional deep beams, most codes, for example the ACI 318-08 [2008], the Eurocode [2004] and the CSA [2004], individualize the STM model with special clauses or appendixes (Appendix A, clause 6.5 and clause 11.4, respectively) to clarify STM model design procedure for deep beams. Given the advancement in the use of FRP materials and their adoption in reinforced concrete structures, the development of an STM-design procedure for FRP-reinforced concrete deep beams for the ACI 440 code will be of interest. Also the effectiveness of the STM approach in CAN/CSA-S806-12[2012] needs to be validated further with experimental results.

1.2. Statement of the problem:

Studies on the behaviour of deep beams reinforced by FRP bars are very limited as compared to that on steel reinforced concrete deep beams. The aim of the study is to investigate the structural behaviour of concrete deep beams reinforced by FRP. For a better understanding of deep beam behaviour, the proposed research consists of three parts. The first part focuses on the review of available experimental studies on conventional concrete deep beams and comparison of the code provisions in prominent jurisdictions to gain an insight in the behaviour of such beams so that a design procedure

can be developed for them. The second part focuses on the development of an experimental program in which a set of concrete deep beams reinforced by FRP will be designed, constructed and tested, to study the effect of the key variables and validate the existing provisions of the Canadian standard. The amount of the web reinforcement has been chosen as a variable to study since the experimental results on steel-reinforced deep beams as reported in the literature indicate that web reinforcement is very important in controlling the mid-span deflection, crack width, failure modes, ultimate strengths and the overall behaviour of reinforced concrete deep beams. Moreover, the shear span-to-depth ratio will be studied because of its major effect on changing the behavior of beams as well as on the failure mechanism.

As the existing standard on FRP-reinforced concrete structures ACI 440.1 R-06[2006] does not provide a procedure for designing deep-beams, the present study is aimed at understanding such beams and developing a design procedure. Also this investigation evaluates the STM procedure of the CSA-S806-12[2012] for design of FRP reinforced deep beams, which was adapted from the STM procedure for conventional deep beams as provided in CSA A23.3-04.

1.3. Objectives and scope:

The objective of the present research is to understand the behaviour of FRP-reinforced concrete deep beams. The behaviour of deep beams is indicated by their levels of ultimate shear strength, mid span deflection, FRP reinforcement strain, crack propagation, and by their type of failure. In addition to the main objective, this study has the following objectives:

1. Review the available experimental studies on conventional reinforced concrete deep beams and identify the critical parameters governing their behaviour.
2. Compare the STM provisions of relevant codes and standards for the design of concrete deep beams, and verify the accuracy and the reliability of the Strut and Tie model (STM) provisions in different codes with respect to the available experimental studies.
3. Develop an experimental program to study the effects of the critical factors in FRP reinforced concrete deep-beams and validate the existing design procedures.
4. Develop a design procedure or modify the existing one for FRP reinforced concrete deep beams based on the results of the present and available experimental studies.

The objectives 1 and 2 have been achieved by utilizing a database of existing experimental studies on conventional deep beams. The effects of governing variables, such as the shear span to depth ratio, amount of web reinforcement, and the compressive strength of concrete were identified and have been explained as observed in the available studies. The results of more than three hundred test specimens from available experimental studies on reinforced concrete deep beams have been used to evaluate and compare the Strut-and-Tie modeling provisions of the codes. An experimental study has been conducted to achieve objectives 3 and, 4 and validate the current design procedure. A design procedure of FRP- reinforced concrete deep beams have been developed based on the design procedure available for conventional deep beams and FRP-reinforced ordinary beams, and compared to the current design procedures.

1.4. Thesis organisation:

The thesis is organized in eight chapters. A general introduction, statements of the problem, the research objectives and the thesis organization is presented in this chapter. The second chapter presents the literature review including: i) review and discussion of the behaviour of deep beams, and description of the modes of failure; ii) review of the Strut-and-Tie Models in provisions of the design codes and standards in three different jurisdictions including Canada; iii) presentation of the available experimental studies on conventional deep beams; iv) identification of the key parameters affecting the behavior of deep beams; and v) overview of the use of Fiber-Reinforced Polymer in deep beams and available experimental studies on FRP reinforced deep beams. Chapter three presents the research methodology and experimental setup. Chapter four presents the comparison of the design Provisions for conventional deep beams in different codes. The effects of governing variables, such as the shear span-to-depth ratio, web reinforcement, and the compressive strength of concrete on the code predictions of the ultimate strength capacity have also been investigated here. The effectiveness of the STM provisions of different codes in predicting the failure modes of concrete deep beams has also been studied in this chapter. Chapter five presents the experimental results of nine FRP reinforced concrete deep beams. The experimental results for each tested beam are presented individually and discussed in this chapter. Chapter six provides a synthesis of the experimental results to highlight the effect of the shear span to depth ratio and the amount of web reinforcement on the behavior of the FRP-RC deep beams. Chapter seven describes the design procedure developed for designing FRP-RC deep beam in the context of Canadian (CSA) and American (ACI) codes which have been compared and validated with the test results

and available provision in the current codes and standards. The summary, conclusions, and recommendation for future work are provided in Chapter seven.

Chapter 2: Literature Review

2.1. Behaviour of Deep Beams:

Nawy [2005] mentioned that the behavior of deep beams is nonlinear; they behave as two-dimensional elements subjected to a two-dimensional state of stress, the strain distribution is nonlinear distribution, the plane sections do not remain planar after bending, and shear deformations will become significant in deep beams, which mean that the assumption of plan section theory cannot be applied. Different codes define deep beams slightly differently, based on the nonlinear variation of strain distribution over the depth of the cross section. A deep beam is defined in ACI 318-08[2008] code as a beam that is loaded on one face and supported on the opposite face, that has a clear span, l_n, equal to or less than four times the overall member depth, and that has regions of concentrated loads within the height of ($a \leq 2h$), where a and h are the shear-span and depth, respectively. According to the Eurocode (EN 1992-1-1-2004-E) [2004], the clear span, l_n, of the beam should be equal to or less than three times the depth, whereas the Canadian code A23-3-04[2004] defines a deep flexure member as a beam having a clear span to overall depth ratio less than 2. The differences between the definitions of the deep beam in different codes are mainly due to the way the codes account for the nonlinear variation in the strain distribution over the depth of the cross section. Deep beams are different from the conventional beams, where the shear strength of deep beams is a function of several variables such as the shear span to depth ratio a/d, the web reinforcements (both in horizontal and vertical directions), concrete compressive strength, and the loading area and support width.

2.2. Modes of Failure:

Michael and Oguzhan [2008], Carlos et al [2006], and Tan et al [1997a] have observed the following failure modes in their experiments: (i) **shear failure**, (ii) **flexural failure**, and (iii) **anchorage failure** (as illustrated in Fig 2-1). The first and the most common type of failure is shear failure, which is brittle in nature. The second type is flexural failure (tensile failure), which occurs at the bottom of the mid-span of a beam at the position of the lower longitudinal reinforcement when there is insufficient reinforcement. The third type is anchorage failure, which happens at the bottom of the beam at the ends of the main reinforcement when the development length or anchorage length is insufficient or when there is no mechanical anchorage at all. The shear failure mode is further classified into three categories:

a) **Diagonal Splitting Failure**. This occurs at the middle of the depth of the beam parallel to the strut. The cracks propagate in both directions towards the loading plate and the bearing plate. Without sufficient reinforcement, this failure can occur suddenly due to the splitting of a concrete strut. This type of failure cannot be predicted by the STM provisions of any of the three selected codes;
b) **Diagonal Compression** (strut crushing) **Failure**. This occurs at a beam's mid-depth, longitudinally between the end of the loading plate and the beginning of a strut, following the formation of several diagonal cracks; and
c) **Shear Compression Failure** (node failure). This occurs near the loading or bearing plate.

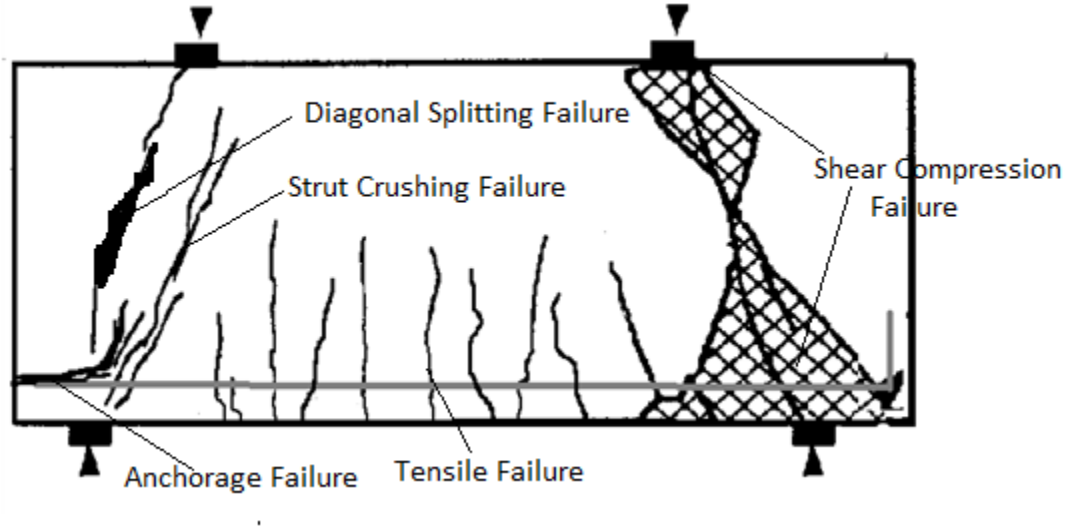

Fig. (2.1) Modes of failure of reinforced concrete deep beams. Michael and Oguzhan [2008], Carlos et al [2006] and Tan et al [1997a]

2.3. Review of the Strut-and-Tie Models in various codes:

2.3.1 General recommendations for designing reinforced concrete deep beams:

The main recommendations for deep beams as provided in these codes are summarized here:

- In the design of deep beams, the nonlinear distribution of strain needs to be considered. Strut-and-Tie Models may be used. The ACI 318-08[2008], Eurocode [2004] and CSA A23-3-04[2004] provide slightly different versions of the STM.
- Lateral buckling shall be considered when a beam is very thin; such that the *h/b* ratio is large (*b* is the width of the beam). This phenomenon has been investigated by many researchers to determine the size effect on the failure shear strength, as discussed below.

- In a study based on experiments, Kani [1967] has determined that with a ratio of *h/b* from 0.5 to 1.8, the width, *b*, has no effect on the failure shear strength. He has suggested that, in other words, the out-of-plane deformation may have no significant effect on the beam strength.
- On the other hand, Kotosoves and Pavlovic [2004] have concluded that the out-of-plane action has a significant effect on the beam strength when the beam cross section is thin or slim. Zhang and Tan [2007] have reached a similar conclusion.

- The definition of the nominal shear strength capacity, V_n, for a deep beam varies from one code to another.
  - ACI 318-08[2008] defines V_n as $0.83\sqrt{f'_c}\, b_w\, d$ (in *SI* units, with b_w and d in mm, and f'_c in MPa).
  - In the Eurocode [2004], V_n is determined by the reaction V_{Ed}, which is equal to $0.5 b_w\, d_v\, f_{cd}$ (in *SI* units). This value may be multiplied by $\beta = a/2d$ if the shear-span is between $0.5d$ and $2d$.
  - CSA [2004] does not specify any limitation on the ultimate shear force, which is calculated from the STM.
- The maximum horizontal and vertical reinforcement in the side faces of a deep flexural member should satisfy the code requirements as discussed below.
  - The provisions of ACI 318-08[2008] specify that the area of the vertical (A_V) and horizontal reinforcement (A_H) should not exceed $0.0025 b_w S_1$ and $0.0015\, b_w S_2$ respectively. As shown in **Figure 2.3**, S_1 and S_2 are spacings

of the bars in the respective directions. The bar spacing S_1 and S_2 should be less than $d/5$ and 12 in or 305 mm.

- The Eurocode [2004] provides that the area of skin reinforcement in the form of the orthogonal mesh should be 0.1% of the beam cross-sectional area, but not less than 150 mm^2/m in each face and direction; and the bar spacing, S, should be less than $2b$ and 300 mm.
- CSA A23-3-04[2004] specifies that web reinforcement is required if the height of a deep beam exceeds 750 mm and shall be uniformly distributed along the exposed side faces for a distance of $[0.5h-(2h-d)]$. In such a case, the area of reinforcement should not exceed $0.002A_c$ in each direction, and the bar spacing, S, should not exceed 300 mm.

- Based on the equation provided in the codes given above for determining and analyzing the beam capacity, the use of web reinforcement appears to have no effect on the way of calculating the strength of the struts. Only in ACI 318-08[2008], especially for a bottle-shaped strut, does the reduction factor β_s become 0.75 if $f'_c \leq 6000$ psi or 40 MPa and if the web reinforcement satisfies equation (A-4) of ACI 318-08[2008] code. Experimental studies, however, as discussed below, show that the web reinforcement may play an important role in enhancing the capacity of a concrete deep beam.
  - Michael and Oguzhan [2008] have assembled a database of tests, the results of which indicate that for a beam with an a/d ratio less than two, the vertical web reinforcement alone is more effective than a combination of horizontal and vertical web reinforcement.

- Zhang and Tan [2007] have conducted experimental tests on beams with and without web reinforcement; their results show that the beams with web reinforcement had higher serviceability loads.

2.3.2 The American Concrete Institute (ACI) Model:

ACI 318-08[2008] Appendix A provides the procedure for calculating the nominal capacities of the elements of the STM, which are the strut (a compression member), nodal zone and the tie (a tension member) as shown in Fig. (2.2).The design of the struts, ties and nodal zone are based on: $\varphi F_n \geq F_u$ where F_u is the largest force in that element for all loading cases, F_n is the nominal strength, and φ is a factor specified by clause 9.3.2.6 in the code.

There are two types of struts defined in the procedure. The first type of strut has a uniform cross sectional area over its length between the applied load and the support plate. The nominal capacity of a strut is given by $f_{ce} = 0.85\ \beta_s f`_c$, where β_s is defined as the efficiency factor. The efficiency factor β_s is the reduction of the ultimate strength of the strut. This factor reflects the ability of the concrete to resist loads at cracking develops or to transfer compression across cracks in a tension zone. The value of β_s ranges from 0.4 to 1 based on the type of the strut. The second type of strut is a strut with a bottle shape as shown in Figure (2.2). The nominal capacity of this type of strut is calculated in the same way as the straight struts, but with a different value for the efficiency factor β_s.

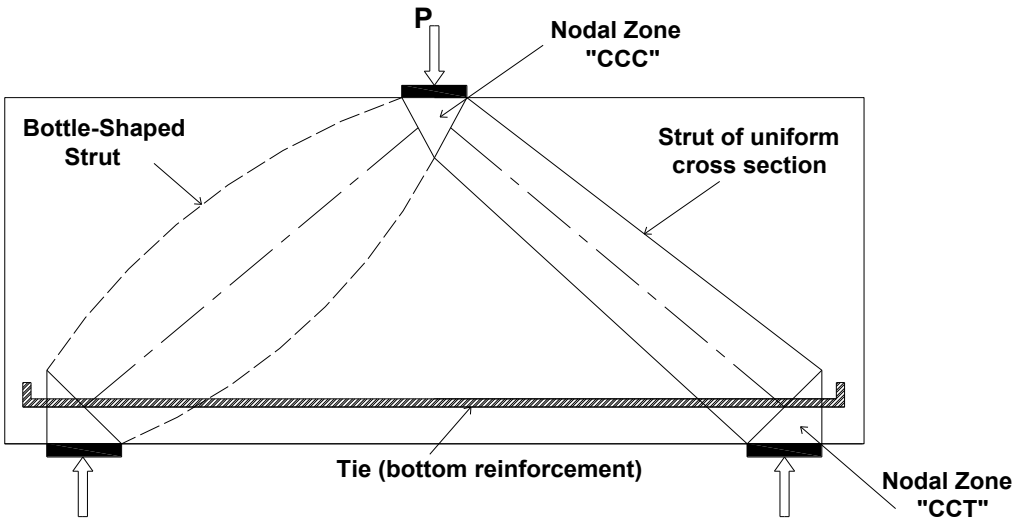

Fig. (2.2) Description of the Strut and Tie model.

For this type of strut, the β_s is taken as 0.75 if f'_c is not greater than 40 MPa and if the web reinforcement satisfies Equation (A-4) of ACI 318-08[2008] as shown in Eq (2.1) below.

$$\sum \frac{A_{Si}}{b_s S_i} \sin\alpha_i \geq 0.003 \qquad (2.1)$$

In the above equation, S_i and A_{Si} indicate spacing and area of a bar for web reinforcement (horizontal or vertical), and b_s indicates the width of the strut as shown in Fig. (2.3).

Michael and Oguzhan [2008] have argued that it is not preferable to use this type of strut since the web reinforcement is less than the required amount and such an amount cannot prevent the diagonal tension crack from growing. In the case of a high-strength concrete f'_c >40 MPa, where the code does not provide any specific guideline, Carlos et al [2006] have assumed a shallower slope of 6:1 for the spread of the compressive force in the strut to avoid an excessive number of web reinforcement. The efficiency factor is

taken equal to 0.6λ for a strut without web reinforcement case and for all other cases that do not meet the above requirements.

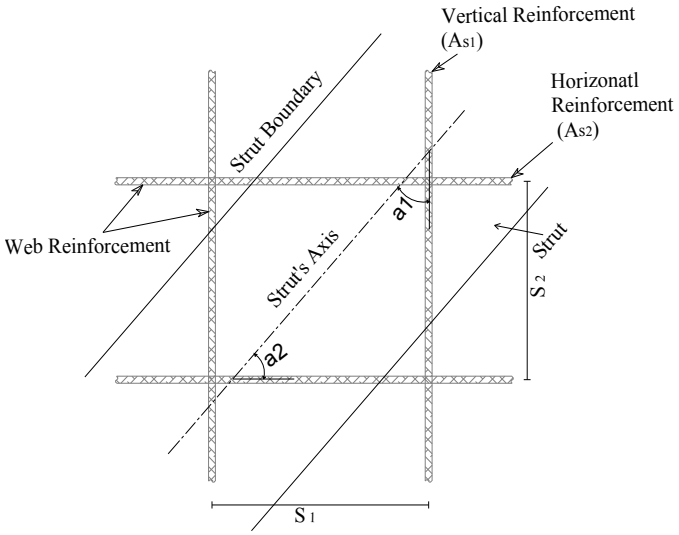

Fig. (2.3) Reinforcement crossing a strut. ACI 318-08 [2008]

Park and Aboutaha [2009] have compared the efficiency factors for different models and have concluded that the results obtained using ACI 318-08 [2008] are not conservative as compared to the experimental results in many cases. However, the code does not specify which type of strut should be used in the design procedure. The provisions of the code allow the designer to choose the type of strut that is used in determining the capacity of the element. Consequently; the procedure may yield multiple solutions.

The nominal compressive strength of a strut is given by $F_{ns} = f_{ce} * A_{cs}$, where A_{cs} is the cross sectional area calculated by multiplying the width of the strut (w_s) by the beam width Figure (2.4), and f_{ce} is the effective compressive strength of concrete. F_{ns} is

calculated at each end of a strut and the lesser value is considered. The strength of the node zone must be checked at the minimum face area of the node by following equation $F_{nn} = f_{ce} A_{nz}$ where A_{nz} is the area of the face of the nodal zone on which F_u acts and $f_{ce} = 0.85 \beta_n f`c$,where β_n is taken as 0.6,0.8 and 1 for CTT, CCT and CCC nodes, respectively, where C and T indicate whether an interacting member at that node is in a compression or a tension. In the first two cases, the strength of the nodal interface is adjusted by the strength of the strut.

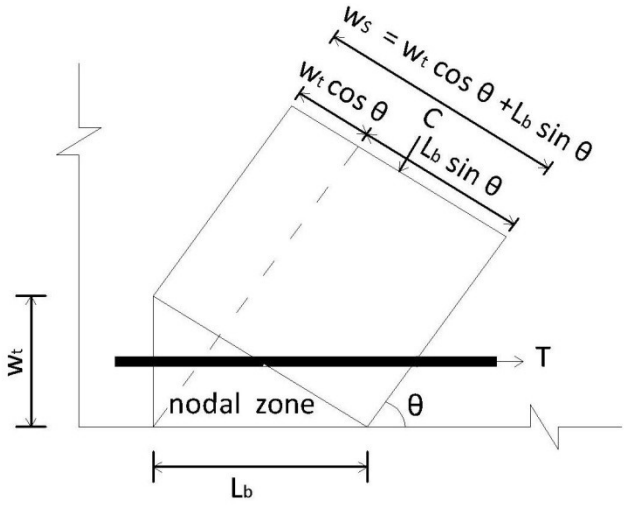

Fig. (2.4) Bottom nodal zone for one layer of steel.

The strength of ties is given by following the equation $F_{nt} = A_{ts} f_y + A_{tp}(f_{se} + \Delta f_p)$ where the second part of the equation is related to pre-stressed members. The code provides some recommendations for applying the tie reinforcement which are: the axis of the reinforcement and the axis of the tie coincide together, and shall be anchored by mechanical devices – standard hooks-or sufficient straight bar. ACI 318-08 [2008] gives

the limitation for the angle θ between the axis of the strut and tie as not less than arc tan ½ = 26.5° to mitigate cracking and to avoid incompatibilities.

2.3.3 The Eurocode Model:

The compressive force in a strut is apportioned by the compression strength of the cylindrical concrete f_{ck}. According to the Euro code, there is only one type of strut which is the strut with a uniform cross section, as in the CSA code [2004]. However, unlike the strut described in the CSA code [2004], this type of strut may have two different efficiency factors based on the transverse tension within the strut. For the first category, when the strut without transverse tension, the factor is equal to $1/\gamma_c$, where γ_c is a partial factor for the concrete in transient design situations and is equal to 1.5, and for accidental design situations is equal to 1.2. For the second case, the efficient factor of a strut with transverse tension is given by $v = 1 - f_{ck}/250$. The compressive strength has a large effect on calculating the efficiency factor in the second category, for example $v=0.9$ for f_{ck}=25 N/mm^2 whereas ν=0.84 for f_{ck}=40 N/mm^2. As stated by the Euro code EN 1992-1-1-2004(E) [2004] there are three nodal zones CCC, CCT, and CTT that are based on the node region and the direction that anchoring by tie. The compressive stress in these nodes CCC, CCT and CTT should not exceed the compressive stress of concrete $\sigma_{Rd,max}$, reducing it by K_1, K_2 and K_3 respectively for each type of node where K_1=1, K_2=0.85 and K_3=0.75.

2.3.4 The Canadian Standard Association (CSA) Model:

The CSA code [2004] provides that all struts are to be assumed to have uniform cross sections and the compressive force in a strut must not exceed $\phi_c f_{cu} A_{cs}$, where

$$f_{cu} = f`_c /(0.8+170\varepsilon_1) \leq 0.85 f`_c \quad (2.2)$$

and

$$\varepsilon_1 = \varepsilon_f + (\varepsilon_f + 0.002)\cot^2\theta_s \quad (2.3)$$

where, θ_s is the smallest angle between the strut and the adjoining tie. In the above equation, the nominal capacity of the strut will be reduced by $\phi_c / (0.8+170\varepsilon_1)$, which is not to exceed $0.85\phi_c$.

Table (2.1) The reduction factor of the effective compressive strength for ACI 318-08, Euro code EN 1992-1-1-2004(E) and Canadian code A23-3-04

Type		ACI318-08		Euro code EN 1992-1-1-2004(E)			Canadian code A23-3-04	
		Features	v	Features		v	Features	v
Strut	Uniform cross section	occur in compression zone	0.85	With transverse tension	transient	0.67	wherever occur	0.55
		occur in tension zone	0.34					
	bottle- shaped	satisfying equation (A-4)	0.64		accidental	0.83		
		not satisfying equation (A-4)	0.51					
	not clarifying	other than above	0.51	without transverse tension for f_{ck}=40 N/mm^2		0.84		
Node	CCC	compression reign	0.85	compression reign for f_{ck}=40 N/mm^2		0.84	CCC	0.55
	CCT	compression reign + one tie	0.68	compression reign + one tie for f_{ck}=40 N/mm^2		0.714	CCT	0.49
	CTT	compression reign + two tie or more	0.51	compression reign + two tie or more for f_{ck}=40 N/mm^2		0.63	CTT	0.43

The following three nodal zones are specified in CSA A23-3-04 [2004] based on the node region and the direction that anchoring by tie, CCC, CCT and CTT, such that the compressive stress in these nodes does not exceed $f`_c$ reduced by $0.85\phi_c$, $0.75\phi_c$ and $0.65\phi_c$ respectively. Also the tensile force in a tie should not exceed $\phi_s f_y A_{st}$. The

Canadian code recommends that the tie reinforcements be adequately anchored and that the angle θ between the axis of a strut and a tie be not less than $29+7000\varepsilon_x$. Table (2.1) contains a comparison of the reduction factors of the effective compressive strength of struts and of the nodes as defined in the codes. The reduction factor is defined as $\mu = \beta\phi$, where β is the efficiency factor and Φ is the strength coefficient.

2.4. Available experimental studies on conventional deep beams:

A number of experimental studies have been conducted in the past on deep-beams to study their behavior. An extensive literature review has been performed to collect the information about the available experiential studies on deep beams and compile database for the specifications of the test specimens utilized in these studies. The results of test specimens from available experimental studies on reinforced concrete deep beams have been used for the present study to evaluate and compare the Strut-and-Tie modeling provisions of the codes from three different jurisdictions: Canada, USA and Europe. The effectiveness of the Strut-and-Tie modeling provisions of the three different codes in predicting the ultimate strength and failure modes of deep beams has been evaluated against the actual behavior of such beams observed in experimental studies. Table (2-2) contains a brief summary of all the specimens in the database. The detailed description for all testes are provided in appendix A. They are deep beams subjected to one or two concentrated loads. The experimental samples contain a wide range of the compressive strength of concrete (f'_c from 16.5 MPa to 120 MPa). The shear-span to depth ratio of the samples ranging from 0.27 to 3.5 has been selected in accordance with the definition of deep beams provided in the above codes covering the entire range of deep beams and those transitioning from deep to shallow beams.

Table (2.2) Description of collected specimens

Reference	Number of samples	f'_c (MPa)	*a/d* ratio
Zhang and Tan [2007]	12	25.9-32.4	1.1
Nathan and Breña [2008]	12	27.0-35.6	1.0-2.0
Tan and Lu [1999]	12	30.8-49.1	0.56-1.13
Oh and Shin [2001]	53	23.72-73.6	0.50-2.0
Smith and Vantsiotis [1982]	52	16.1-22.1	0.77-2.01
Walraven and Lehwalter [1994]	12	17-21.3	1.0
Tan et al. [1997a]	19	56.2-86.3	0.85-1.69
Tan et al. [1997b]	22	54.8-74.1	0.28-3.14
Foster and Gilbert [1996]	16	77-120	0.76-1.88
Shin et al. [1999]	30	52 -73	1.5-2.5
Yang et al. [2003]	21	31.4-78.5	0.53-1.13
Kong and Rangan [1998]	42	63.6-89.4	1.51-3.30
Aguilar et al. [2002]	4	28	1.14-1.27
Tan et al. [1995]	19	41.06-58.84	0.27-1.62
Rigotti [2002]	11	16.5-34.5	1.87-2.33
Garay & Lubell [2008]	10	43-48	1.19-2.38
Total	**347**		

2.5. The effect of web reinforcements on the behavior of deep beams:

There are many studies available in the literature that provide more information on the effect of web reinforcements, mid-span deflection, crack width, failure modes, ultimate strengths and the behavior of reinforced concrete deep beams. Based on the results of the experimental studies as compiled here, the effect of web reinforcements on the behavior of deep beams has been investigated, and it has been observed that web reinforcements play an important role in enhancing the ultimate capacity, stiffness, etc. The effects of web reinforcement as observed in the experimental studies are briefly discussed below.

2.5.1 Beam stiffness:

Tan et al [1997a] have observed, judging from the mid-span deflection, that the web reinforcements increase the beam stiffness, and the effect of web reinforcement on the stiffness is more significant at $a/d \geq 1.13$. Smith and Vantsiotis [1983] have observed that a minimum amount of vertical and horizontal web reinforcement should be applied to increase beam stiffness and control cracks. Also Kong et al[1970] have found that web reinforcements have an effect on the beam stiffness, to a degree that becomes significant based on the arrangement and amount of web reinforcement depending on L/d and a/d ratios. They have also found that the vertical web reinforcement is more effective in enhancing the beam stiffness when the shear span-to- depth ratio $a/d \geq 0.7$.

2.5.2 Crack-control:

Smith and Vantsiotis [1983] have observed that at the same load level the crack widths are smaller and more uniform for beams with web reinforcement than for those without. Smith and Vantsiotis [1983] and Shin et al [1999] have also found that the web reinforcement produces no effect on the propagation of cracks, where the propagation of cracks in all beams is the same. Tan et al [1997a] have observed that web reinforcements have a significant effect in controlling the diagonal cracks, and the beams with web reinforcements exhibit higher serviceability loads. However, the control of the diagonal cracks varies according to the positioning of the shear reinforcements where the web is the most effective. Kong et al [1970] have concluded that the effect of web reinforcement on the crack width and length is dependent on the beam stiffness.

2.5.3 Modes of failure:

Most of the researchers Smith and Vantsiotis [1983], Tan et al [1997a] and Shin et al [1999] have clearly demonstrated that beams with web reinforcements exhibit the same modes of failure as compared to the beams without web reinforcements. However, Rogowsky et al [1986] have observed that a large amount of vertical web reinforcement may alter the mode of failure to ductile failure.

2.5.4 Ultimate shear strength:

Smith and Vantsiotis [1983] have indicated from their test results that the vertical web reinforcements of 0.18% to 1.25% can improve the ultimate shear strength, where the horizontal web reinforcements of 0.23% to 0.91% have a little or no effect on the ultimate shear strength. Smith and Vantsiotis [1983] have observed in their experimental study that the web reinforcements increase the ultimate shear strength from 0 to 30% but not beyond $4bd\sqrt{f'_c}$. Rogowsky et al [1986] have proved that only the vertical web reinforcements have a significant effect on the ultimate shear strength. Tan et al [1997a] have also confirmed that the vertical web reinforcements are more effective in increasing the shear strength than are the horizontal web reinforcements in the case of beams with high strength concrete. Using the test results of Tan et al [1997a] it was observed that the contribution of web reinforcements on the ultimate shear strength for high strength concrete varied from 0 to 50%, and the maximum contribution did not exceed $2bd\sqrt{f'_c}$. Oh and Shin [2001] have observed that the vertical web reinforcements increase the ultimate shear strength slightly, and the contribution of shear reinforcement is a function of the shear-span to depth ratio *a/d*. They also found that the horizontal web reinforcement has little effect on the ultimate shear strength. Table (2.3) contains a brief

description of the specification (e.g., compressive strength, $f`_c$; shear span depth ratio; vertical reinforcements, ρ_v%; horizontal reinforcements, ρ_h%; and web reinforcement, ρ_v%+ρ_h%) of experimental specimens used by the researchers to study the effect of web reinforcements.

Table (2.3) Details of the available experimental studies

Reference	$f`_c$ (MPa)	*a/d*	ρ_v%	ρ_h%	{ρ_v%-ρ_h% }
Tan et al [1997a,b]	56.3 to 92.7	0.85, 1.13, 1.69	0, 1.43, 2.86	0,1.59, 3.17	{0-0}, {2.86-1.59}, {1.43-1.59},
Kong et al [1970]	Avg of 22.13	0.23 to 0.7	0, 0.85, 2.45	0, 0.85, 2.45	{0-0}, {1.23-1.23}
Smith & Vantsiots [1982]	16.07 to 22.68	0.77, 1.01, 1.34	--	--	{(0.28,0.63,1.25)-(0.23to0.91)} {(0.24,0.63,0.77,1.25)-(0.23to0.91)} {(0.18,0.31,0.56,0.77)-(0.23to0.91)}
Oh andShin [2001]	23 to 74	0.5, 0.85, 1.25, 2	--	--	{0-0},{(0.12,0.22,0.34)-0.43},{0.13-(0.23,0.47,0.94)},{0.13-(0,0.023,0.47,0.94)}
Shin et al [1999]	52 & 73	1.5, 2, 2.5	--	--	{0 -0}, {(0.45to1.81)-0.5}
Rogowsky et al. [1986]	26.1 to 46.8	1, 1.5, 2	0.0015, 0.006, 0.0019, 0, 0.0057, 0.0014.	0.0016, 0.0018, 0.0011, 0.0032, 0.0013, 0.0039	{(0.0,0.0015)-(0.0,0.0016)},{(0.0,0.0019)-(0,0.0011)},{(0,0.0014)-(0,0.0012)}

2.6. The effect of shear-span to depth ratio on the behavior of deep beams:

The shear-span to depth ratio, *a/d*, has a major effect on the change of the stress pattern from linear to non-linear. The *a/d* ratio is an important variable that is used for

defining a deep beam. According to the common definition for a deep beam, the load from a support is closer than about twice the effective depth (i.e. $a/d<2$). Tan and Lu [1999] indicated that the stress-deflection curve was gentler in the beams that had higher *a/d*, and they also observed that with an increase in *a/d* ratio the beam becomes more flexible. MacGregor [2000] demonstrated that the *a/d* ratio has a major effect on the failure mechanism, and when $a/d<1$, the behavior changes from beam action to truss action. On the other hand, for the beams whose *a/d* ratio ranges between 1 and 2.5, failure occurs at less than the flexure moment capacity. Nathan and Breña [2008] noted that the influence of *a/d* on the crack patterns for the beams that have *a/d* ratio between 1 to 1.5 is consistent with a tied-arch mechanism of load transfer, in contrast to beams with $a/d=2$, where the crack formation indicates a truss mechanism of load transfer.

2.7. Further development of Strut and Tie models:

Many researchers proposed modification to the Strut and Tie models and the results showed some improvements. A brief account of some of the proposed Strut and Tie models for deep beams are presented below:

- **Matamoros and Wong [2003]** developed a STM models and calibrated them using experimental results from 175 simply supported beams having maximum shear span to depth ratio of 3. The forces in the strut were calculated by using four models, where the first model (Fig 2.5 a and b) uses a direct strut neglecting the contribution of web reinforcements, and the other two models (Fig 2.5 c and d) account for the contribution of web reinforcement using a truss with vertical ties (Fig 2.5 c) to represent the vertical reinforcements or horizontal ties (Fig 2.5 d) to represent the horizontal reinforcements.

However the fourth model (Fig 2.6) is a statically indeterminate strut-and-tie model that represents a combination of the above three models.

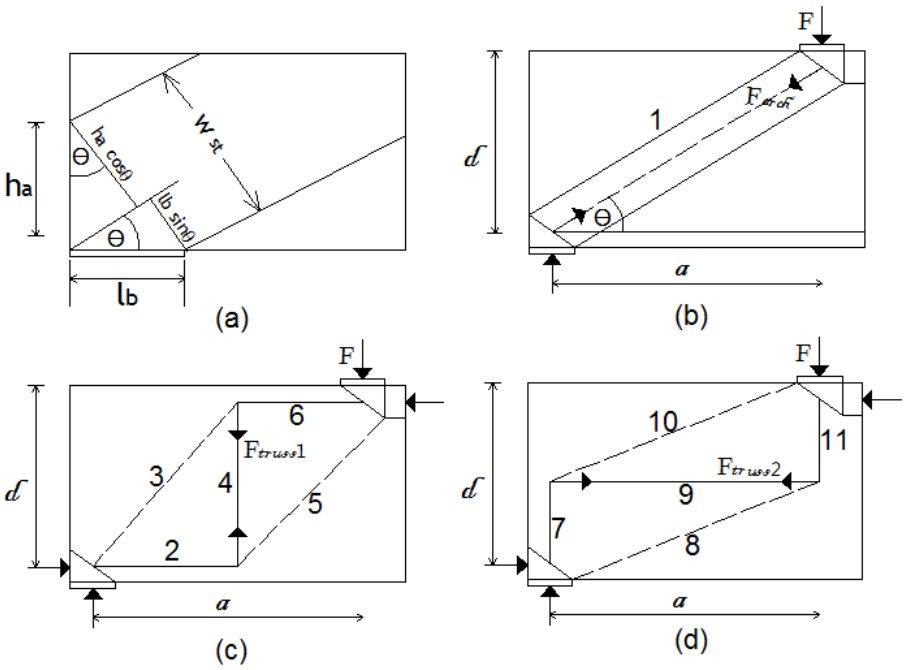

Fig. (2.5) (a) Dimensions of nodal zone; (b) compression strut mechanism; (c) vertical truss mechanism; and (d) horizontal truss mechanism. Matamoros and Wong [2003]

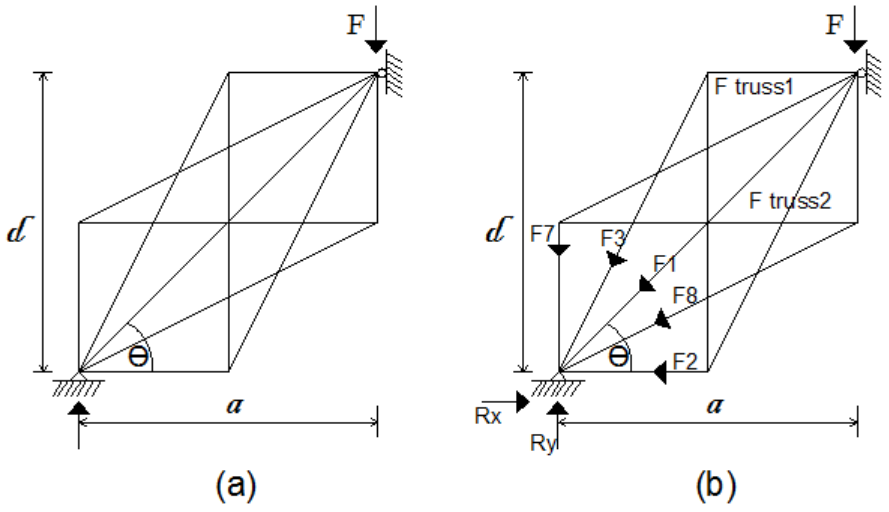

Fig. (2.6) Combined strut-and-tie models. Matamoros and Wong [2003]

The total shear force is carried by each of three mechanisms and can be presented by following equation (2.4):

$$V = C_c S_{strut} + C_{wv} S_{tv} + C_{wh} S_{th} \quad (2.4)$$

where, S_{strut} is the nominal strength of the strut by using only the contribution of the compressive strength of the concrete , S_{tv} is the nominal strength of the strut by using only the contribution of the vertical web reinforcement, S_{th} is the nominal strength of the strut by using only the contribution of the horizontal web reinforcements and C_c, C_{wv} and C_{wh} are the strength parameter, vertical web reinforcement coefficient and horizontal web reinforcements coefficient, respectively.

The resulting formula provides a comparable prediction of the shear strength according to a guideline by the Architectural Institute of Japan (AIJ) (Aoyama 1993). The proposed equation is also found to provide a safer estimate of capacity for beams with *a/d* ratio less than one.

-**Park and Kuchma [2007]** proposed a strut-and-tie-based method for calculating the strength of reinforced concrete deep beams. A strut-and-tie statically determinate model shown in Fig (2.7) is used for describing the flow of forces of a deep beam. The model is used in the development of a general approach that considers the compression softening and web splitting phenomena as influenced by transverse tensile straining. The proposed compatibility-based strut-and-tie model procedure uses an iterative secant stiffness formulation, employs constitutive relations for concrete and steel, and considers strain compatibility. The strain compatibility relation used in this study requires that the sum of normal strain in two perpendicular directions is an invariant. Also they assumed that the effective depth of the top horizontal concrete strut will be calculated by: $w_c = kd$, where d is the effective depth of the deep beam and *k* is derived from the classical bending theory

for a singly-reinforced beam section as: $(k = \sqrt{(n\rho)^2 + 2n\rho} - n\rho)$. In this case, n is the ratio of steel to concrete elastic modules and ρ is the longitudinal reinforcement ratio.

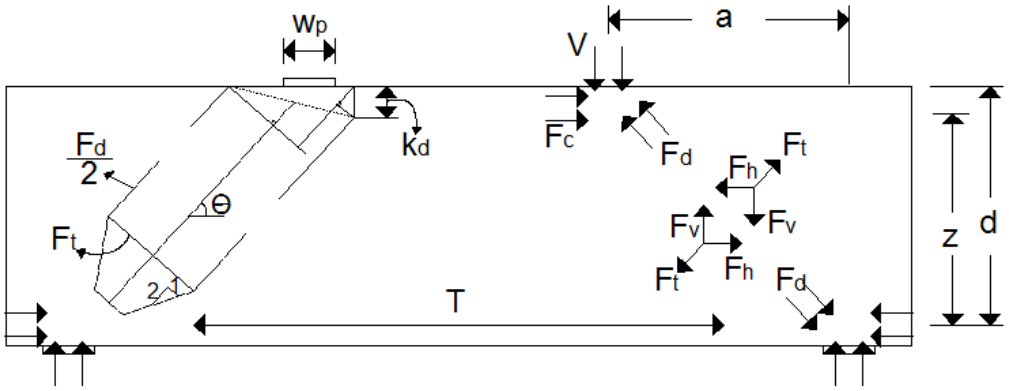

Fig. (2.7) Strut-and-tie model for deep beam. Park and Kuchma [2007]

This model was compared by Park and Kuchma [2007] with the strut-and-tie given in ACI 318-05 and CAN/CSA A23.3-04 code provisions in predicting the capacity of 214 deep beams which were tested to failure. The comparison showed that the proposed method consistently predicts the strengths of deep beams with a wide range of horizontal and vertical web reinforcement ratios, concrete strengths, and shear span-to-depth ratios (*a/d*) well.

-**Zhang and Tan [2007]** proposed a modified strut-and-tie model (STM) for determining the shear strength of reinforced concrete deep beams. The model is a modification to the original model proposed by Tan et al. [2003] with a direct strut-and-tie model for pressurised deep beams, and the model proposed by Tan et al. [2003] representing a direct method for deep beams with web reinforcements.

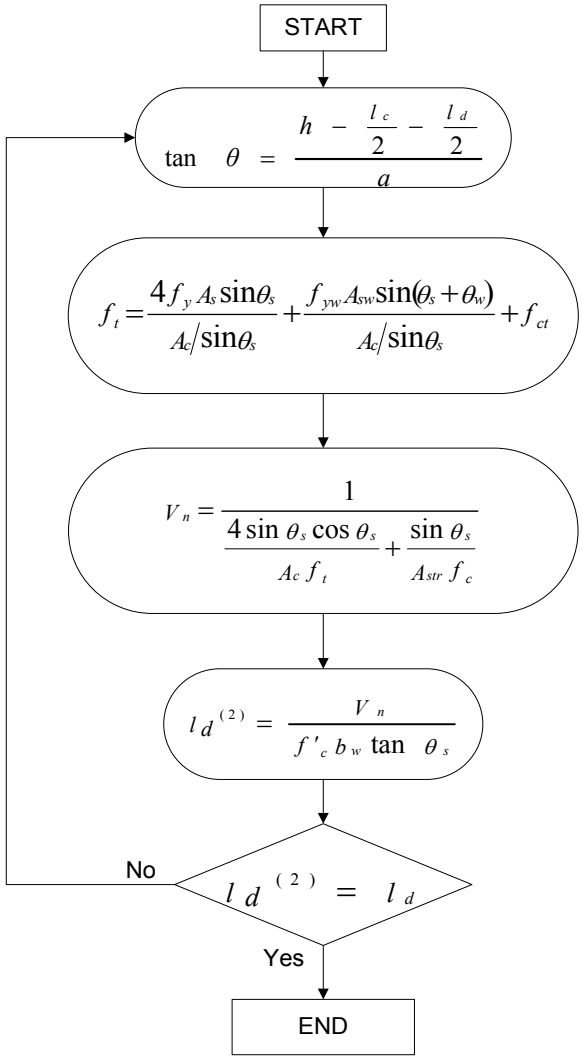

Fig. (2.8) Iteration procedure for computing the ultimate strength of for simply supported deep beams - Zhang and Tan [2007]

Figure (2.8) shows the iterative procedure for calculating the ultimate strength of deep beams by the modified model for the purpose of implementation. The assumption of proposed model can be summarized in the following: concrete tension–stiffening properties are used instead of concrete tensile strength to improve model prediction consistency. The component force of tension tie in the direction of the concrete diagonal strut is also included in the model for completeness. The softening effect of concrete strength due to the presence of transverse tensile strain is implicitly taken into

consideration. The stress distribution factor k is derived from the consideration of both force and moment equilibrium. The modified model for simply supported deep beams is evaluated using 233 test results and it was shown to be in a better agreement with the experimental results than the original model.

2.8. The use of Fibre-Reinforced Polymer (FRP) in deep beams

Since reinforced concrete deep beams have been used in many structural applications where they are often exposed to severe conditions, those conditions have often led to the deterioration of the concrete and led to the corrosion of rebars. The corrosion considered as the main factor behind the deterioration of the majority of concrete structures. Rebar corrosion will shorten the lifespan of a structure. Fiber-Reinforced Polymers (FRPs) have proven to be effective in concrete structures as an alternative to steel reinforcement. Compared to conventional steel reinforcement, Fiber-Reinforced Polymers (FRP) is up to five or six times stronger, lighter and not susceptible to corrosion. It is also used as an external confinement of the existing concrete structural elements to enhance the shear strength, the axial strength and the deformability of the members.

The increasing application of fibre-reinforced polymers (FRPs) as internal reinforcement in concrete prompted many researchers to conduct experimental and numerical studies to understand the behaviour of FRP-reinforced concrete structures. Further research is still needed particularly in terms of the shear behaviour of concrete members reinforced with FRP bars. A brief review of research programs was conducted in this chapter to investigate the behaviour of concrete members reinforced with FRP reinforcement. It is interesting to note that while some research is available on the behaviour of FRP-reinforced regular (shallow) beams, there are not many studies

available for FRP-reinforced concrete deep beams. The following review includes studies on deep beams or beams which are close to deep beams.

-El-Sayed et al. [2006a] tested nine large-scale reinforced concrete beams without stirrups with shear-span to depth ratio of 2.5. The test beams included three beams reinforced with glass FRP bars, three beams reinforced with carbon FRP bars, and three control beams reinforced with conventional steel bars. The dimensions of the beams were 3250 mm in length, 250 mm in width, and 400 mm in depth. And all beams were tested in bending with four-point loading. The details of test specimens are given in Table (2.4) and shown in Figure (2.9). The main variables considered were the reinforcement ratio and the modulus of elasticity of the longitudinal reinforcing bars. The beams were subjected to two point loads at the top.

Table (2.4) Details of the test specimens

Specimen No	f'_c (MPa)	b (mm)	d (mm)	L_e (mm)	a/d	Main reinforcement	f_{fu} (MPa)	ε_{fu}	Vertical & Horizontal reinforcement	ρ (%)
SN-1	50.0	250	326	2750	3.06	7No.15 M steel bars	460	0.0023	N/A	0.86
SN-2	50.0	250	326	2750	3.06	5No.15 M steel bars	460	0.0023	N/A	1.24
SN-3	50.0	250	326	2750	3.06	7No.15 M steel bars	460	0.0023	N/A	1.72
CN-1	44.6	250	326	2750	3.06	10 No. 10 CFRP bars	1536	0.0156	N/A	0.87
CN-2	44.6	250	326	2750	3.06	8 No. 13 CFRP bars	986	0.0180	N/A	1.24
CN-3	44.6	250	326	2750	3.06	11 No. 13 CFRP bars	986	0.0180	N/A	1.72
GN-1	43.6	250	326	2750	3.06	10 No. 10 GFRP bars	608	0.0120	N/A	0.87
GN-2	43.6	250	326	2750	3.06	5 No. 16 GFRP bars	754	0.0074	N/A	1.22
GN-3	43.6	250	326	2750	3.06	7 No. 16 GFRP bars	754	0.0074	N/A	1.71

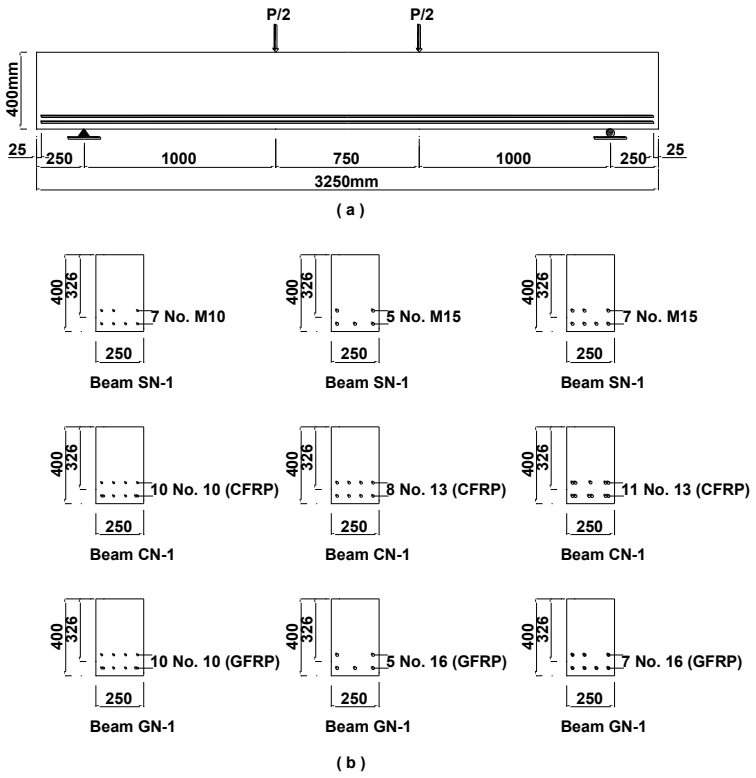

Fig. (2.9) (a) Test setup and dimensions; and (b) Sectional details. El-Sayed et al. [2006a]

From test results it was shown that the relatively low modulus of elasticity of FRP bars resulted in reduced shear strength as compared to the shear strength of the control beams reinforced with steel. The reduction of the shear strength can be attributed to the fact that the cross section using FRP flexural reinforcement develops wider and longer cracks as opposed to a steel reinforced section, and thus has a smaller depth to the neutral axis. It was observed that the most dominant failure mode was diagonal tension failure except in the control beams which experienced steel yielding simultaneous with the diagonal tension when failure occurred. Figure (2-10) shows the crack patterns at failure of the tested beam CN-3. A proposed modification to the current ACI 440.1R design

equation based on the obtained experimental results was presented and verified against test results of other researchers.

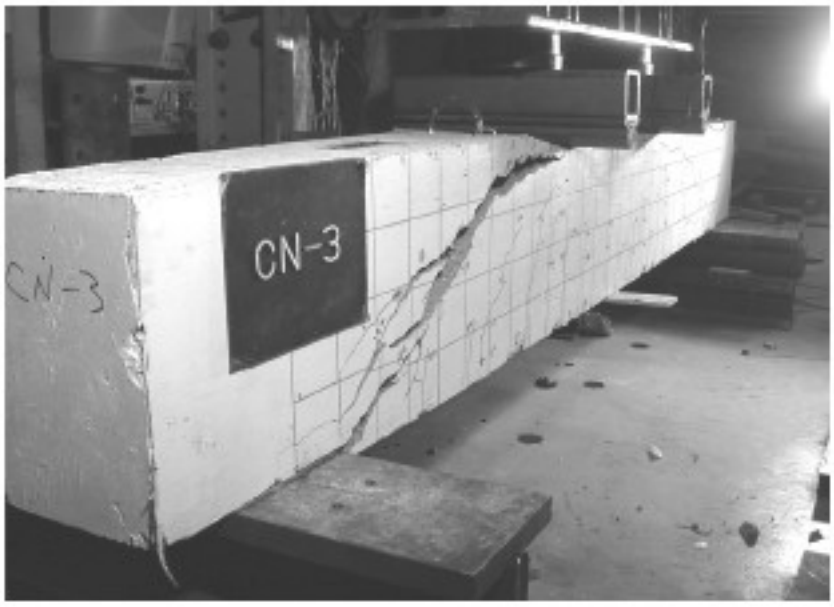

Fig. (2.10) Typical failure mode (Beam CN-3). El-Sayed et al. [2006a]

-El-Sayed et al. [2006b] carried out investigations on the influence of concrete strength, reinforcement ratio, and modulus of elasticity of the longitudinal reinforcing bars on six large-scale reinforced concrete beams with high-strength concrete (HSC), and three beams using normal-strength concrete (NSC). Carbon and glass FRP bars and conventional steel bars were used as longitudinal reinforcement in this investigation. All beams were without web reinforcement, and had ratio of shear-span to depth ratio of 2.5. The beams were 3250 mm long, 250 mm wide, and 400 mm deep, and they were tested in bending with four-point loading. The beams were tested under symmetrical loading conditions. The details of test specimens are given in Table (2.5) and shown in Fig. (2-11).

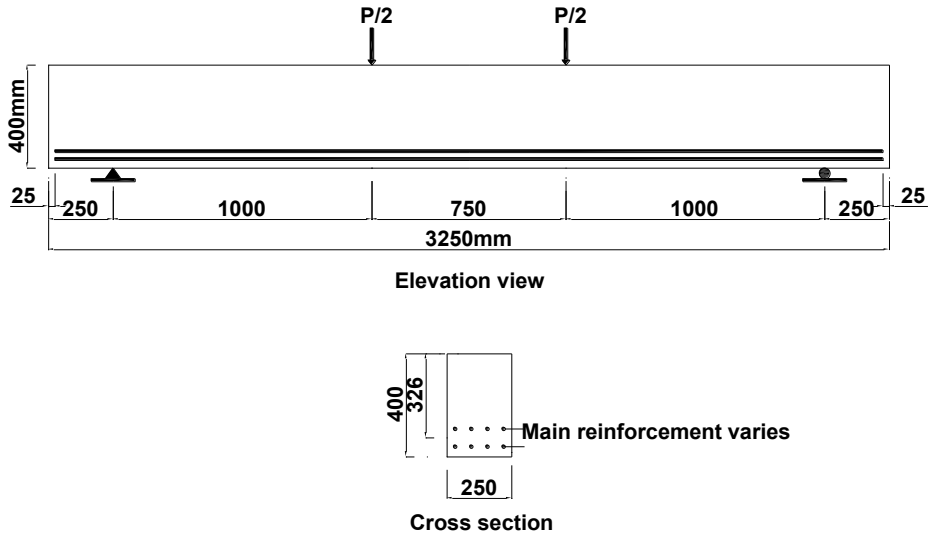

Fig. (2.11) (a) Test setup and the dimensions; and (b) sectional details. El-Sayed et al. [2006b]

Table (2.5) Details of the test specimens

Specimen No	f'_c (MPa)	b (mm)	d (mm)	L_e (mm)	a/d	Main reinforcement	f_{fu} (MPa)	ε_{fu}	Vertical & Horizontal reinforcement	ρ (%)
SN-1.7	35	250	326	2750	3.06	7No.15 M steel bars	460	0.0023	N/A	1.72
CN-1.7	35	250	326	2750	3.06	11 No. 13 CFRP bars	986	0.0074	N/A	1.72
GN-1.7	35	250	326	2750	3.06	7 No. 16 GFRP bars	754	0.0180	N/A	1.71
SH-1.7	65	250	326	2750	3.06	7No.15 M steel bars	460	0.0023	N/A	1.72
CH-1.7	65	250	326	2750	3.06	7 No. 16 CFRP bars	769	0.0074	N/A	1.71
GH-1.7	65	250	326	2750	3.06	7 No. 16 GFRP bars	754	0.0180	N/A	1.71
SH-2.2	65	250	326	2750	3.06	9No.15 M steel bars	460	0.0023	N/A	2.21
CH-2.2	65	250	326	2750	3.06	9 No. 16 CFRP bars	769	0.0074	N/A	2.20
GH-2.2	65	250	326	2750	3.06	9 No. 16 GFRP bars	754	0.0180	N/A	2.20

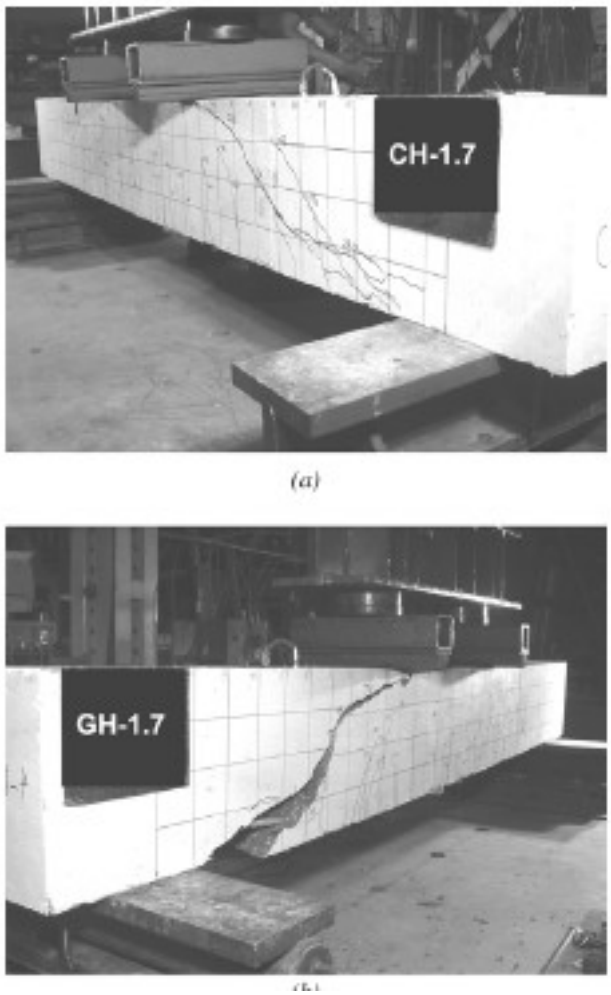

Fig. (2.12) Diagonal tension failure mode: (a) associated with no concrete splitting (Beam CH-1.7); and (b) associated with concrete splitting (Beam GH-1.7). El-Sayed et al. [2006b]

Test results showed that the high-strength concrete beams exhibited slightly lower relative shear strength as compared to normal-strength concrete beams. Figure (2.12) shows the crack patterns at failure of the tested beams CH-1.7 and GH-1.7. Also they concluded that the HSC beams exhibited lower normalized shear strength as compared to the control NSC beams.

-Farghaly and Benmokrane [2013] undertook a study on the shear strength of 4 full-scale deep beams reinforced with longitudinal carbon- and glass-Fiber Reinforced Polymer (FRP) bars and without any stirrups or web reinforcements. The variables included the longitudinal reinforcement ratio and the reinforcement type. The shear-span to depth ratios ranged from 1.13 to 1.15. The beams were supported over a 3,000-mm span with a projection of 1,000 mm on each side, with a cross section of 300 mm in width and 1,200 mm in depth, and tested to failure under four-point loading. The details of test specimens are given in Table (2.6) and shown in Fig. (2.13).

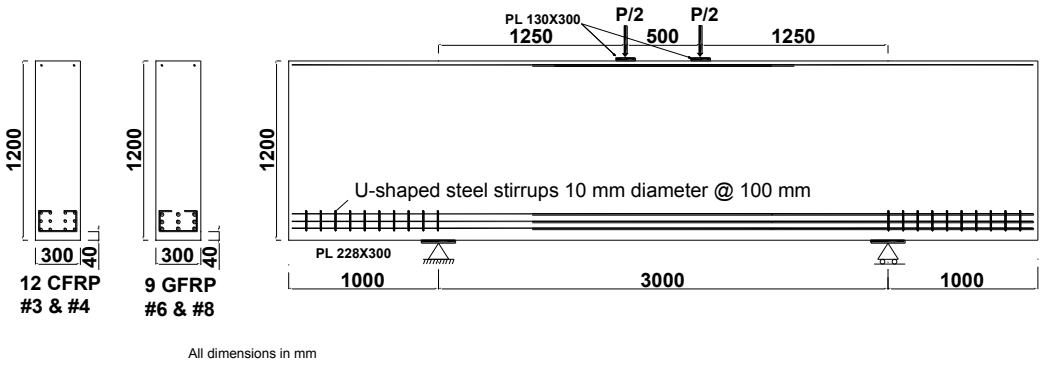

Fig. (2.13) Dimensions of beam sections and details of reinforcement configuration. Farghaly and Benmokrane [2013]

Table (2.6) Details of the test specimens

Specimen No	f'_c (MPa)	b (mm)	d (mm)	L_e (mm)	a/d	Main reinforcement	f_{fu} (MPa)	ε_{fu} (%)	Vertical & Horizontal reinforcement	ρ_f (%)
G8N6	49.3	300	1097	3000	1.14	8 No.6 GFRP bars	460	1.66	N/A	0.69
G8N8	49.3	300	1088	3000	1.15	8 No. 8 GFRP bars	460	1.45	N/A	1.24
C12N3	38.7	300	1111	3000	1.13	12 No. 3 CFRP bars	380	1.33	N/A	0.26
C12N4	38.7	300	1106	3000	1.13	12 No.4 CFRP bars	380	1.32	N/A	0.46

It was observed that reinforcement type had no clear effect on the behavior of the tested beams. Also it was found that the reinforcement ratio and concrete compressive strength had a clear effect on the ultimate capacity and deflection characteristics. Figure (2.14) shows the failure modes of the tested beams.

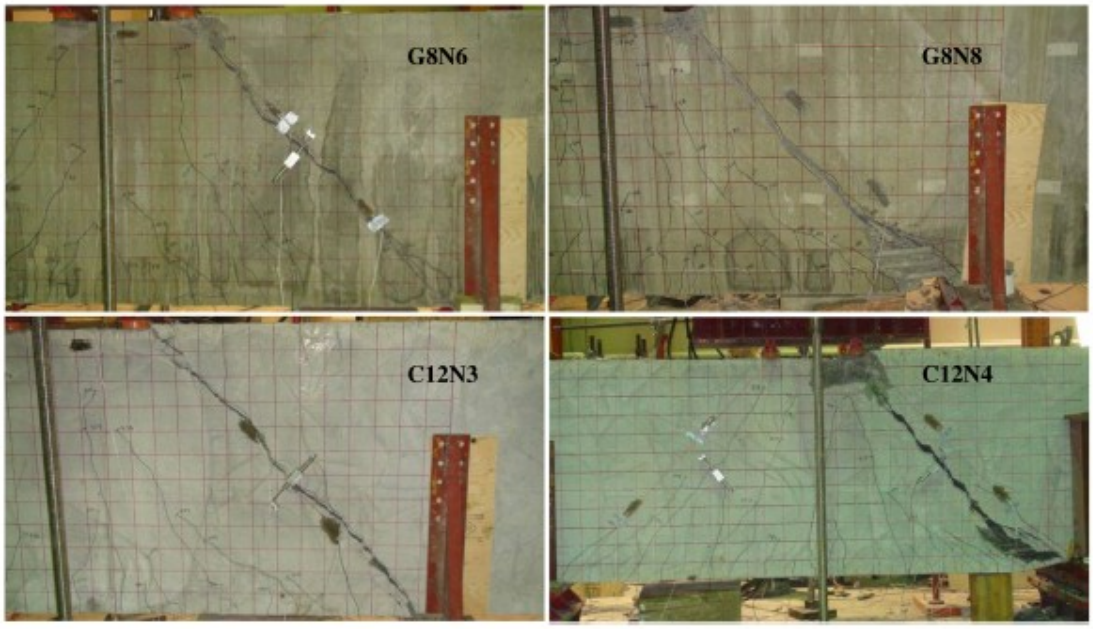

Fig. (2.14) Failure of the tested deep beams. Farghaly and Benmokrane [2013]

The results confirmed the formation of the tie action, where the strain in the longitudinal reinforcement distributed nearly uniform. It is important to note that these are the only studies available so far on FRP-RC deep beams.

Chapter 3: Research Methodology and Experimental Setup

3.1. Overview:

The research methodology includes the comparison of the STM provisions of ACI 318-08 code [2008], EN 1992-1-1-2004(E) [2004] and the Canadian code CAN/CSA A23-3-04 [2004] in designing conventional deep beams. The comparative study is intended to capture the effect of most important variables on the estimation of the ultimate strength of deep beams using the STM provisions of various codes. Also a design method for FRP reinforced concrete deep beams is developed based on the provisions for conventional RC deep beams and FRP reinforced ordinary beams. In addition the effectiveness of the STM provisions of the CAN/CSA-S806-12[2012] in predicting the capacity of concrete deep beams has been verified. An experimental program was conducted to study the behaviour of FRP-reinforced concrete deep beam and to investigate the effect of the critical variables. Based on the experimental results, the suggested design procedure will be fine-tuned and the appropriate quantity of the FRP web reinforcement in deep beams will be determined. The proposed design methodology, the details of the geometry and reinforcement configurations, the material properties and the test set up for the specimens are explained in this chapter.

The main tasks undertaken in the present research are as follows:

1. Review the existing experimental studies on reinforced concrete deep beams and collect the detailed data on the experimental specimens and parameters.

2. Compare the impact of the current codes provisions for designing reinforced concrete deep beams using STM on the capacity and failure mode with respect to the results of the available experimental studies.
3. Identify critical parameters governing the behaviour of deep beams using available experimental data.
4. Develop a design method for FRP-reinforced concrete deep beams and use it in the design of the experimental specimens used in the present study.
5. Experimentally evaluate the behaviour of FRP-reinforced deep beams and evaluate the influence of the critical parameters on their behaviour.
6. Validate the existing code provisions and update the proposed design method using the results of the experimental study.

3.2. Comparison of the STM procedures for conventional deep beams provided in the three selected codes:

The results of more than three hundred test specimens from available experimental studies on reinforced concrete deep beams have been used for the present study to evaluate and compare the Strut-and-Tie modeling provisions of the codes from three different jurisdictions: Canada, USA and Europe. Figure (3.1) shows a typical deep beam and possible STM configurations. The effectiveness of these code provisions in predicting the ultimate strength and failure modes of deep beams have been evaluated against the actual behavior of such beams observed in experimental studies.

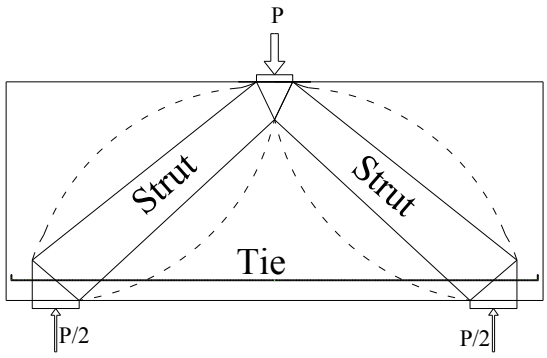

(a.

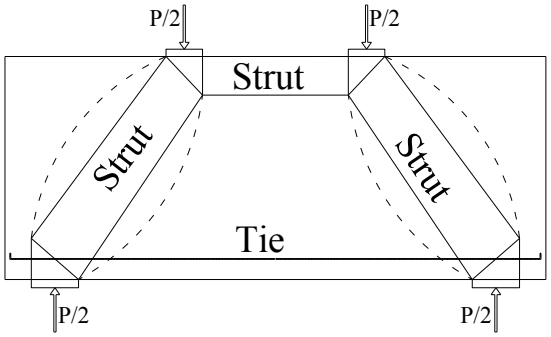

(b.

Fig. (3.1) Strut and Tie Models: (a) beam specimen loaded by a single point load, (b) beam specimen loaded by two point loads

The capacity of each specimen has been computed using the STM provisions of the three codes as selected here. ACI-318 provides a straight and a bottle-shaped strut, while other codes provide only straight struts. For the ACI, bottle-shaped strut has been used here for its superior performance, and the efficiency factor β_s is assumed to be 0.75 as suggested in the code (ACI 318-08 [2008] - Appendix A).The Eurocode procedure provided in EN 1992-1-1-2004(E) [2004] has been used with the modification of the predicted ultimate shear force by multiplying this value by $\beta = a/2d$ as suggested in the code.

No modification is suggested in the Strut and Tie model procedure specified in Canadian standard CSA A23-3-04 [2004]. The effects of governing variables, such as the shear span to depth ratio, web reinforcement, and the compressive strength of concrete on the capacity determined by the Strut-and-Tie Model (STM) procedures of the selected codes have also been investigated.

3.3. Design methods for FRP-reinforced concrete deep beams:

At the beginning of this current research, the strut and tie model was not available in any of the relevant design codes and standards for design of FRP reinforced concrete deep beams. At that time, the existing standard on FRP-reinforced concrete structures CAN/CSA-S806-02 [2002] did not permit FRP-RC deep-beams as relevant design methods were not provided. Thus, a design procedure for FRP-RC deep beams was developed in this research based on the corresponding design provisions for conventional deep beams as provided in CSA A23.3-04 [2004], which have been modified for FRP materials. Later, the current version of CSA-S806-12 [2012] was published which provided an STM procedure for FRP-RC deep beams that is mostly based on the provisions of CSA A23.3-04 applicable for conventional deep beams, but modified for FRP materials. The ACI and Eurocode still do not provide similar methods for designing FRP-RC deep beams. This section briefly discusses the design procedure adopted for the test specimens prior to the publication of CSA-S806-12, the relevant provisions of CSA-S806-12 and a proposal for an STM procedure in ACI for designing FRP-RC deep beams based on the modified procedure for conventional RC deep beams as provided in ACI 318-08 [2008].

3.3.1. The STM design procedure adopted for the test specimens based on CSA A23.3-04 [2004] and CSA S806-02 [2002]:

The STM model for concrete deep beams provided in CSA A23.3 [2004] has been adapted to FRP reinforced concrete deep beam for strut and node elements which represent the compression element (concrete), while the equation of the tie element is revised to consider the rupture of the FRP that will cause the failure of a tie section. This proposal was consistent with what was later on adopted in the new edition of the Canadian code CAN/CSA-S806-12[2012]. The Canadian code in its new edition CAN/CSA-S806-12[2012] adopts the STM approach of conventional beam with similar adjustments that take into account of the properties of FRP.

Since the ACI 440.1 R-06[2006] standard does not provide a procedure for designing RC deep beams reinforced with FRP bars as yet, an STM design procedure for FRP-reinforced concrete deep beams is also developed here. The proposed design procedure for FRP-reinforced concrete deep beams is similar to the STM approach for conventional deep beams as provided in ACI 318-08 with some adjustments to account for the properties of FRP. The design method and proposed STM for FRP-reinforced concrete deep beams are described below.

3.3.2. STM procedure in the CAN/CSA-S806-12 [2012] code:

In the newer edition, the CSA-S806-12[2012] adopts the STM approach for conventional RC beams, with appropriate adjustments to account for the properties of FRP. For example the compressive force in a strut is calculated in a similar way as to CSA-A23.3-

04 [2004] where the strut is apportioned by the compression strength of the concrete and the principal tensile strain in cracked concrete due to factored loads.

The force in a strut in the CSA-S806-12 [2012] procedure as given by Equation (2.2) is calculated slightly differently from that in the CSA-A23.3-04 [2004] procedure where the principal tensile strain ε_1 is estimated based on the ultimate strain in FRP instead of steel, but the other parameters in calculating ε_1 are not changed (Equation 3.1).

$$\varepsilon_1=\varepsilon_f+(\varepsilon_f+0.002)cot^2\theta_s \quad (3.1)$$

where θ_s is the smallest angle between the strut and the adjoining tie and ε_f is the strain in the FRP reinforcement.

As for nodal zones, the CSA-S806-12 [2012] still adopted the same nodal zones CCC, CCT, and CTT (here, C and T indicate compression and tension, respectively in a member connecting to the node) that are described in the CSA-A23.3-04 [2004] without any change. The compressive stress in these nodes, CTT, CCT and CCC should not exceed the compressive stress of concrete $\phi_c f_c'$, reduced by 0.65, 0.75 and 0.85, respectively. The CSA-S806-12[2012] calculated the tensile force in a tie similarly to the CSA A23.3-04 [2004] code but using only 65% of the tensile strength of FRP reinforcement instead of the yield strength of steel. The strength of ties strengthened by FRP can be calculated by using the following equation

$$F_{nt}=0.65\ \phi_F A_{FT} f_{Fu} \quad (3.2)$$

where A_{FT} is the total area of FRP reinforcement and f_{Fu} is the designed tensile strength of the FRP.

Unlike to the CSA-A23.3-04[2004] which used only the yield strength of steel multiplied by (x/l_d) to calculate the limitation of the stress for straight bars extending a distance, x beyond the critical location (l_d is the development length), the CSA-S806-12[2012] includes the area of FRP reinforcements in the corresponding equation that calculate the stress limit, which is inconsistent.

Both the CSA-A23.3-04[2004] and the CSA-S806-12[2012] recommend application of specified amounts of web FRP reinforcements that may enhance the beam stiffness and satisfy the serviceability requirements. Although the FRP stirrups have lower dowel resistance and lower modules of elasticity as compared to the steel stirrups, the FRP web reinforcement can perform the same functions of the steel stirrups such as, restrict the growth of diagonal cracks and provides some confinement to the concrete in the compression zone. The difference between the two codes is in the recommended amount of the web reinforcements. The CSA-S806-12[2012] determined this ratio to be less than 0.004 (of the normal area between two adjacent stirrups for vertical reinforcements) for GFRP and AFRP, and 0.003 for CFRP, while CSA-A23.3-04 [2004] recommends (for steel reinforced deep beams) the ratio not to be less than 0.002 in each direction. CSA-S806-12[2012] requirements for the web reinforcement appear to be quite conservative and may result in a very close spacing of the web reinforcements. For example the minimum spacing between the GFRP stirrups for beam of width equal to 230 mm is 62 mm, while that for a beam of width 450 mm is 31mm, which is very small and not practical.

3.3.3. Procedure for shear design in flexural regions in the CAN/CSA-S806-12 code:

The philosophy of the FRP shear design in the standard is in accordance with the sectional design method. The shear strength of an FRP-reinforced member is determined from the nominal resistance of the concrete V_c and the contribution of the FRP shear reinforcement $V_{sf.}$ The code provides an equation to calculate the shear capacity of the concrete for sections having an effective depth not exceeding 300 mm.

$$V_c=0.05\lambda \phi_c k_m k_r (f'_c)^{1/3} b_w d_v \quad (3.3)$$

where

$$k_m=\sqrt{(V_f d/M_f)}\leq 1.0 \quad (3.4)$$

$$k_r=1+(E_f \rho_{Fw})^{1/3} \quad (3.5)$$

V_c provided by S806-12 [2012] is modified by the factor k_s for members with effective depth greater than 300 mm and with less transverse shear reinforcement.

$$k_s= 750/ (450+d) \leq 1.0 \quad (3.6)$$

By using the same method as that used in CSA-A23.3-04 [2004] and using the properties of FRP with a reduction of 40%, the shear contribution of the FRP stirrups, V_{sf} , can be calculated as

$$V_{sf}= (0.4 \phi_F A_{Fv} f_{FU} d_v/s) \cot\theta \quad (3.7)$$

3.3.4. Procedure of shear design in flexural regions in the ACI 440.1R-06 code:

The philosophy of the FRP shear design in ACI 440.1R-06 [2006] is in accordance with the strength design method. The shear strength of an FRP-reinforced member is determined from the nominal resistance of the concrete V_c and the FRP shear reinforcement V_f. The code mentions that many researchers have observed the influence the stiffness and of the tensile reinforcement on the concrete shear strength. Despite the similarity of the general structural behavior of concrete beams reinforced by FRP and those reinforced by steel, the lower axial stiffness of FRP reinforcement reduces the compression region of the cross section. Therefore, the shear resistance provided by concrete in cross section using FRP is smaller than those using steel reinforcement.

The shear capacity of the concrete V_c as provided by the ACI 318-08 [2008] code is modified by a factor of ([5/2]k) to account for the axial stiffness of the FRP reinforcement, as follows.

$$V_c = (\frac{5}{2}k)2\sqrt{f`c\ b_w d} \qquad (3.8)$$

By using the same method as used in ACI 318-08 [2008], the shear contribution of the FRP stirrups, V_f, can be calculated as

$$\mathrm{V}_f = \frac{A_{fv} f_{fv} d}{s} \qquad (3.9)$$

To avoid failure at the bent portion of the FRP stirrups, the stress level in the FRP shear reinforcement is limited by following equation as per ACI 440.1R-06 [2006].

$$f_{fv} = 0.004\, E_f \leq f_{fb} \qquad (3.10)$$

Similar to what is applied in ACI 318-08 [2008] for the minimum requirements of shear reinforcement to prevent brittle shear failure, ACI 440.1R-06 [2006] recommends the application of the minimum amount of FRP shear reinforcement taking in to consideration of the properties of the FRP.

3.3.5. Proposed procedure for design designing FRP-RC deep beams based on ACI code:

Chapter nine of the ACI code does not provide any procedure to design deep beams reinforced with FRP bars. The relevant procedure for conventional steel reinforced concrete deep beams as provided in ACI 318-08 [2008] is modified here for FRP RC and used here along with other relevant provisions of ACI 440.1R-06 [2006] code to design the FRP-reinforced concrete deep beams. Appendix B of the ACI 318-08 [2008] provides the procedure for calculating the nominal capacities of the elements of Strut-and-Tie models for conventional concrete deep beams, which are the strut (a compression member), the nodal zone and the tie (a tension member). The design of the struts, ties and nodal zones are based on: $\varphi F_n \geq F_u$ where F_u is the largest force in that element for all loading cases, F_n is the nominal strength, and φ is a factor specified in the code. Two types of struts are defined in the procedure: strut of uniform cross section; and bottle shaped strut. The nominal capacity of a strut is given by $f_{ce} = 0.85\ \beta_s\ f'_c$, where β_s is defined as the efficiency factor. The value of (β_s) for uniform cross section strut ranges from 0.4 to 1 based on where the strut is placed. While for the bottle shaped strut the efficiency factor β_s can be taken as 0.75 if the web reinforcement satisfies the provisions of ACI 318-08 [2008] as given in Eq. (2.1) in this thesis. The nominal compressive strength of a strut can be determined as

$$F_{ns} = f_{ce}\, A_{cs} \qquad (3.11)$$

where A_{cs} is the cross sectional area. To calculate the strength of a nodal zone, the procedure in ACI 318-08 [2008] can be used as is, without any changes. The compressive stress in these nodes, CTT, CCT and CCC, should not exceed the compressive stress of concrete $0.85f'_c$ reduced by 0.6, 0.8 and 1, respectively. Here, the nodes are designated by the type of truss members meeting at the node, where T denotes Tensions, and C denotes Compression.

The strength of ties consisting of FRP reinforcements can be calculated by using the following equation

$$F_{nt} = A_{tf} f_{fu} \qquad (3.12)$$

where A_{tf} is the total area of FRP reinforcement and f_{fu} is the design tensile strength of FRP, considering the reduction factors as per ACI 440.1R-06 [2006]. For deep beam design, all the recommendations prescribed by the ACI 318.08 [2008] should be applied and taken into consideration, for example, the application of the minimum of web reinforcement.

3.4. Experimental Plan:

The experimental work was carried out in the Structures Laboratory of the Concordia University. Different parameters were examined for their effect on the behaviour of the beam specimens. These parameters were the shear span to depth ratio (*a/d*) and the amount of the FRP web shear reinforcement. A total of nine concrete deep beam specimens were tested. The beams were divided into three groups of similar shear span to depth ratio. The first group, A, contains 4 beams with shear-span to depth ratio *a/d* =1 with different quantities of the FRP web shear reinforcement: ρ_w= 0, 44%, 68%, and

100%, where ρ_w= 100% indicates the quantity of shear reinforcement corresponding to the maximum allowable spacing of the web reinforcement to control cracks in a beam as required by the earlier edition of the Canadian code for GFRP reinforcements, CAN/CSA S806-02 [2002]. It should be noted that when the present experimental study was planned and the specimens were made, the current version of the CSA standard, CSA-S806-12 was not available and the earlier version did not provide any design provisions for FRP-reinforced concrete deep beams (i.e., no STM procedure was available in CSA-S806). For that reason, the web reinforcements were provided in the studied samples based on the crack control provisions of the earlier version of CSA-S806. The present version of the standard provides an STM model for FRP-RC deep beams, and the required amount of web reinforcements is significantly higher than the crack control reinforcements which seems to be overly conservative and can lead to very closely spaced web reinforcements. The second group B, includes only one beam having shear-span to depth ratio, a/d =1.5 with 100% of required FRP web shear reinforcement ratios. The third group, C, comprises 4 beams with shear-span to depth ratio a/d =2 and different FRP web shear reinforcement ratios: ρ_w= 0, 38%, 60%, and 100%. All the beams were tested to failure under three-point loading (i.e. one concentrated vertical load).

3.4.1. Details of Test Specimens:

All nine beams were designed according to the design procedures developed for this research which is based on the design provisions for conventional deep beams as provided in CSA A23.3-04. The design of the beam specimens took into consideration the required anchorage length, the web reinforcement requirement and main reinforcement ratio. All beams have a constant width of 230 mm, and a total span of

1800 mm. However, different height was utilized to obtain shear span to depth ratios (*a/d*) of 1, 1.5 and 2. The depth *d* was varied as 328, 447 and 600 mm to achieve the three different *a/d* ratios. The stress in each reinforcement layer will vary depending on its distance from the neutral axis because the behaviour of the FRP materials is elastic up to failure. Therefore, in case of multiple layers of reinforcement and combinations of different FRP types, the analysis of the flexural capacity should be based on a strain-compatibility approach. Because all the beams have two layers of the same type of FRP reinforcement and the distance between the two layers is very small as compared to the depth of the deep beam, the stress in the FRP reinforcement in the two layers are almost equal. Therefore, the effective depth of the section was taken as the distance of the centre of the layers of the main rebars from the top face of the beam. It should also be noted that the deep beams are not expected to behave in flexure and the strain distribution is not proportional to the distance from the neutral axis. In this case, the strain of the main longitudinal reinforcements in different layers are expected to be very close to each other and the bars in different layers are expected to act in a group to provide the tie effect in the context of an STM model.

Each group has a longitudinal main GFRP reinforcement ratio ranging between ρ =1 to 1.197 percent. The stirrups were all GFRP with diameter of 6 mm. Top reinforcement consisted of two 10 mm GFRP bars. Bearing plates at the loading point and at the supports were of 200 mm length x 230 width x 30 mm height. The details of the specimens are given in Table (3.1).

In order to simplify the nomenclature of the samples, the following abbreviations are used. With each group with constant *a/d*, only the variable of web reinforcements is

changing. Each specimen is labeled in the following way: *Gf/p*, where *G* indicates the group name, *f* represents the value of the *a/d* ratio (i.e., 1, 1.5 or 2), and *p* indicates the nominal level of web reinforcement in percentage (i.e., 00, 50, 75 or 100). As for example, the specimen in Group A which had *a/d* ratio of 1 and 100% of web reinforcement will be labeled as A1/100.

Table (3.1) Details of the experimental specimens

Specimen No	f'_c (*MPa)*	*b (mm)*	*d (mm)*	L_e *(mm)*	*a/d*	Main reinforcement	f_{fu} *(MPa)*	ε_{fu}	ρ *(%)*	ρ_v *(%)*
A1/100	49.8	230	621	1240	1	6 # 6(19 mm)	656	0.0153	1.197	0.141
A1/75	52.2	230	621	1240	1	6 # 6(19 mm)	656	0.0153	1.197	0.095
A1/50	52.5	230	621	1240	1	6 # 6(19 mm)	656	0.0153	1.197	0.061
A1/00	52.7	230	621	1240	1	6 # 6(19 mm)	656	0.0153	1.197	N/A
B1.5/100	51.8	230	447	1340	1.5	3 # 6(19 mm) 3# 4 (13 mm)	656 708	0.0153 0.0170	1.201	0.145
C2/100	50.8	230	328	1310	2	6 # 4(13 mm)	708	0.0170	1	0.158
C2/75	51.0	230	328	1310	2	6 # 4(13 mm)	708	0.0170	1	0.095
C2/50	51.3	230	328	1310	2	6 # 4(13 mm)	708	0.0170	1	0.061
C2/00	51.3	230	328	1310	2	6 # 4(13 mm)	708	0.0170	1	N/A

Details of Specimens of Group A:

Full detailing of specimen dimensions and reinforcement are illustrated in Figures (3.2) through (3.5). All four beams have a width of 230 mm, the beams have effective span l_e 1240 mm while the total length is 1800 mm. The depth, *d* is 621 mm for the specimens of group (A). Each beam has a longitudinal main FRP reinforcement ratio ρ of 1.197 percent. The specimens of group (A) consisting two rows of three 19-mm diameter FRP rebars. However, different amount of vertical and horizontal FRP reinforcement was applied to obtain different quantities with ρ_w= 0, 44, 68, and 100 percent for A1/00, A1/50, A1/75 and A1/100 specimens, respectively. Closed-loop FRP stirrups of 6 mm

diameter with different spacing *S* of 196, 290 and 450 mm were used as the vertical reinforcement for A1/100, A1/75 and A1/50 specimens, respectively. The FRP stirrups were pre-fabricated by the manufacturer at the plant. Also two FRP bars with diameter of 6 mm at 190 mm spacing on each side were used as horizontal web reinforcement for specimens A1/100. While, the specimens A1/75 and A1/50 have only one FRP bar in each side with diameter of 10 and 6 mm at the mid height of the beam, respectively.

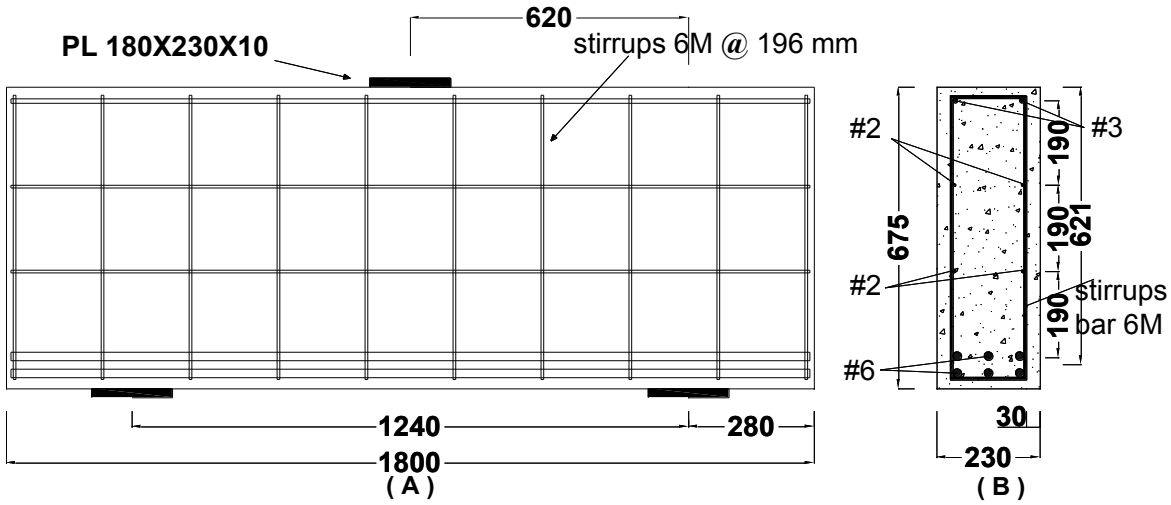

Fig. (3.2) Beam A1/100: (A) elevation (B) cross section

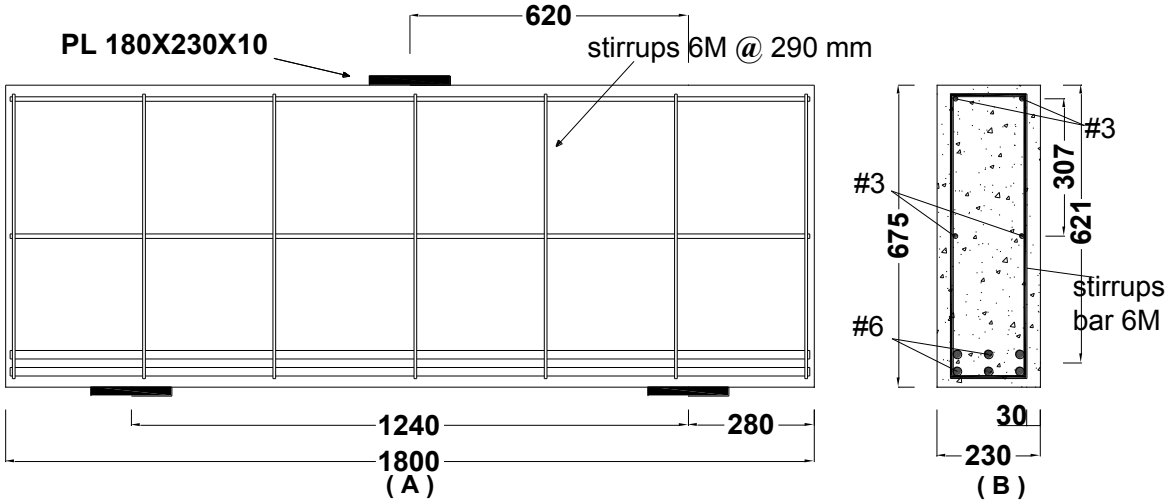

Fig. (3.3) Beam A1/75: (A) elevation (B) cross section

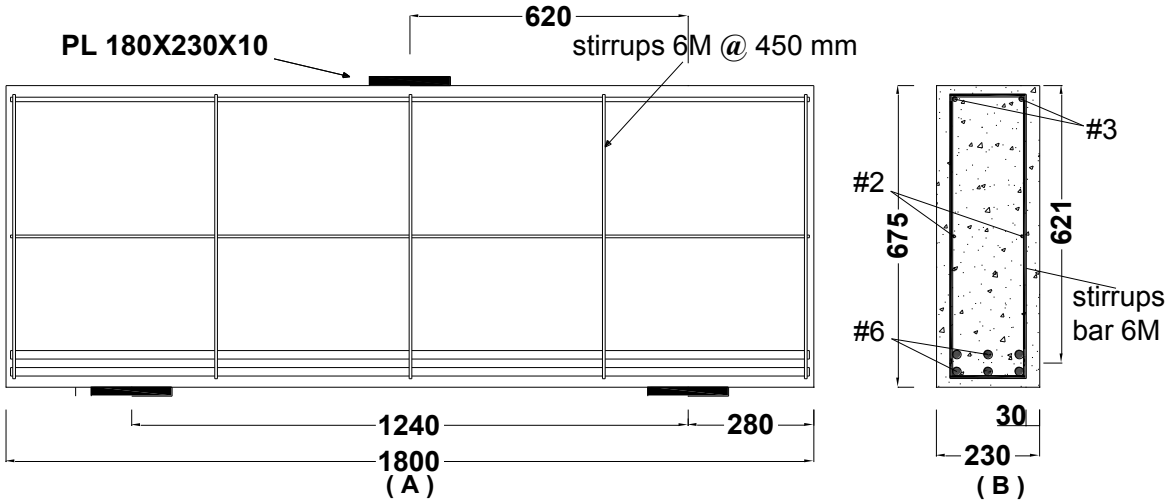

Fig. (3.4) Beam A1/50: (A) elevation (B) cross section

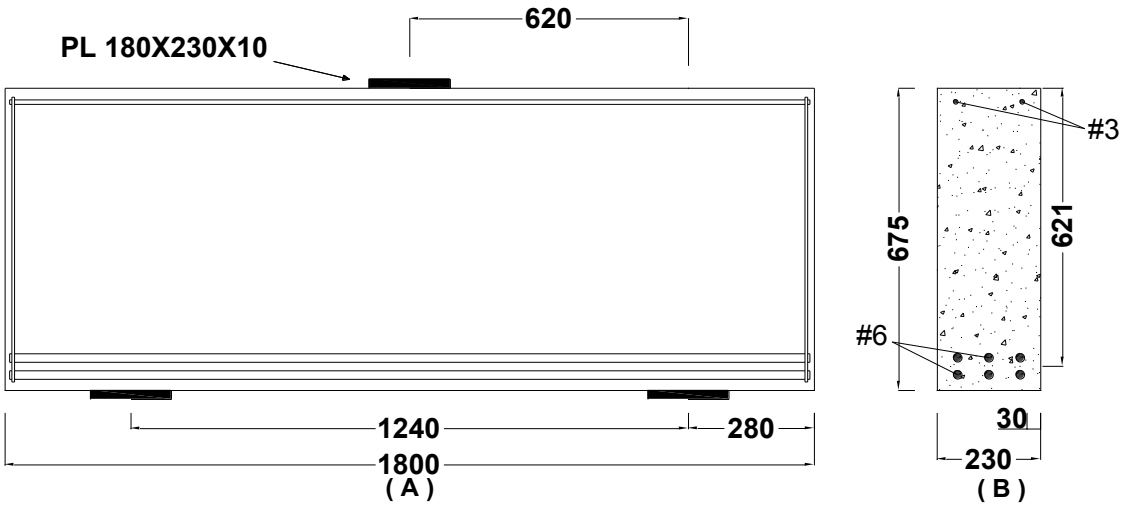

Fig. (3.5) Beam A1/00: (A) elevation (B) cross section

Details of Specimens of Group B:

Full detailing of specimen dimensions and reinforcing are illustrated in Figure (3.6). The beam has a width of 230 mm, also it has effective span (l_e) is 1340 mm while the total length is 1800 mm. The depth, d is 447 mm for the specimen of group (B). The

beam has a longitudinal main FRP reinforcement ratio ρ of 1.201 percent. The longitudinal reinforcement consists of two layers of FRP rebars; three 19-mm diameter bars at the bottom layer, and three 13-mm diameter bars at the upper layer. The vertical web reinforcement consists of pre-fabricated closed-loop FRP stirrups of 6 mm diameter with a spacing *S* of 196 mm. Also one FRP bar with diameter of 6 mm was used in each side of the beam as horizontal web reinforcement.

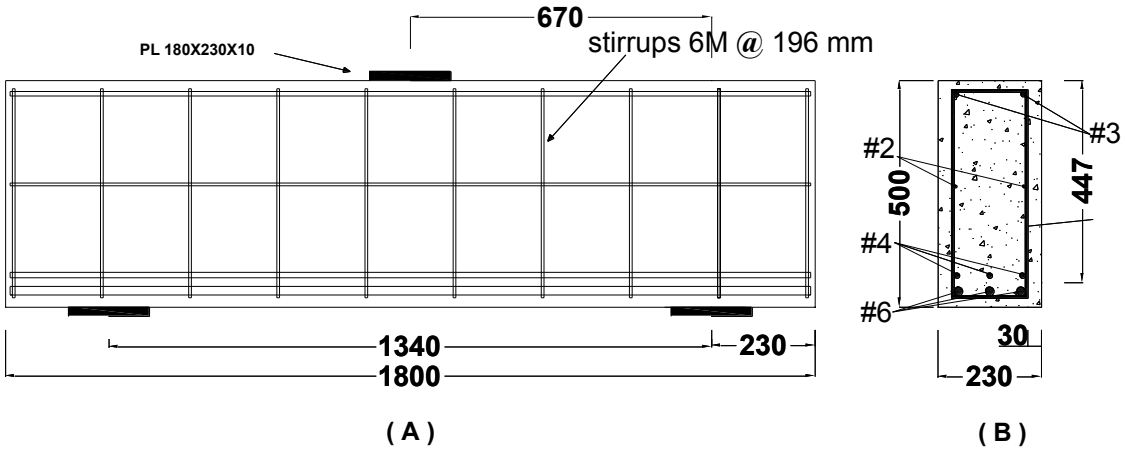

Fig. (3.6) Beam B1.5/100: (A) elevation (B) cross section

Details of Specimens of Group C:

Full details of the specimen dimensions and reinforcements are shown in Figures (3.7) through (3.10). All four beams have a width of 230 mm, the beams have effective span l_e 1310 mm while the total length is 1800 mm. The depth, *d* is 328 mm for the specimens of group (C). Each beam has a longitudinal main FRP reinforcement ratio ρ of 1.00 percent. The specimens of group (C) consisting of two rows of three 13-mm diameter FRP rebars. However, different amount of vertical and horizontal FRP reinforcements was applied to obtain deferent quantities of web reinforcements, ρ_w= 0, 38, 60, and 100 percent for

C2/00, C2/50, C2/75 and C2/100 specimens, respectively. Pre-fabricated closed-loop FRP stirrups of 6 mm diameter are used with a spacing *S* of 175, 290 and 450 mm for C2/100, C2/75 and C2/50 specimens, respectively. Also one FRP bar with diameter of 6 mm in each side at the mid height of the beam was used as horizontal web reinforcement for specimens C2/100 and C2/75.

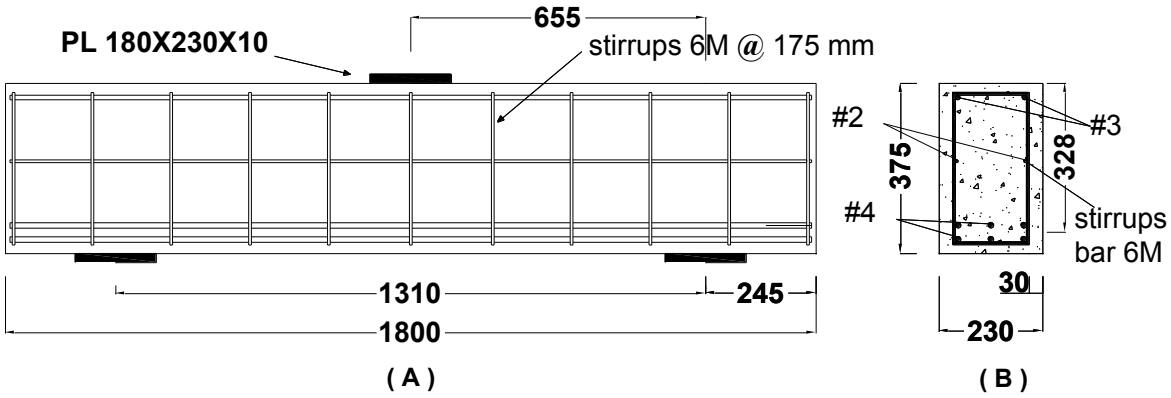

Fig. (3.7) Beam C2/100: (A) elevation (B) cross section

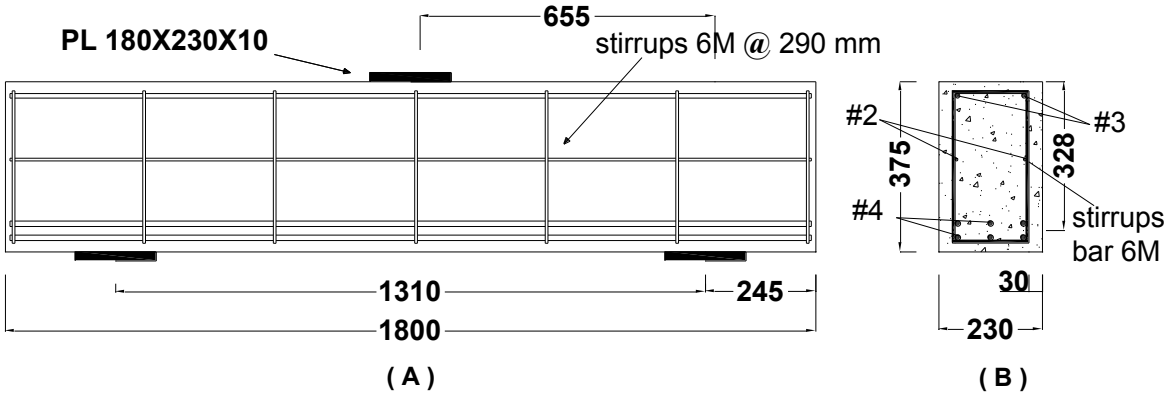

Fig. (3.8) Beam C2/75: (A) elevation (B) cross section

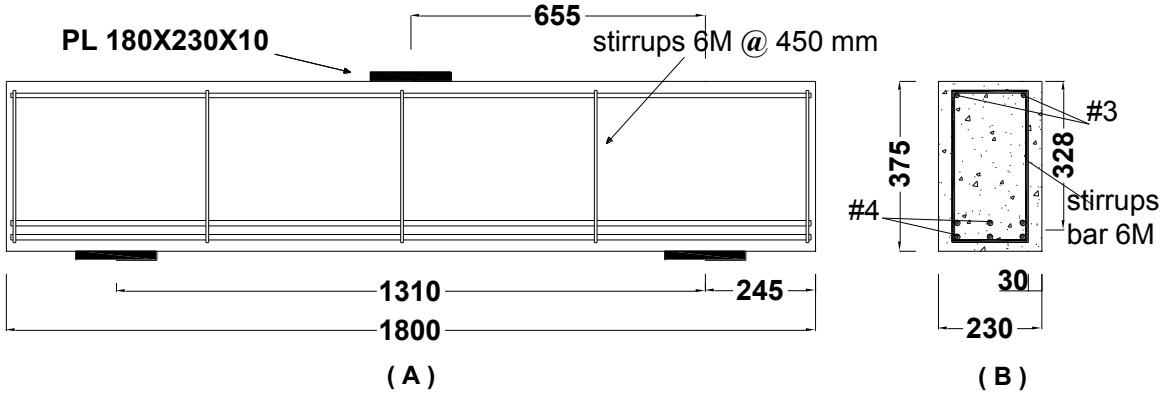

Fig. (3.9) Beam C2/50: (A) elevation (B) cross section

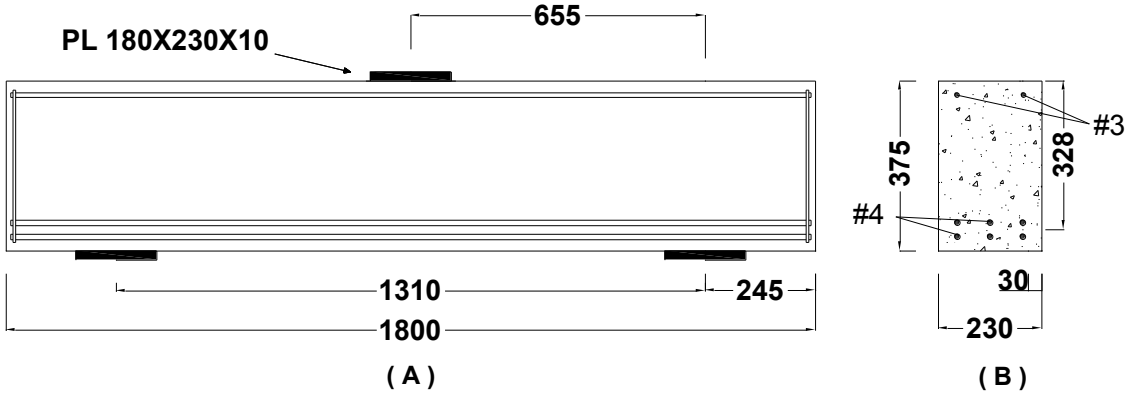

Fig. (3.10) Beam C2/00: (A) elevation (B) cross section

3.4.2. Materials:

Concrete:

A single batch of concrete with a target compressive strength of about 35 MPa supplied by a local ready-mix concrete company was used in the construction of the beam specimens. Table (3.2) describes the details of the concrete mixture used in this study.

During the casting of the beams, eight 100 mm diameter and 200 mm high concrete cylinders were also prepared.

Table (3.2) Concrete mixture details

Concrete mixture	
w/c	0.39
Water, kg/m^3	161.9
Cement type	Type GU
Cement content, kg/m^3	415.0
Fine aggregate content, kg/m^3	875.0
Coarse aggregate size	5-14 mm
Coarse aggregate content, kg/m^3	870.0
Air, %	5-8%
Slump, mm	80±30 mm
Additives	
Micro Air ml/m^3	260.0
Glenlum 7500, ml/m^3	1090.0

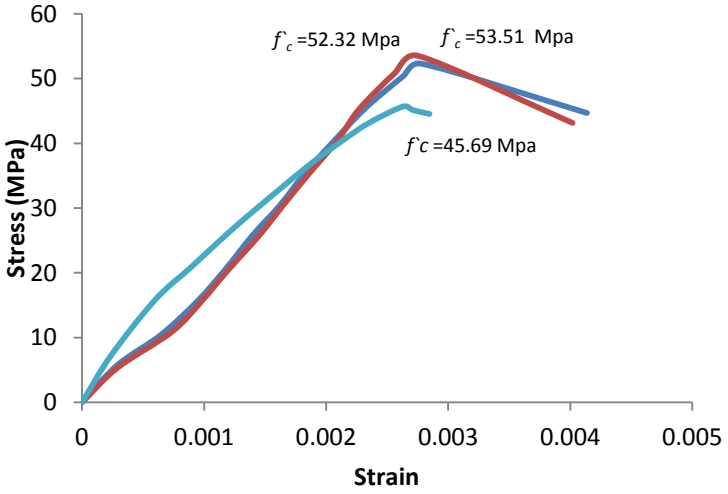

Fig. (3.11) Concrete compressive stress-strain relationship

Fig. (3.12) Compression test of concrete cylinder

The compressive strength was obtained by testing three cylinders according to Canadian standard A23.2-9C-09 [2009] Fig. (3.12). Also two cylinders were tested for the assessment of splitting tensile strength of concrete according to Canadian standard A23.2-13C [2009]. The stress-strain diagram of a few concrete cylinders tested for determining the strength of concrete is presented in Figure (3.11). As can be seen in Figure (3.11), the stress-strain curve consists of two portions: the elastic and the inelastic range. In the elastic range where the transition zone cracks remain stable, the curve is a linear.

Table (3.3) Average concrete strength determined from test cylinders

Age of the sample (days)	f'_c (MPa)	f_t (MPa)
28	45.69	--
60	--	6.55
112	49.61	--
166	52.92	--

The stress-strain plot in the inelastic range becomes non-linear because the cracks begin to propagate. After the ultimate stress is reached, the stress decreases while the

strain grows until the failure occurred. A summary of the concrete strength is provided in Table (3.3). Another three cylinders from the same mix were also tested, one at the beginning and two at the end of the beam tests. A linear relationship between the compressive strength and number of days was developed which has been used to find the actual compressive strength for each beam.

Glass FRP Reinforcement Bars:

Only one type of glass FRP manufactured by Pultrall Inc., Quebec, was used here. The sand coated glass FRP bars were used as flexural reinforcement with following three sizes: No. 10, No. 13, and No. 16. The stirrups were pre-fabricated by manufacturer from sand coated glass FRP bar with size No. 6 according to the dimensions provided based on the design of the specimens. Figure (3.13) shows the stress-strain diagrams of the glass FRP rebars. All the rebars show an elastic phase up to failure point in tension. The characteristics of the glass FRP used in this study are summarized in Table (3.4) according to the data sheet provided by the manufacturer.

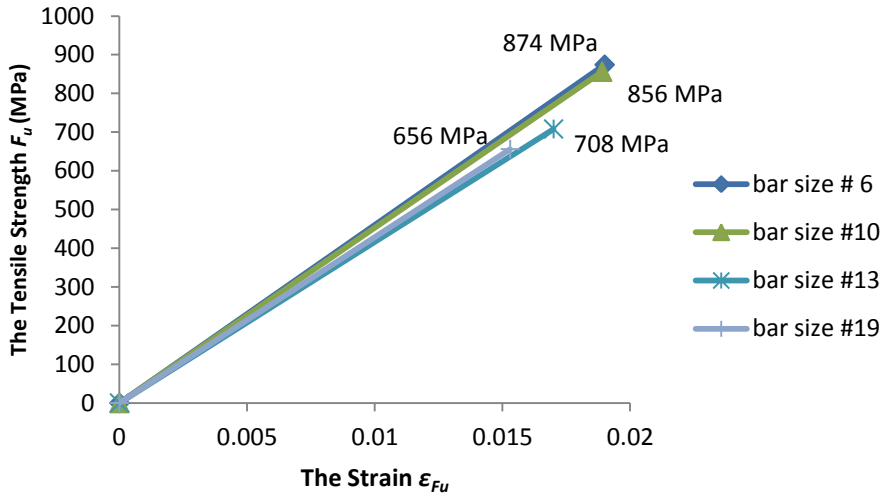

Fig. (3.13) Glass FRP stress-strain relationship

Table (3.4) Manufacture's properties of Glass FRP bars

Soft Metric Size	Diameter (mm)	Area (mm^2)	Tensile Modulus of Elasticity E_t (GPa)	Ultimate Tensile Strength f_u (MPa)	Ultimate Strain in Tension ε_{Fu} (%)	Poisson's Ratio μ
# 6	6.350	31.7	46.1	874	1.90	0.25
#10	9.525	71.3	45.4	856	1.89	0.21
#13	12.700	126.7	46.3	708	1.70	0.26
#19	19.050	285	47.6	656	1.53	0.25

3.4.3. Instrumentation:

External instrumentation for each beam consists of two linear potentiometers located at the mid-span to record the beam deflection; where one potentiometer was connected on each side of the beam to measure the differential displacement of the both sides during the test. The full stroke range (F.S) of the potentiometers was 635 mm with accuracy of 0.25% of F.S. Three uniaxial strain gauges of model KFG-10-120-C1-11 with 10 mm length were bonded on the longitudinal bars at the mid-span. Also the same type of uniaxial strain gauge was bonded on both ends of the longitudinal bars in each beam. The FRP web reinforcements on both sides of a beam at critical section were instrumented with Kyowa Model KFG-2-120-C1-11 Uniaxial strain gauges with 2 mm length. The instruments at the installation phase and their locations on the FRP are illustrated in Figures (3.14) and (3.15).

Fig. (3.14) The installation phase of strain gages in specimen A1/50.

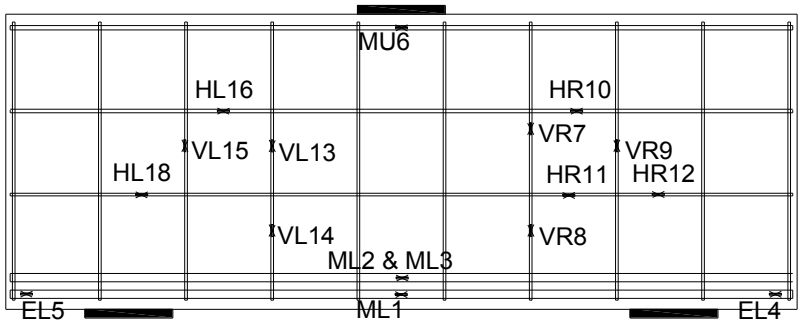

Fig. (3.15-a) The location of strain gages for specimen A1/100.

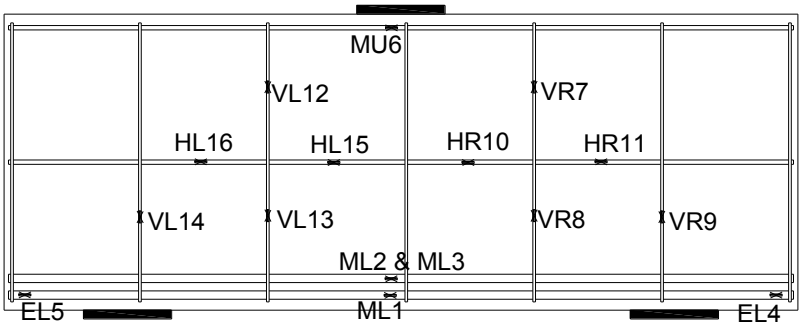

Fig. (3.15-b) The location of strain gages for specimen A1/75.

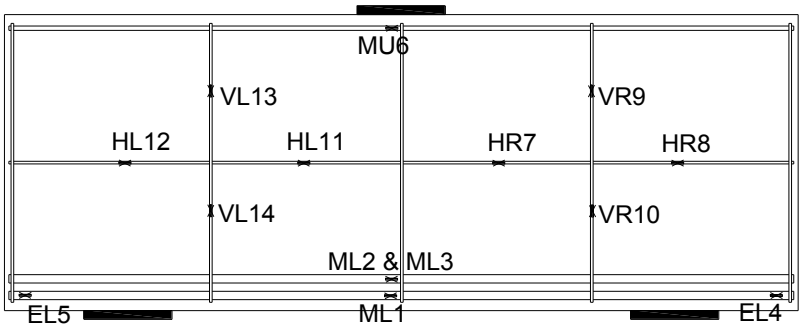

Fig. (3.15-c) The location of strain gages for specimen A1/50.

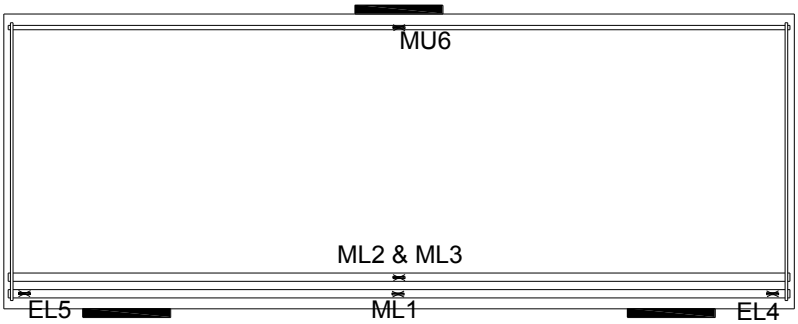

Fig. (3.15-d) The location of strain gages for specimen A1/00.

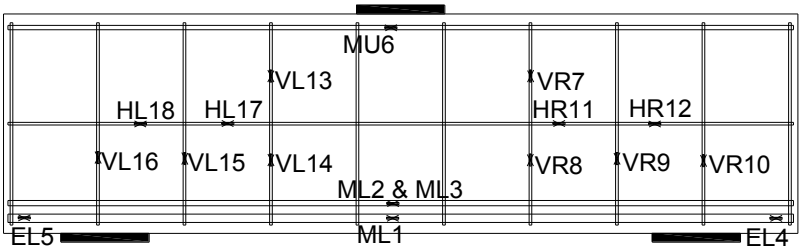

Fig. (3.15-e) The location of strain gages for specimen B1.5/100.

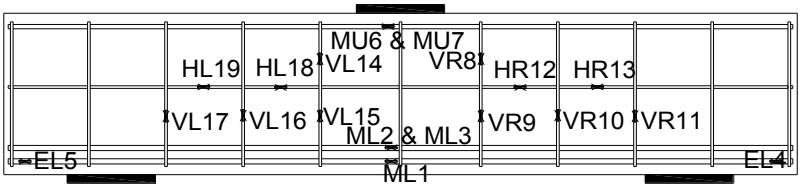

Fig. (3.15-f) The location of strain gages for specimen C2/100.

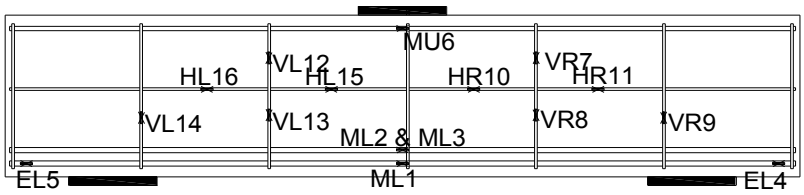

Fig. (3.15-g) The location of strain gages for specimen C2/75.

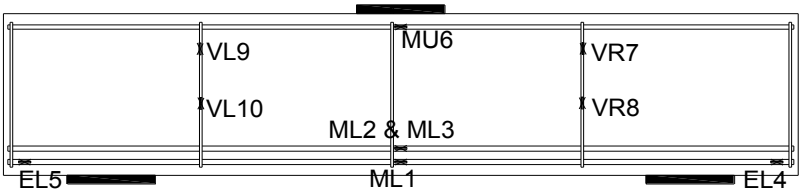

Fig. (3.15-h) The location of strain gages for specimen C2/50.

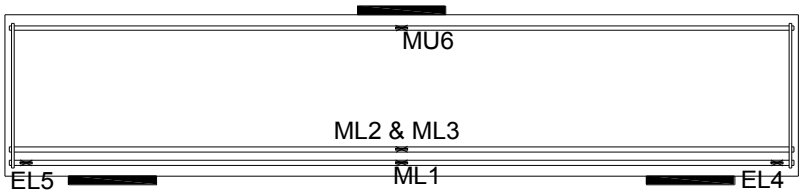

Fig. (3.15-i) The location of strain gages for specimen C2/00.

3.4.4. Fabrication and Casting of Beams:

Wood forms were used in the fabrication of the beams. The inside of the forms was painted before the reinforcement cage was placed in its position to prevent the wood from absorbing the water of the concrete mixture. The concrete mix was then placed and vibrated using electrical vibrator. Next day of casting, the beams were covered with damp canvas. The canvas was watered once daily for 14 days. The formwork was removed after 35 days after the day of casting as shown in Figure (3.16).

Fig. (3.16) The stages of specimen preparation during and after the concrete casting.

3.4.5. Test Procedure:

All the specimens were simply supported as shown in Figures (3.17) and (3.18). All the beams were tested to failure under three-point loading (i.e. one concentrated vertical load at the mid-span). Steel roller restrained in the horizontal direction was used to ensure that only the concentrated load would be applied at the loading point. A 2000 kN capacity actuator was used to apply the load at the top of the mid span of the specimens. Steel plates were placed at the point load and the support location. The bearing plates with the dimensions of 180 mm length x 230 mm width x30 mm height were attached by plaster paste at the loading point and at the supports to obtain uniform contact and to prevent the plates from slipping. To reduce the possibility of a stability failure, the centralization of the beam position and its vertical alignment were verified during the erecting process. Both surfaces of the beam were painted white and with grids to monitor the crack development during the test.

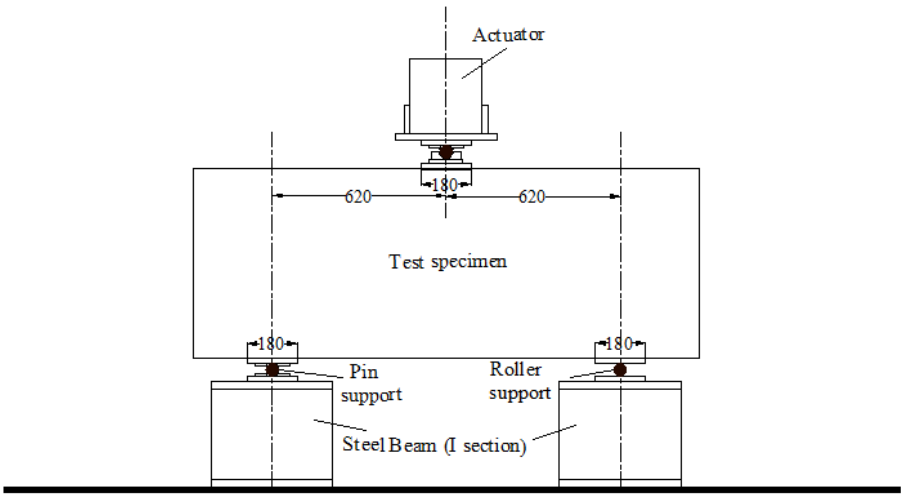

Fig. (3.17) Typical test setup for any beam in group A

All wiring of strain and deflection gauges was connected to the data acquisition system and initialized to zero. Throughout the test procedure, the load capacity, FRP strain and mid-span deflection data at each load increment was recorded. Measurements were taken at half-second intervals. Global information, obtained from the data acquisition system, photographs and recorded observations, were utilized to interpret the results of each test. The average time to beam failure was approximately 28, 24 and 16 minutes for beams in group A, B and C, respectively. The load was applied at a rate according to C293-08 of the ASTM standards - Section 4 - Construction [2013]. The loading rate for flexural test of simply-supported concrete beams with center-point loading in the ASTM standards should be constant and calculating as followed:

$$r = 2S\,h\,d^2 / 3l \qquad (3.13)$$

where r is the loading rate (N/min), S is the rate of increase in the maximum stress on the tension face (0.9-1.2 MPa/min), b is the average width (mm), h is the average depth (mm) and l is the effective length (mm). Table (3.5) shows the minimum and the maximum of the loading rate that should be applied to the beams in group A, B and C according to the Equation (3.4).

Table (3.5) The loading rate of the beams in group A, B and C

Specimens	The loading rate	
	Min (kN/sec)	Max (kN/sec)
Group A	0.72	0.95
Group B	0.34	0.46
Group C	0.19	0.25

A constant rate of load was applied with rate of 0.36, 0.49, 0.87 and 0.93 kN/sec for the specimens in the group A: A1/00, A1/50, A1/75 and A1/100, respectively. While the loading rate of the beam B1.5/100 was 0.43kN/sec. the specimens in group C: C2/00, C2/50, C2/75 and C2/100 were loaded up to failure with loading rate of 0.16, 0.23, 0.21 and 0.25kN/sec, respectively. While the loading rate is consistent with that suggested in the relevant ASTM standard for most of the tested specimens, it was smaller in the cases of A1/00 and A1/50 because of the manual control of loading. However, the lower rate of loading for these two specimens was not expected to affect the behaviour of the beams which was later conformed form the results of the tests.

Fig. (3.18) The test arrangement for beam A1/100

3.5. Objective of the Experimental Program:

The objective of the experimental program was to measure the strain distribution, as well as to monitor the load-deflection response. Also to study the structural behaviour of FRP reinforced concrete deep beams by using the experimental data. The test beams were designed with sufficient width to avoid the effect of lateral buckling. Beams were also designed with and without stirrups for a different shear span-to-depth ratio *a/d* to determine their effect on the deep beam behaviour and its failure modes. The experimental results are to be used to validate the proposed and current design methods for FRP-reinforced concrete deep beams and suggest suitable modifications, if required.

Chapter 4: Comparison of the Different Design Provisions for Conventional Deep Beams

4.1. Introduction:

A set of 347 experimental test results have been gathered from the literature and used here to evaluate and compare the Strut-and-Tie modeling provisions of the codes from three different jurisdictions: Canada, USA and Europe. The effect of the governing variables such as the shear-depth to span ratio, web reinforcement and the compressive strength of concrete on the capacity predicted by the Strut–and-Tie model (STM) provisions of the codes have also been investigated. Also the predictions of failure occurrence in deep beams as determined using the models have been examined. The Canadian code (CSA A23.3-04) is found to provide the most efficient and robust procedures for estimating the ultimate capacity of reinforced concrete deep beams using the strut and tie model. The study also indicates that none of the selected codes provide adequate procedures to determine the location and mode of failure accurately and reliably as compared to the experimental results.

4.2. Calculating the capacity using the STM procedures:

The geometry of the strut and tie model is determined by calculating the maximum lever arm, which is determined by balancing the internal compressive forces *C* and tensile forces *T* in steel, for example. In the Canadian code, the height of the bottom node is assumed to be 1.13 times the height of the top node and is obtained by dividing the compressive stress of the CCT node by the compressive stress of the CCC. The

multiplication factors are 1.25 and 1.34 for both the ACI and the Eurocode, respectively. Figure (4.1) shows the strut and tie model of a beam loaded by a single point load.

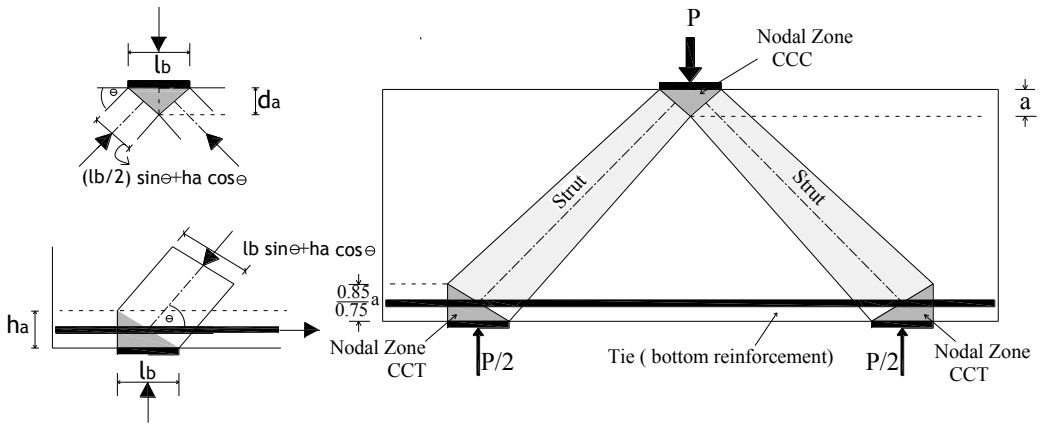

Fig. (4.1) Description of strut and tie model

Thus, based on the geometry of the truss, the dimension of all struts, nodes and ties can be calculated. From the truss geometry and the dimensions of the nodes and beam member, the strut angles "θ" can be determined and compared with the allowable minimum strut angle. If the calculated angle exceeds the limit, the geometry will be modified according to the modified angle. Based on this manipulation, all the possibilities of the applied loads and the resulting forces in each element can be determined using the provisions of each code.

The maximum applied load (i.e. failure load) can be determined from the strength of the weakest element. The calculation covered five different categories. The ACI cases have been divided into two types based on the strut shape. ACI represents the strut with a uniform cross section and the bottle-shaped struts, for which the efficiency factor β_s is different from the efficiency factor of the uniform strut. There is also Euro Option-2, which is similar to the procedure provided in the Eurocode with modifying the prediction

of the ultimate shear force by multiplying this value by $\beta = a/2d$. Additionally, the ultimate shear forces are calculated by using the Canadian code and Eurocode Option-1 without any adjustment. An example of application of the STM provisions in the Canadian code (CSA- A23.3-04) is given in Appendix-A.

4.3. Comparison between the Strut-and-Tie model and the traditional (sectional) beam theory:

Figure (4.2) shows a comparison between the Strut-and-Tie model and the traditional (sectional) beam theory in predicting the dimensionless shear stress capacity (v) of beams as a function of the a/d ratio. To illustrate this comparison, the dimensionless shear stress value is calculated as follows:

$$v = V_{calc}/bdf'_c \qquad (4.1)$$

where, b is the beam width; d is the effective depth; and f'_c is the concrete compressive strength. The results shown in Figure (4.2) confirm the influence of this factor on the specimens with a/d less than or equal to two, where the specimens with small shear span-to-depth ratio has higher shear strength. And the results also emphasize the efficiency of the Strut and Tie model in designing deep beams. In addition, it can be seen that for $a/d<3$, the sectional model (i.e. traditional beam theory) in the provisions of any of the selected codes, does not provide an accurate estimate of capacity. In this case, the STM model, especially with the provisions of the Canadian code (CSA-A23-3-04[2004]), provides a very good estimate of the capacity when compared to the experimental results.

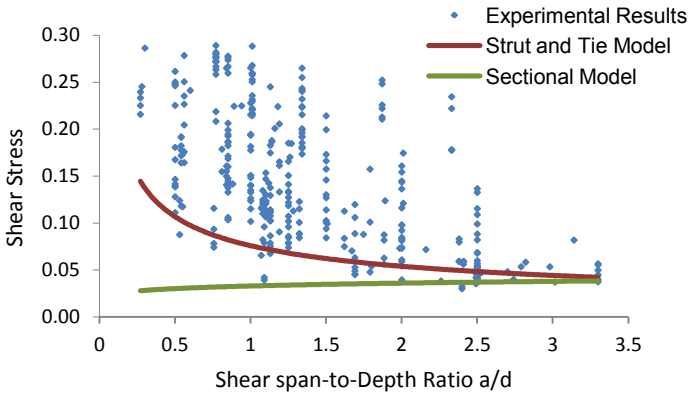

a.)

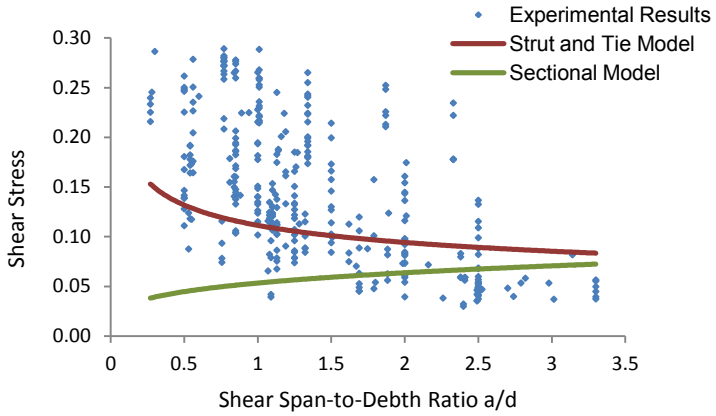

b.)

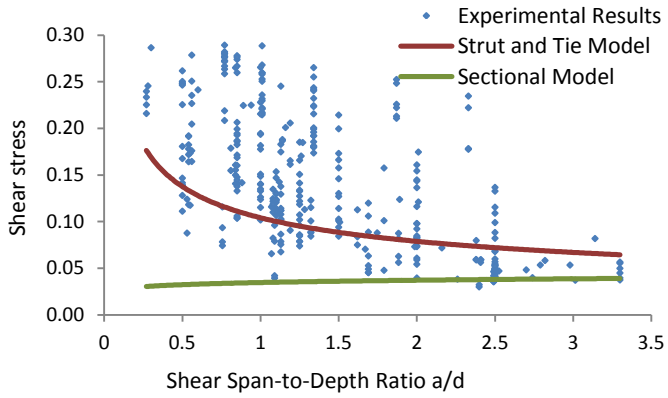

c.)

Fig. (4.2) Use of strut and tie model and sectional mode to predict the strengths of a series of beams l: a.) Canadian code (A23.3-04); b.) Eurocode (EN 1992-1-1-2004E), and c.) ACI code (ACI 318-08).

The prediction of the capacity from the Canadian code is conservative as compared to that obtained using the other two codes. It should be noted that the provisions for determining the capacity using the sectional model varies slightly from one code to another, as evident from Figure (4.2).

4.4. The codes prediction of ultimate shear strength of deep beams:

Figure (4.3) shows the percentage of samples for which the ratio of the predicted shear strength calculated using the code provisions (V_{calc}) to the actual shear strength from the experimental results (V_{exp}) is lower than 1 indicating that V_{calc} is conservative. Those results come from all the experimental specimens, including those that are not covered by the provisions of the codes, such as the specifications of web reinforcements and the strength of concrete.

Based on the results, it is found that the Canadian code provides the most conservative provisions with an average of 89.34% of the test specimens have higher capacity than that provided in the code, while just a 66.28% and 68.01% of the total specimens exceed the capacity predicted using the ACI and the Eurocode Option-1 respectively. Also the results as shown in Fig. (4.3) indicate a noticeable improvement when Eurocode Option-2 is used and the percentage increased to 79.54%. The results of ACI improve only by 12.11% when bottle-shaped struts are used instead of uniform cross section struts.

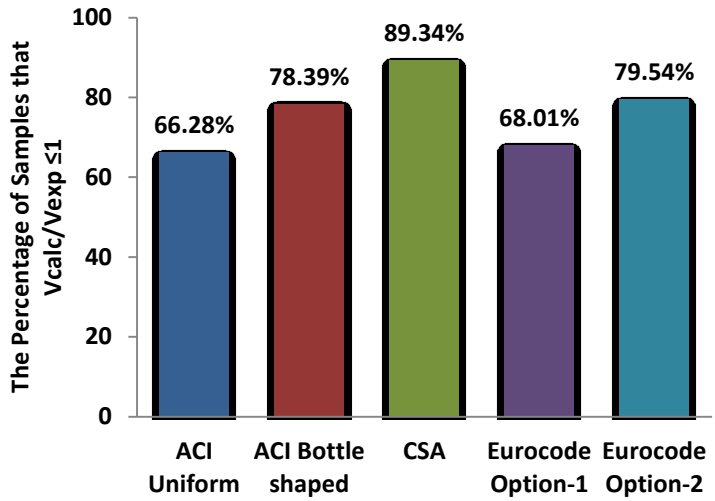

Fig. (4.3) The percentage of samples that $V_{calc}/V_{exp} \leq 1$ for all specimens

4.5. Comparison between the nominal and factored capacity of shear strength of deep beams calculated by using the code provisions:

The plot in Figure (4.4) shows a comparison between the nominal and factored shear strength capacity calculated using the code provisions ($\boldsymbol{V_{calc}}$). The comparison was done based on the percentage of samples for which the ratio of the nominal and factored capacity calculated using the provisions of the three codes ($\boldsymbol{V_{calc}}$) to the actual shear strength from the experimental results ($\boldsymbol{V_{exp}}$). The results contain only the experimental specimens that have shear span-to depth ratio less than 2.5. The results show that the factored capacities calculated by using the Canadian code provides the most consistent results with an average of 90.99% and 77.48% of the test specimens having higher capacity than the capacity calculated using the code provisions considering the factored and nominal strengths, respectively. In calculating the factored capacity, the resistance factor of the material ϕ was taken as 0.65 for the concrete and 0.85 for reinforcing bars.

The nominal capacities of the beams were found to be approximately 14% higher than the corresponding factored capacities. The predicted capacity by using the nominal strength of the STM in the Canadian code was found to be scattered with mean value of V_{calc}/V_{exp} as 0.81, standard of deviation (SD) of 0.40 and coefficient of variation (COV) of 0.49. Considering these results, the Canadian code can be said to provide a conservative estimate to predict the ultimate strength. When the factored strength is used in the STM in the Canadian code, the results were quite conservative and scattered with mean values of 0.59, SD of 0.26 and COV of 0.44.The mean, SD and COV of the result predictions of the three codes are presented in the table (4.1).

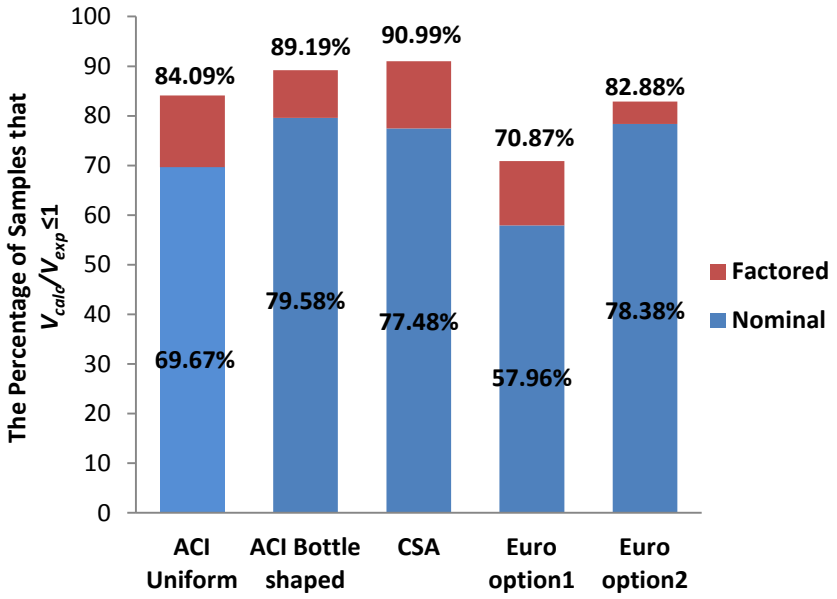

Fig. (4.4) The percentage of samples that $V_{calc}/V_{exp} \leq 1$ for all specimens

Although the ACI code applied a constant reduction factor for factored force in the all elements of the STM (struts, ties, and nodal zones), the improvement in the percentage of the prediction by using uniform strut in the ACI code for the factor force was higher than

that in the case of bottle shaped strut. In other words, these results indicate that the decrease in the nominal force by about 25% enhanced the conservativeness of the ACI provisions with uniform strut by passing 84.09% of the specimens instead of 69.67%. On the other hand, the prediction of the ACI provisions with bottle shaped strut was improved only by 9.61%, in which case 89.19% of the test specimens had higher capacity than that calculated using the code provision. The mean, SD and COV of V_{calc}/V_{exp} using ACI uniform strut was found to be 0.92, 0.49 and 0.53, respectively. For V_{calc}/V_{exp} using the bottle shaped strut, the mean, SD and COV were found to be 0.78, 0.41 and 0.52, respectively. These values in the two procedures of the ACI decreased after using the factor strength of the STM, where the mean value of V_{calc}/V_{exp} becomes 0.73 and 0.62 for uniform and bottle shaped struts, respectively. The result also indicated that the factored capacity calculated using the bottle shaped strut provided more conservative estimate than that using uniform strut.

Table (4.1). Statistical analysis of the prediction of the ultimate shear strength by different codes (V_{calc}/V_{exp})

Shear Strength		ACI Uniform	ACI Bottle shaped	CSA	Euro option1	Euro option2
Nominal	Mean	0.92	0.78	0.81	1.03	0.76
	Standard Deviation (SD)	0.49	0.41	0.40	0.44	0.51
	coefficient of variation(COV)	0.53	0.52	0.49	0.42	0.67
Factored	Mean	0.73	0.62	0.59	0.93	0.68
	Standard Deviation (SD)	0.35	0.27	0.26	0.45	0.50
	coefficient of variation(COV)	0.48	0.44	0.44	0.49	0.74

The results as shown in Figure (4.4) indicate a noticeable improvement when Eurocode Option-2 for nominal strength is used and the percentage increased to 78.38% comparing to Eurocode Option-1. Although the two options of the Eruocode applied a similar reduction factor for concrete to calculate the factored force, the Eruocode Option-1 improves up to 12.91% while the Eruocode Option-2 improves only 4.50% and becomes 82.88% of the test specimens having higher capacity than that provided in the code. The least improvement in the prediction of the shear strength is found in the Eruocode Option-2 after using factor strength. This variation between the two options of the Eurocode clearly appeared in Table (4.1) where Eurocode Option-1 produces the mean value of V_{calc}/V_{exp} as1.03 with SD of 0.44 for nominal strength which shows a slight overestimation of the shear strength; and for the mean value of V_{calc}/V_{exp} and SD are found to be 0.93 and 0.45, respectively for factored strength.

4.6. The effect of web reinforcement on the code predictions of the ultimate strength:

To study the effect of web reinforcement on the ultimate shear strength and on that estimated by using the code provisions, the samples from the database of available experimental results (Table 2-2) as compiled in this study have been divided into four groups depending on the distribution of web reinforcement. In this case the following groups are formed: (1) the samples that have vertical and horizontal web reinforcements are referred to as “only web”; (2) samples having web reinforcements in the vertical direction only are referred to as “only vertical”; (3) samples having web reinforcement in the horizontal direction only are referred to as “only horizontal”; and (4) the samples without any web reinforcement are referred to as “without web”. Figure (4.5) shows the

percentage of samples that have ($\boldsymbol{V_{calc}/V_{exp} \leq 1}$) for the above four groups. The only variable taken into consideration in producing the results shown in Figure (4.5) is the distribution of web reinforcement regardless of the shear-span to depth ratio and the compressive strength of concrete. When using Eurocode Option-1 or ACI (uniform strut) for determining the shear strength capacities of the available samples with web reinforcement, 86.52% and 87.23% samples, respectively, have been found to have $V_{calc}/V_{exp} \leq 1$ (Fig. (4.5)).

Using the bottle-shaped strut instead of the uniform strut section, the results are found to be improved to 96.45%. Similar improvement in the V_{calc}/V_{exp} ratio is obtained using Eurocode Option-2 in which case 97.87% of the samples are found to have a capacity higher than the predicted capacity using the code procedure (i.e., $V_{calc}/V_{exp} \leq 1$). In the case of the Canadian code provisions, 98.58% of the samples are found to have $V_{calc}/V_{exp} \leq 1$, indicating that the CSA procedure yields the most conservative estimate of the shear strength capacity of concrete deep beams with web reinforcements.

From Figure (4.5) it is observed that, in the case of concrete deep beams with only vertical or horizontal web-reinforcements, and also in the case of no web-reinforcements, the Canadian code provisions still yield conservative estimates the shear strength capacity as compared to the other code provisions. The mean, SD and COV of the estimated ultimate shear strength by different codes considering the effect of web reinforcement are presented in the Table (4-2). The predictions by using the Canadian code for specimens with web reinforcement scattered with mean values of V_{calc}/V_{exp} as 0.52, SD of 0.18 and COV of 0.34. The mean value of V_{calc}/V_{exp}, SD and COV considering the nominal strength for the ACI uniform strut are found to be 0.77, 0.23 and 0.21, respectively.

While using the bottle shaped strut, the mean, SD and COV are found to be 0.71, 0.21 and 0.30, respectively. The mean (V_{calc}/V_{exp}), SD and COV of the predictions by using the Eruocode Option-1 are obtained as 0.77, 0.23 and 0.30, respectively. With Eruocode Option-2 the estimated V_{calc}/V_{exp} is found to be lower and scattered with mean value of 0.48, SD of 0.20 and COV of 0.42.

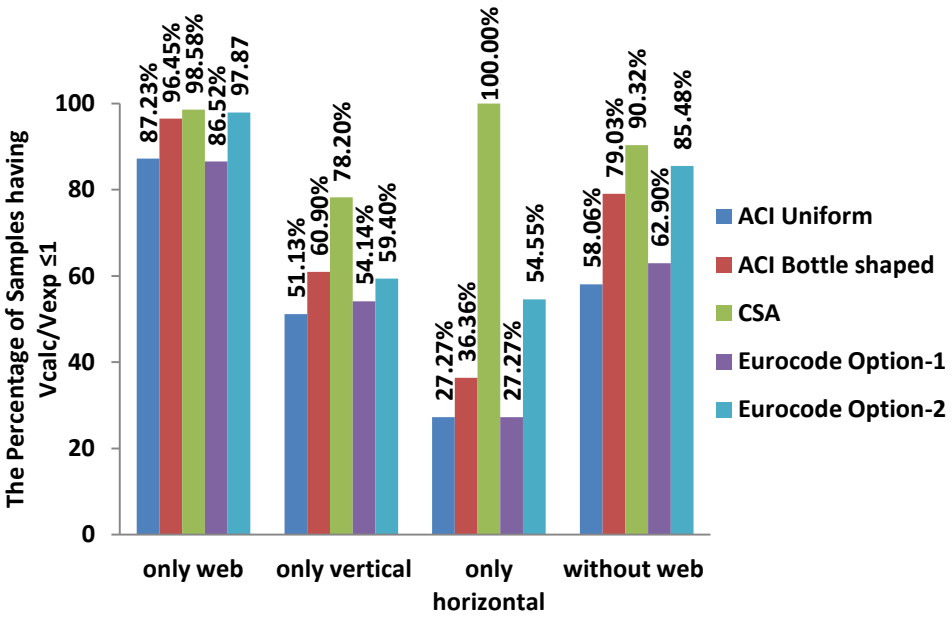

Fig. (4.5) The percentage of samples having $V_{calc}/V_{exp} \leq 1$ considering the effect of web reinforcement

Eruocode Option-2 and ACI bottle shaped strut provided less conservative estimate of the ultimate shear strength as compared to Eruocode Option-1 and ACI uniform strut. ACI uniform and Eurocode Option-1 produces more conservative results, especially in the cases when vertical or horizontal web reinforcement are used (Figure 4.5). The Canadian code is found to provide the most conservative estimate of the ultimate strength considering the available experimental results.

Table (4.2). Statistical analysis of the prediction of the ultimate shear strength by different codes considering the effect of web reinforcement

Distribution of the web reinforcement		ACI Uniform	ACI Bottle shaped	CSA	Eurocode option-1	Eurocode option-2
only web	Mean	0.77	0.71	0.52	0.77	0.48
	Standard Deviation (SD)	0.23	0.21	0.18	0.23	0.20
	coefficient of variation(COV)	0.30	0.29	0.34	0.30	0.42
only vertical	Mean	1.02	0.85	0.65	0.94	0.80
	Standard Deviation (SD)	0.58	0.48	0.31	0.60	0.64
	coefficient of variation(COV)	0.57	0.56	0.48	0.64	0.80
only horizontal	Mean	1.22	1.18	0.67	1.23	0.82
	Standard Deviation (SD)	0.44	0.41	0.16	0.48	0.51
	coefficient of variation(COV)	0.36	0.35	0.25	0.39	0.62
without web	Mean	0.95	0.74	0.61	0.86	0.52
	Standard Deviation (SD)	0.40	0.38	0.27	0.42	0.36
	coefficient of variation(COV)	0.42	0.51	0.44	0.49	0.69

Figures (4.6) and (4.7) show the effect of the web reinforcement with respect to the compressive strength of concrete. As can be observed from the figures, the provisions of all three codes yield conservative results when the compressive strength is equal to or less than 40 MPa. With the ACI bottle-shaped strut, fewer than 5% of the samples exhibit the actual capacities to be less than the predicted capacities calculated using the code provisions (Figure (4.6)), which is contrary to the findings of Michael and Oguzhan [2007].

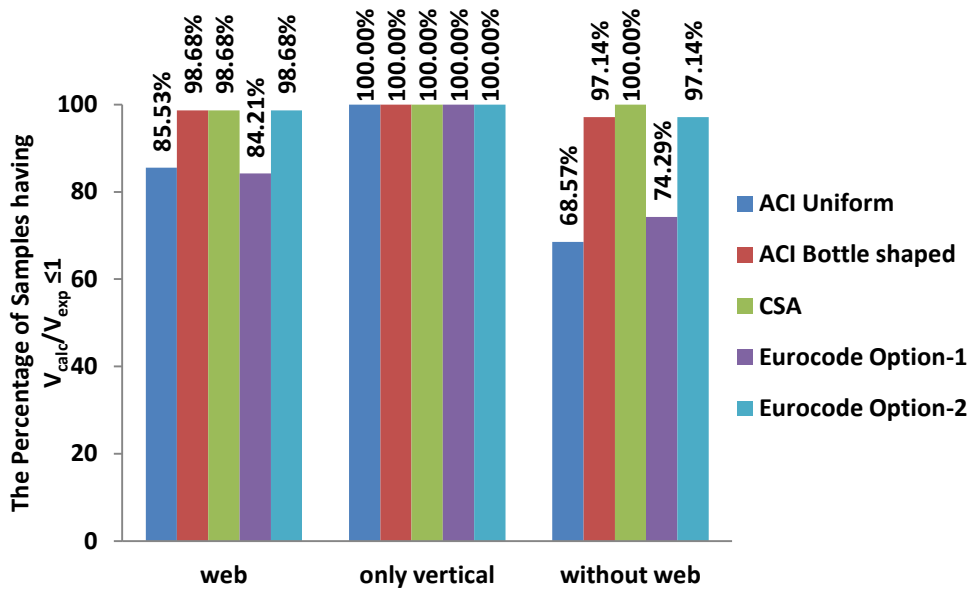

Fig. (4.6) The percentage of samples having $V_{calc}/V_{exp} \leq 1$
(for specimens with $f`c \leq 40$ MPa)

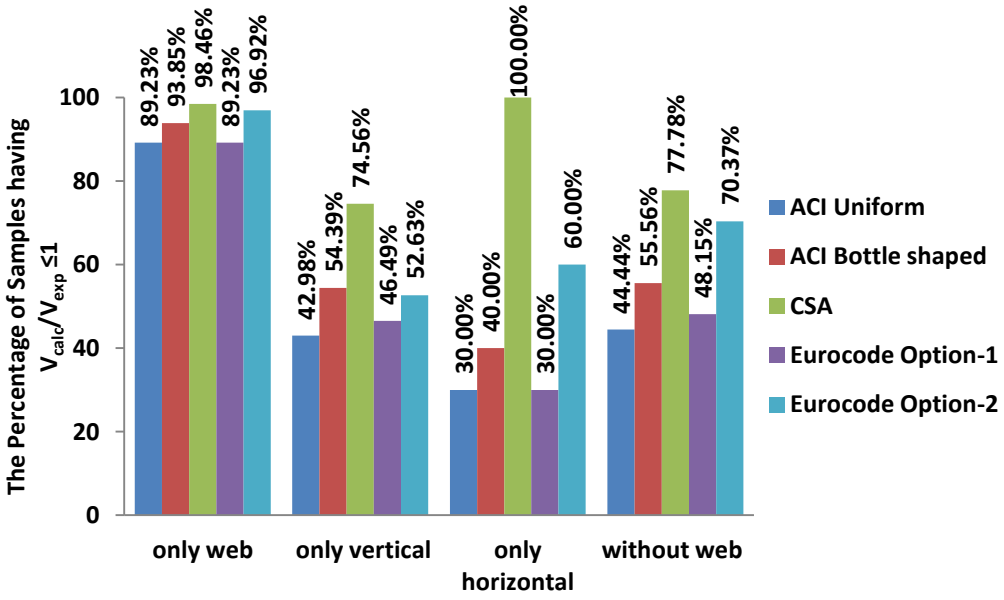

Fig. (4.7) The percentage of samples having $V_{calc}/V_{exp} \leq 1$
(for specimens with $f`c > 40$ MPa)

For high-strength concrete samples where the compressive strength of concrete is assumed to be equal to or more than 40 MPa, the results are very conservative. In this

case, Eurocode Option-2, the ACI bottle-shaped strut and the CSA code produce a conservative estimate of capacity for 96.92%, 93.85%, and 98.46% of the samples, respectively (Figure (4.7)).

4.7. The effect of shear-span to depth ratio on the code predictions of the ultimate strength:

To study the effect of the shear-span to depth ratio on the code provisions in predicting the ultimate strength, the samples of the experimental results are divided into four categories. The beam samples grouped according to the *a/d* ratio, as follows: (1) specimens having ($a/d \leq 1$), (2) specimens having ($1<a/d \leq 2$), (3) specimens having ($2<a/d \leq 2.5$), and (4) specimens having ($a/d > 2.5$). For the available experimental specimens having ($a/d \leq 1$), the capacity estimated by using the code provisions is found to be conservative as compared to the actual capacity.

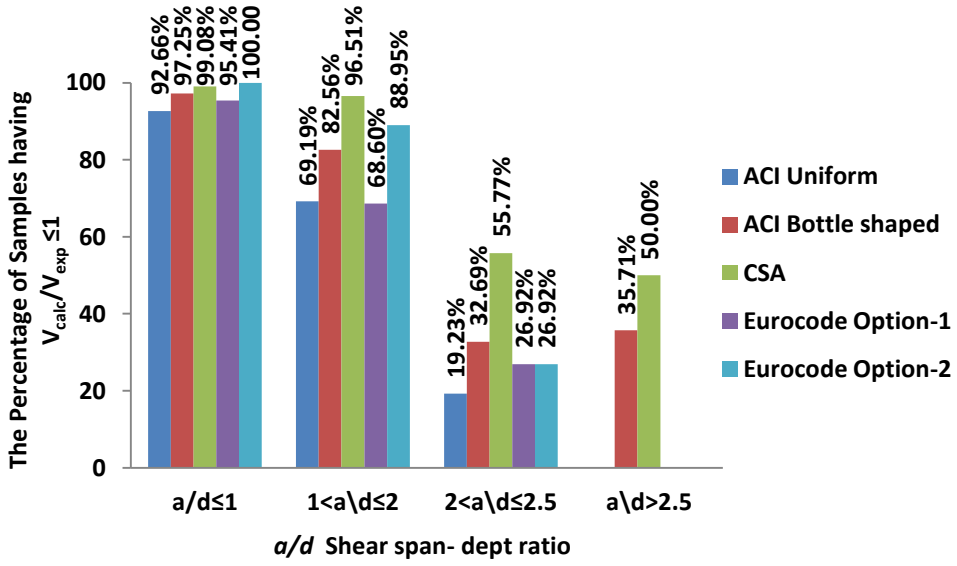

Fig. (4.8) The percentage of samples having $V_{calc}/V_{exp} \leq 1$ considering a/d ratio

As observed in Fig. (4.8), the code provisions, especially the Eurocode Option-2 and the Canadian Code underestimate the capacity for 100% and 99.08% of the samples,

respectively. The best results for the specimens with an *a/d* ranging between 1 and 2 are represented by the Canadian provisions, with 96.51% of the specimens having a higher capacity than that predicted using the code provisions (Fig. (4.8)).

For the specimens with ($a/d > 2$), the capacity predicted using the code provisions is not conservative in many cases (Figure (4.8)). The capacity of 50% of the samples is overestimated using the provisions of the Canadian code when the *a/d* ratio is higher than 2.5, whereas the provisions of the other codes produce even worse results, as shown in Figure (4.8). The above results indicate that the STMs available in the selected codes are not applicable when ($a/d > 2$).

Table (4.3) compares between the mean, the standard of deviation and the coefficient of variation of the predictions of the ultimate shear strength, V_{calc}/V_{exp} by different codes considering the effect of shear span-to-depth ratio. The predictions by using the STM in the Canadian code for beams with $a/d \leq 1$ and $1 < a/d \leq 2$ were almost similar with mean values of V_{calc}/V_{exp} as 0.57 and 0.52, SD of 0.21 and 0.20 and COV of 0.37 and 0.39, respectively. On the other hand, for beams with $2 < a/d \leq 2.5$ and $a/d \geq 2.5$, the predictions by using the STM in the Canadian code produced the mean values of V_{calc}/V_{exp} as 0.87 and 0.79, SD of 0.37 and 0.35 and COV of 0.42 and 0.44, respectively.

The higher standard deviation indicates higher scatter in the predicted values (using the code provisions) of the ultimate strength of the beams with shear span-to-depth ratio higher than two, as shown in Figure (4.8). The bottle shaped strut provides a lower mean value of V_{calc}/V_{exp} and SD as compared to the ACI uniform strut to predict the ultimate strength of the beams $a/d \leq 1$ and $1 < a/d \leq 2$ which shows an increased number of the test

specimens having higher capacity than that provided by ACI bottle shaped strut (Figure 4.8).

Table (4.3). Statistical analysis of the prediction of the ultimate shear strength by different codes considering the effect of shear span-to-depth ratio

Shear span-to-depth ratio		ACI Uniform	ACI Bottle shaped	CSA	Eurocode option-1	Eurocode option-2
a/d≤1	Mean	0.76	0.69	0.57	0.68	0.37
	Standard Deviation (SD)	0.26	0.26	0.21	0.23	0.21
	coefficient of variation(COV)	0.35	0.38	0.37	0.34	0.56
1<a/d≤2	Mean	0.88	0.75	0.52	0.87	0.60
	Standard Deviation (SD)	0.40	0.36	0.20	0.43	0.35
	coefficient of variation(COV)	0.45	0.47	0.39	0.50	0.59
2<a/d≤2.5	Mean	1.44	1.12	0.87	1.29	1.29
	Standard Deviation (SD)	0.64	0.53	0.37	0.70	0.70
	coefficient of variation(COV)	0.45	0.48	0.42	0.54	0.54
a/d≥2.5	Mean	1.28	0.87	0.79	1.24	1.24
	Standard Deviation (SD)	0.49	0.53	0.35	0.53	0.53
	coefficient of variation(COV)	0.38	0.61	0.44	0.43	0.43

In contrast, the two procedures of the ACI provides un-conservative results for the beams with $2<a/d\leq2.5$ and with $a/d\geq2.5$. For the beams with $2<a/d\leq2.5$ and $a/d\geq2.5$, both procedures have the mean value of V_{calc}/V_{exp} higher than 1 except the ACI bottle shaped strut which produces the mean value of V_{calc}/V_{exp} as 0.87. Table (4-3) shows that the predicted capacity by the Eurocode Option-1 and Option-2 which are found to be un-conservative for the beams with $2<a/d\leq2.5$ and with $a/d\geq2.5$ and gave similar results as in the cases of AQCI provisions. The similarity is caused due to parameter β that modifies the ultimate shear force provided in Eurocode Option-1, and it is equal to one

for all the specimens with $a/d \geq 2$. Compared to the above results, the Canadian code provides a conservative estimate to predict the ultimate strength for all cases that have different shear span-to-depth ratio.

4.8. The prediction of the failure occurrence in deep beams:

Figure (4.9) shows the level of accuracy with which the failure mode and its location can be predicted for 310 specimens using the code provisions. A total of 213 [68.71%] test specimens failed in the second category (i.e., diagonal compression) of the first type of failure mode (i.e., shear failure), resulting in strut crushing as reported in the experimental studies. Using the uniform strut section of the of the ACI code [2008] provision, only 53 [24.88%] specimens were correctly predicted to fail by strut-crushing failure (Figure (4.9)). When the bottle-shaped strut was used in the ACI provisions, the accuracy of the prediction of the failure mode improved where 155 [72.77%] specimens were found to have failed by strut-crushing. These results indicate that the decrease in the efficiency factor β_s by about 25% in the case of bottle-shaped struts instead of the uniform strut section significantly enhanced the accuracy of the prediction of the strut-crushing failure mode. Using the provisions of the CSA code [2004], 138 [64.79%] specimens were predicted to fail in the strut-crushing mode, whereas only 57 [26.76%] specimens were predicted correctly by Eurocode [2004] (Option-1) to have the same failure mode. There was no significant change when Eurocode Option-2 was applied, and the total number of specimens that were predicted correctly to have the strut-crushing mode of failure was found to be just 58 [27.23%]. Figure (4.9) shows the accuracy of the prediction of the failure mode for the failure at the bearing plate (regardless of its location, whether at the loading plate or the support plates). Using the provisions of the

Canadian Code [2004] for only 22 out of 44 specimens [50.00%], the bearing plate failure was predicted correctly. However, a good accuracy was achieved when the ACI [2008] provisions (uniform strut) were used, where 35 [79.55%] specimens were correctly predicted to have failure at the bearing plate. By using the bottle-shaped strut in the ACI provisions only 27.27% (12 specimens out of 44 specimens) of the failure mode can be predicted correctly.

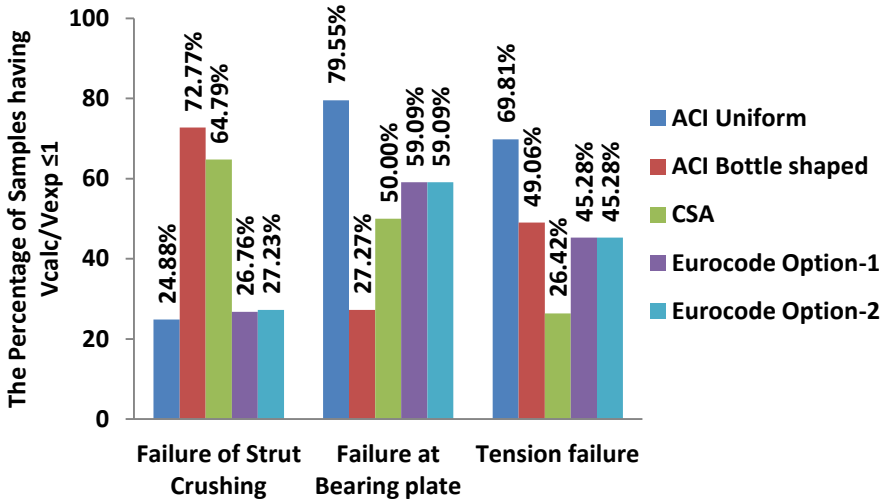

Fig. (4.9) The prediction of failure occurrence by the STM provision of codes.

The use of the bottle-shaped strut in the ACI provisions produced a far worse result than did the uniform strut in predicting the failure at a bearing plate. In the case of the Eurocode provisions, the failure at the bearing plate was correctly predicted for only 26 specimens [59.09%] even after it was adjusted (i.e. Option-2). For the tension failure mode, using the provisions of ACI [2008] with uniform strut sections, 37 [69.81%] specimens were correctly predicted to have failed in that mode, whereas 24 [45.28%] specimens were correctly predicted by the provisions of the Eurocode [2004] (Option-1).

Using the provisions of the Canadian Code A23-3-04[2004], only 14 [26.42%] specimens were correctly predicted for the failure at the tie member. Therefore, unlike its conservativeness in predicting the shear strength capacity of a deep beam, the CSA code provisions are not found to be effective in predicting the failure mode in deep beams. In fact, none of the codes predicted the failure mode and its location in concrete deep beams accurately. While the bottle-shaped strut of ACI provisions is useful in predicting the strut-crushing mode of failure, it is not effective in predicting the failure at the bearing plates or ties (i.e., tension failure), in which cases the uniform strut option is found to work better. The Eurocode provisions were not at all effective in predicting any of the failure modes as shown in Fig. (4.9).

4.9. Proposed modification to ACI code provision:

Based on the study presented earlier in this chapter, the STM model provided in the ACI code with bottle shaped strut was found to perform better than that with uniform strut. The ACI version of the STM procedure with bottle shape strut is investigated further here to improve its performance. One of the key parameters in this case is the efficiency factor. The efficiency factor for each element calculated by ACI bottle shaped strut will be determined according to the results of the collected data.

To determine the efficiency factor β_s for a bottle shape, the actual capacity of the experimental specimens were compared to that calculated by the ACI STM procedure and plotted in Fig. (4.10). The results of the experimental studies indicate that the shear span depth ratio factor has important effect on the efficiency factor β_s. This observation is consistent with that reported in Foster and Malik [2002]. Foster and Malik [2002] found that the shear span-to-depth ratio factor is a significant factor affecting the

efficiency factor and is more dominant than the influence of concrete strength.

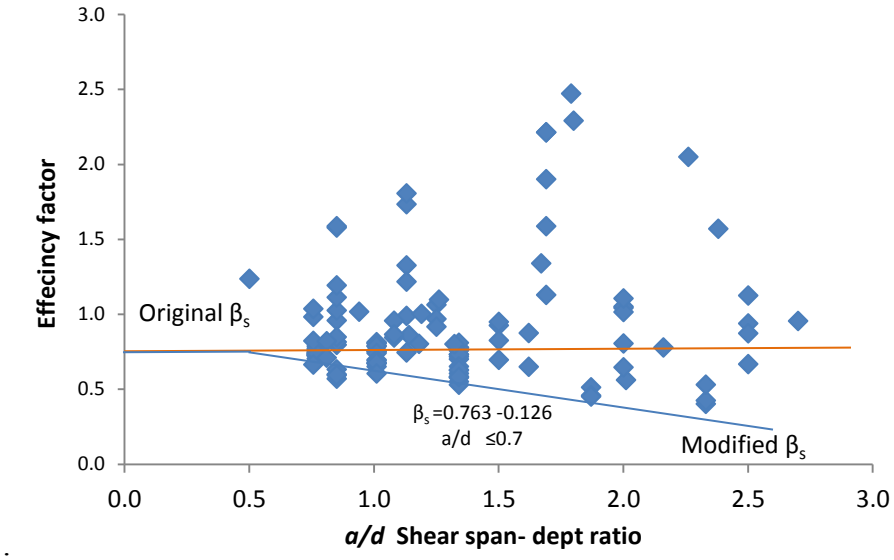

Fig. (4.10) Ratio of actual-to-calculated shear strength versus shear span-to-depth ratio for specimens with web reinforcement.

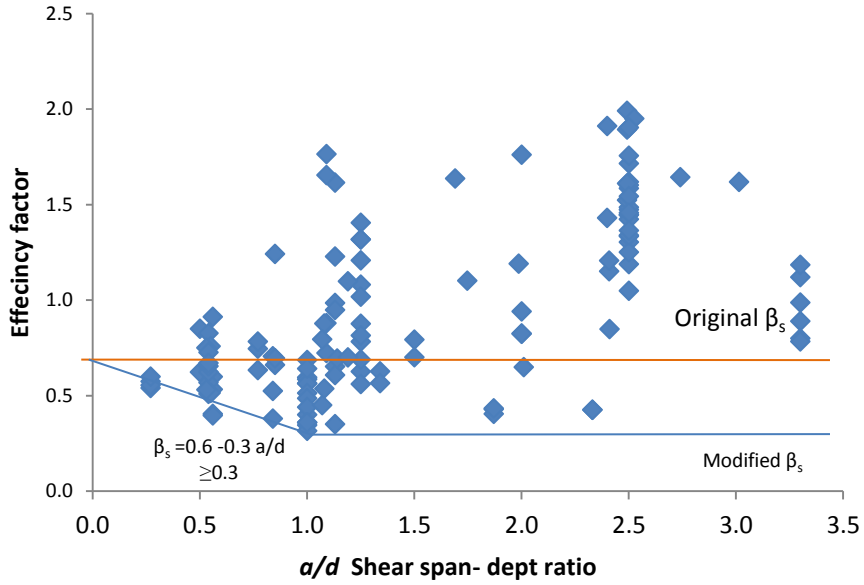

Fig. (4.11) Ratio of actual-to-calculated shear strength versus shear span-to-depth ratio for specimens without web reinforcement.

Figure (4.10) shows the plot of efficiency factor against *a*/*d* for all the specimens that had web reinforcement and satisfied the provisions of of ACI 318-08 [2008] and failed in a shear compression (diagonal splitting or strut crushing failure). The efficiency factor β_s for a bottle shape strut that satisfies Eq (2.1) can be determined as function of the *a/d* according to the following equation (Eq. 4.2):

$$\beta_s = 0.763 - 0.126(a/d) \leq 0.7 \quad (4.2)$$

Figure (4.11) shows the plot of the efficiency factor against *a*/*d* for all the specimens that had no web reinforcement or did not satisfy Eq. (2.1) and failed in a shear compression (diagonal splitting or strut crushing failure). The efficiency factor β_s for a bottle shape strut which does not satisfy Eq. (2.1) can be modified from 0.6 to be also calculated as function of the *a/d* according to the following equation:

$$\beta_s = 0.6 - 0.3(a/d) \geq 0.3 \quad (4.3)$$

Fig (4.12) shows the comparison of the capacity of the beams obtained from the tests and that calculated using original and modified ACI STM models bottle shaped struts. As can be observed from Figure 4.10, the capacity estimated by using the modified model is slightly improved as compared to the original model. The modified model underestimates the capacity of 100% of the samples with *a/d* ratio less than one. But for the specimens with *a/d* ranging between 1 and 2, the modified model underestimates the capacity of only 94.25% of the samples which is higher than the results obtained by using the original model. When the *a/d* is less than 2, the modified model yields conservative estimate of the capacity for 96.44% samples which is 8.18% higher than that obtained using the original model.

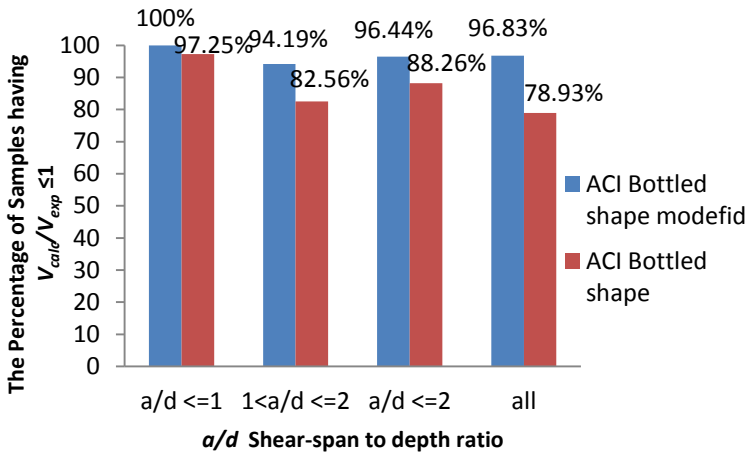

Fig. (4.12) The percentage of samples having $V_{calc}/V_{exp} \leq 1$ considering *a/d* ratio

Considering all specimens taken together, the original model predicts the capacity of only 78.93% of samples conservatively, while the modified model yields conservative estimate of the capacity for 96.83% of the samples, highlighting its improvement. Based on the results provided in Figure (4.12), it can be concluded that the suggested modification in the efficiency factor as a function of *a/d* provides a more conservative estimate of the capacity of a deep beam when ACI bottle shaped strut is considered. The prediction of the failure modes and locations using the original ACI bottle shaped struts and the modified model are shown in Fig. (4.13). The modified procedure with the bottle shaped struts provide a better prediction of the failure mode than the original model when the most common mode of failure (i.e., strut crushing) occurs. The modified STM predicts the failure by strut crushing 13.42% more than the original STM (86.19%). However, for the other types of failure, the modified procedure does not perform as well, and in these cases the prediction is worse than that by the original model.

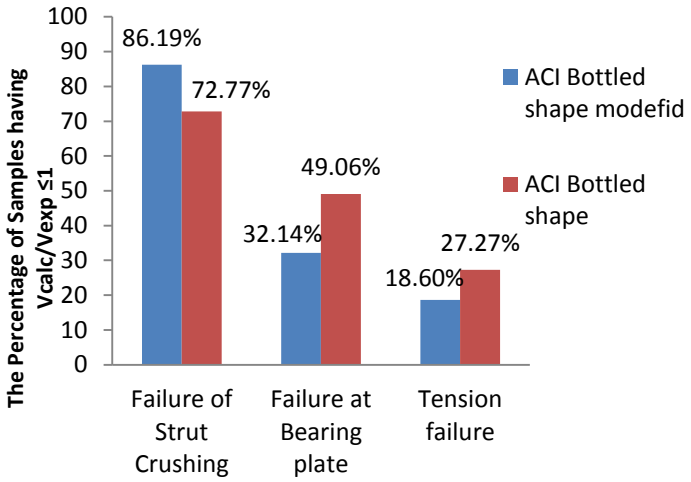

Fig. (4.13) The prediction of failure modes by using the ACI STM original and modified model

4.10. Summary:

The effectiveness of the Strut and Tie Model of reinforced concrete deep beams as provided in the design codes from Canada (CSA A23.3-04 [2004]), USA (ACI 318-08 [2008]) and Europe (EN 1992-1-1-2004E [2004]) has been evaluated based on the experimental results of 397 test samples compiled from the literature. The influence of certain variables on the codes' ability to predict the ultimate strength of deep beams is also studied. The investigation confirms that the Strut and Tie model is in general an appropriate method for the design and evaluation of beams with shear span-to-depth ratio less than or equal to two. It has been found that the code provisions are more accurate for beams with web reinforcement. The CSA code provisions appear to be very robust in estimating the capacity of deep beams, as compared to the other two codes. However, the provisions of all the selected codes do not have the ability to predict the failure mode and location accurately and reliably. The STM procedure in ACI code in bottle shaped strut is found to be more suitable than the uniform strut in predicting the ultimate capacity.

Based on the database of the experimental results, a modification has been suggested in the way the efficiency factor is calculated for the ACI bottle shaped struts, as function of shear span-to-depth ratio. With the suggested modification to the efficiency factor of bottle shaped struts a conservative estimate of the capacity of reinforced concrete deep beams can be obtained. The modified procedure is found to provide an improved prediction of the most common failure mode (i.e. strut crushing) as compared to the original model. In contrast, the modified procedure does not provide an accurate prediction for the other two failure modes. However, since the other two failure modes are less common than the strut crushing mode of failure, the proposed modification represents an improvement on the existing procedure for determining the failure modes.

Chapter 5: Results of the Experimental Study

5.1. Introduction:

In this chapter the experimental results are presented for nine FRP reinforced concrete deep beams described in chapter three. The load-deflection and the load-strain response for all the strain gages and LVDTs are provided in graphs presented in this chapter for each beam tested individually. The crack patterns of each experimental specimen were charted in this chapter. Also, the loads measured at different stages of the experimental tests (e.g., first flexural crack, first diagonal crack and failure) are presented.

Table (5.1) Summary of all experimental results

Specimen No	f'_c (MPa)	a/d	V_{cr} (kN)				V_{max} (kN)	Δ (mm)	Mode of Failure
			Visual Observation		Measured Data				
			Initial Flexural Cracking	Initial Strut Cracking	Initial Flexural Cracking	Initial Strut Cracking			
A1/100	49.8	1	105.85	205.85	100.50	192.05	560.25	8.22	Shear Compression
A1/75	52.2	1	125.35	220.85	108.35	172.70	552.39	8.43	Shear Compression
A1/50	52.5	1	115.85	212.85	112.80	193.50	493.69	10.33	Diagonal splitting
A1/00	52.7	1	109.85	172.35	105.10	175.70	416.89	8.91	Diagonal splitting
B1.5/100	51.8	1.5	67.48	117.48	52.96	77.21	322.38	11.93	Shear Compression
C2/100	50.8	2	39.86	71.86	27.72	60.62	125.91	12.04	Shear Compression
C2/75	51.0	2	39.36	74.36	22.07	50.32	98.68	8.12	Strut Crushing
C2/50	51.3	2	36.11	66.86	27.12	69.27	102.71	9.12	Strut Crushing
C2/00	51.3	2	28.36	54.36	25.42	56.22	93.47	10.36	Strut Crushing

5.2. Presentation of Test Results:

The Results for each of the individual specimens with crack patterns are provided in section 3 to 12 of chapter four. The result summaries of the tested FRP reinforced concrete deep beams are presented in Table (5.1). Table (5.1) contains the material properties, modes of failure; the shear strength at the initial crack formation (flexural and diagonal). V_{cr}; and the ultimate shear strength, V_{max} of all the specimens.

5.3. Results for the specimens in Group A:

The beams in this group had *a/d* ratio of 1, and except for the amount of web reinforcement, all four specimens in this group are identical. The amount of web reinforcement, ρ_w provided in A1/00, A1/50, A1/75 and A1/100 is 0, 44, 68, and 100%, respectively; where, 100% indicates the minimum web reinforcements required for crack control.

5.3.1. Response of Beam A1/00:

Crack development and failure mode in A1/00:

The formation of the first flexural crack at mid-span appears at 213 kN of loading. The formation of new flexural cracks began to appear and lengthened toward the loading plate as the load increased. Initial diagonal cracks occurred after a load level of 340 kN. The initial diagonal cracks formed approximately at the interior edge of the support propagating toward the loading plate and to a distance lower than the mid height of the specimen. A new diagonal cracks formed in the general direction between supports and load point on the mid-depth of the beam. By increasing the load, more flexural cracks and diagonal cracks were developed.

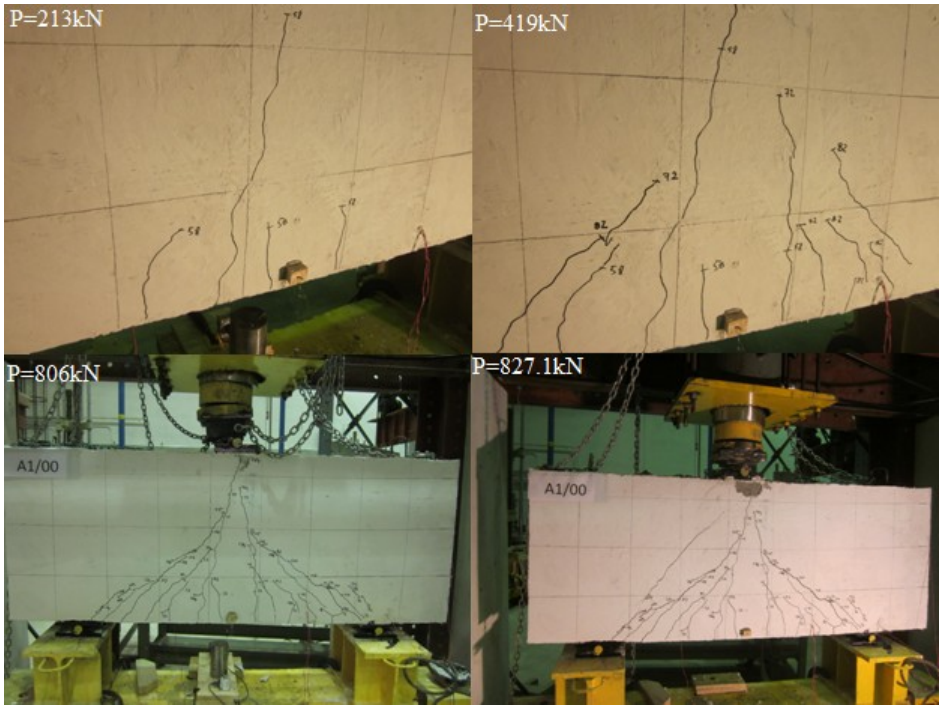

Fig. (5.1) The propagation of the crack patterns in the beam A1/00 at four different loading stages

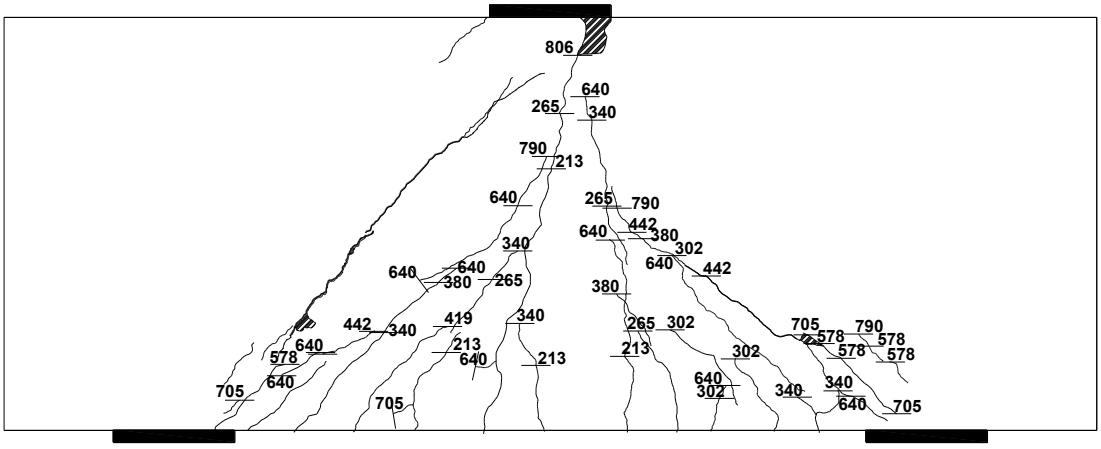

Fig. (5.2) Crack pattern of specimen A1/00

When the load reached 827.1 kN, the beam failed suddenly due to the splitting of the concrete strut (Diagonal splitting failure). The failure occurred at the middle-depth of the beam parallel to the strut. Since there was no web reinforcement in this beam, this type of failure was expected. Figure (5.1) shows the pictures of the propagation of crack patterns for beam A1/00 at four different loading stages, while, Figure (5.2) illustrates the crack patterns at failure with the load level when each crack was first observed. The cracks that caused the failure are marked in bold lines.

Load –Deflection response of A1/00:

The deflection reading was taken at each load increment. When the maximum load was reached, the deflections at the mid span were 8.9 mm and 9.9 mm recorded from the LVDTs placed on for both sides of the beam. After reaching P_{max} and the occurrence of failure, the load started to drop with a decrease in the deflection. The deflections at the mid span were 8.2mm and 8.8 mm as recorded on both sides. The load versus mid-span deflection curves of specimen A1/00 is shown in Figure (5.3).

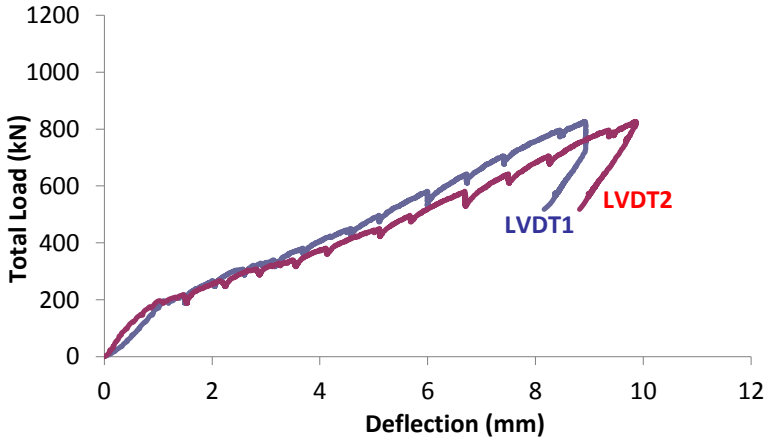

Fig. (5.3) Deflection at mid-span of specimen A1/00

Load –Strain response of the main reinforcements in A1/00:

The strains located on the middle of the upper and the lower main GFRP longitudinal reinforcement for loading stages is shown in Figure (5.4). At a load level of 196.8 kN, the tensile strains began to increase as loading was increased. This level of loads approximately corresponds to the formation of the initial flexural crack as observed from the experimental test. Figure (5.5) shows the strains in the extension edge of the bottom FRP rebars beyond the supporting plate (the nodal zone). From the Figure (5.5) it can be observed that the strain in the rebars in the end node region was within 19.1%, which is much lower than the ultimate strain of GFRP rebar as specified in the manufacturer's data sheet, indicating that the anchorage of the rebar was satisfactory.

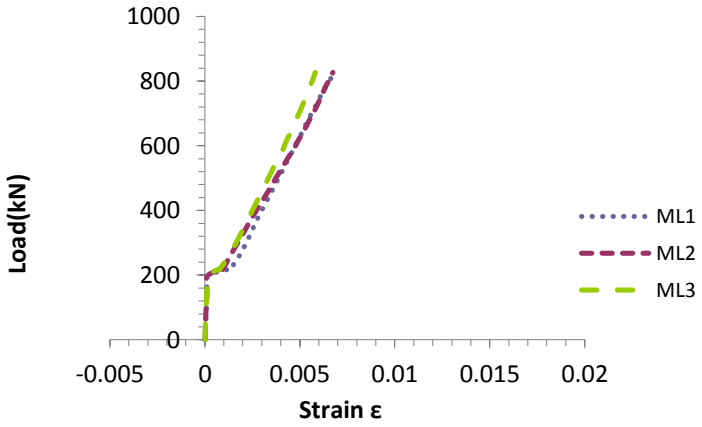

Fig. (5.4) Strains in the middle of the main tension GFRP reinforcement of specimen A1/00

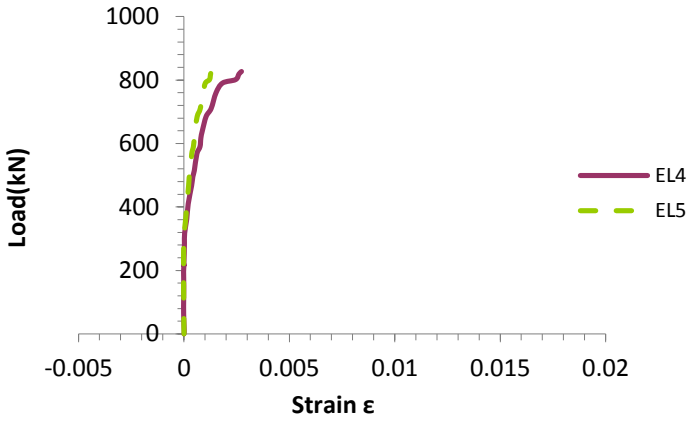

Fig. (5.5) Strains in the end of the main tension GFRP reinforcement of specimen A1/00

The action of the compression zone (node) formed at the supporting plate confirmed that the rebar were subjected to lateral pressure and higher bond stresses developed. The strain-load response at a top longitudinal GFRP rebar is shown in Figure (5.6), and it indicates that the strain in a top rebar is very small and has reached only 0.9% of the ultimate strain of GFRP rebar. Also the negative and small value of the strain indicates that the zone between the loading plate and the action of the two loading compression strut is exposed to negligible stress.

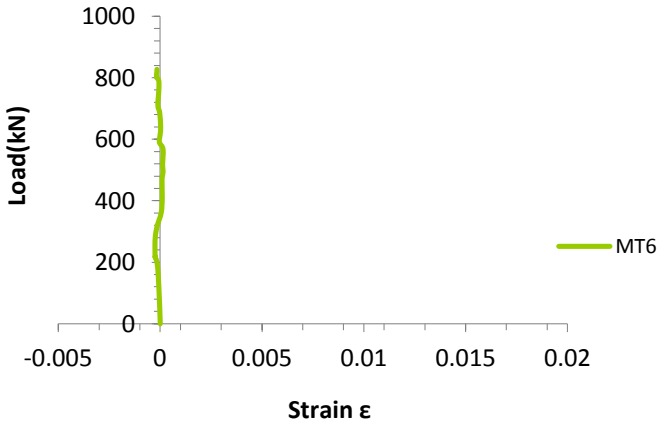

Fig. (5.6) Strains in the middle of the main top GFRP reinforcement of specimen A1/00

5.3.2. Response of Beam A1/50:

Crack development and failure mode in A1/50:

The first flexural crack at mid-span appeared at 225 kN of loading. The new flexural cracks began to appear and lengthened toward the loading plate as the load increased. The propagation rate of flexural cracks in the specimen A1/50 is much lower than that in case of the previous specimen, A1/00. The initial diagonal cracks occurred after 419 kN load was applied. The Initial diagonal cracks formed approximately at the interior edge of the support plate and propagated towards the loading plate to a distance lower than the mid height of the specimen. By increasing the load, more flexural cracks and diagonal cracks developed and the existing ones widened or lengthened toward the compression face of the beams. The formation of new cracks eventually stopped and the existing ones widened, particularly after reaching 65% of P_{max}. A sudden thunderous sound was heard at 75% of $P_{max,}$ indicating a sudden release of energy.

When the load reached the maximum level, 980.68 kN, the beam failed in the same manner as in the case of the previous specimen by splitting of the diagonal strut (Diagonal splitting failure). The failure took place at the middle-depth of the beam parallel to the strut between the end of the loading plate and the support. Figure (5.7) shows the pictures of the crack patterns for beam A1/50 at four different loading stages, while Figure (5.8) illustrates the crack patterns at failure with the load level when each crack was first observed. The cracks that caused the failure are marked in bold lines.

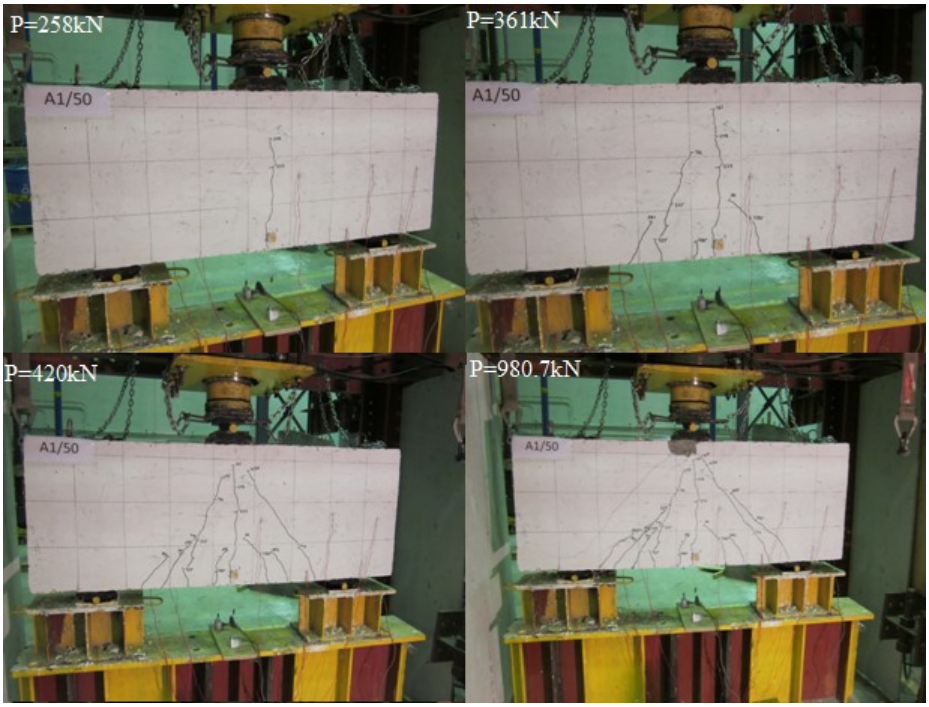

Fig. (5.7) The propagation of the crack patterns in the beam A1/50 at four different loading stages

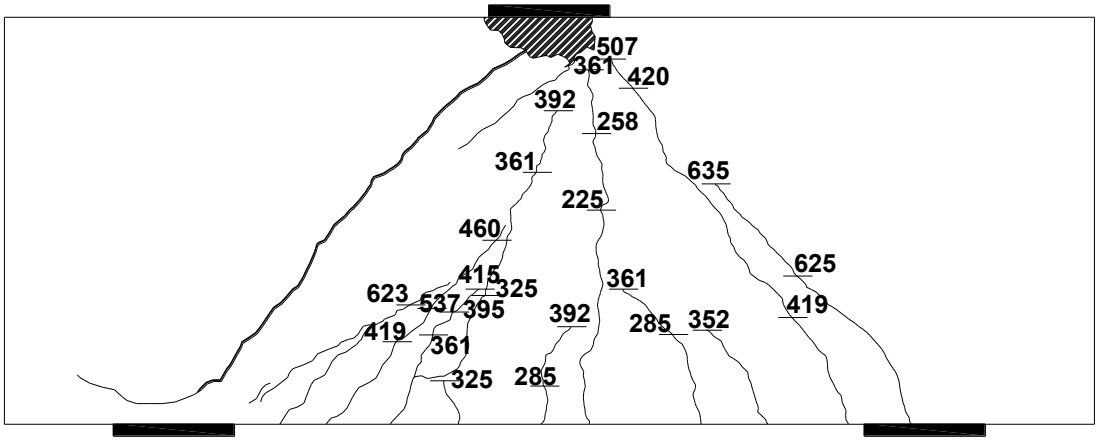

Fig. (5.8) Crack pattern of specimen A1/50

Load –Deflection response of A1/50:

The deflection reading was taken at each load increment. When the maximum load was reached, the deflections at mid span were 10.3 mm and 11.6 mm at both sides. After reaching P_{max}, the load started to drop for increased deflection until failure occurred. The maximum deflections at mid span were 10.85 mm and 11.68 mm on each side. The load versus mid-span deflection curves of specimen A1/50 is plotted in Figure (5.9).

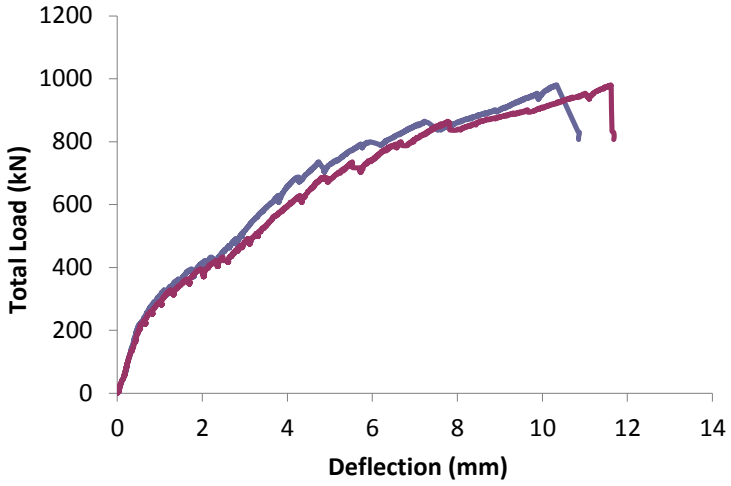

Fig. (5.9) Deflection at mid-span of specimen A1/50

Load –Strain response of the main and web reinforcements in A1/50:

The mid-span strains ML 1, 2 & 3 in main GFRP longitudinal reinforcement at the upper and the lower faces of the beam A1/50 at loading stages are shown in Figure (5.10). At the load of 212.2 kN, the tensile strains began to increase as loading was increased. This load level is in approximate agreement with initial flexural crack that was observed from the experimental test. Figure (5.11) shows the response of strains at the extension edge of the rebar beyond the supporting plate (the nodal zone).

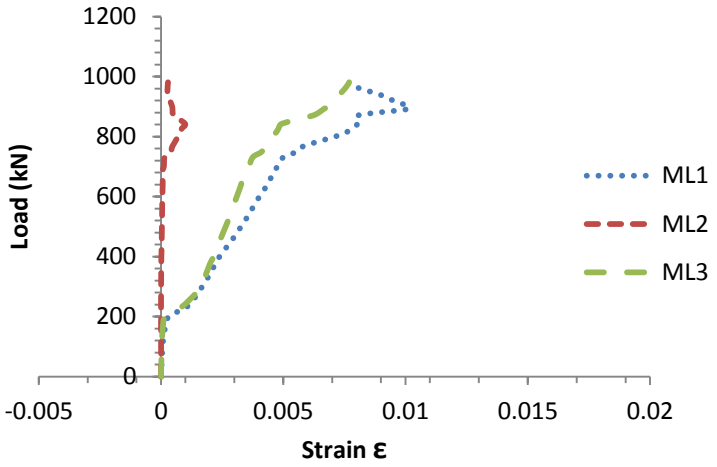

Fig. (5.10) Strain in the middle of the main tension GFRP reinforcement of specimen A1/50

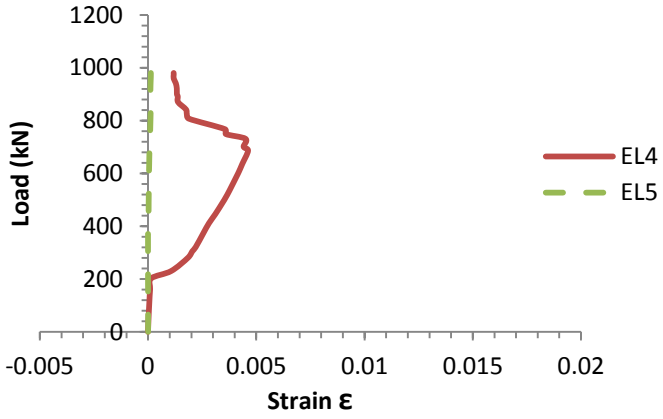

Fig. (5.11) Strain in the end of the main tension GFRP reinforcement of specimen A1/50

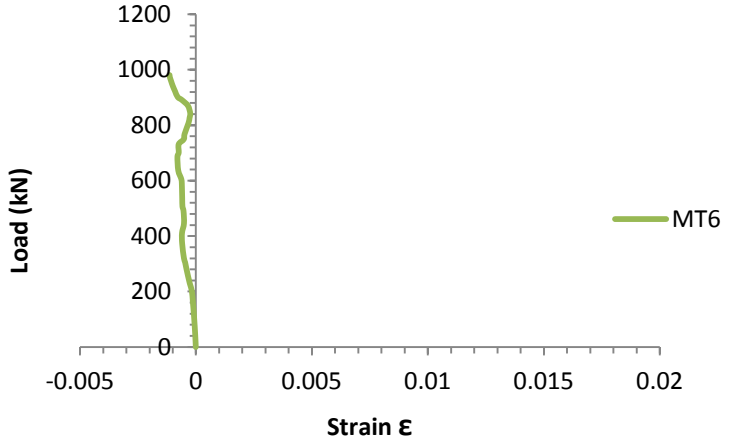

Fig. (5.12) Strain in the middle of the main top GFRP reinforcement of specimen A1/50

From the Figure (5.11) can be observed that only 30.2% of the ultimate strain of GFRP rebar has been reached, indicating that the anchorage of the rebar was satisfactory. The strain-load response of the longitudinal GFRP reinforcement located at the top is illustrated in Figure (5.12). Only 6.9% of the ultimate strain of GFRP rebar in the top rebars has been reached. The strains in the vertical and the horizontal GFRP web reinforcement on both sides of the beam at different loading stages are shown in Figures (5.13) and (5.14). After reaching a load level of 373.6 kN, the tensile strain in the region of the assumed direction of the main struts began to increase as loading was further increased.

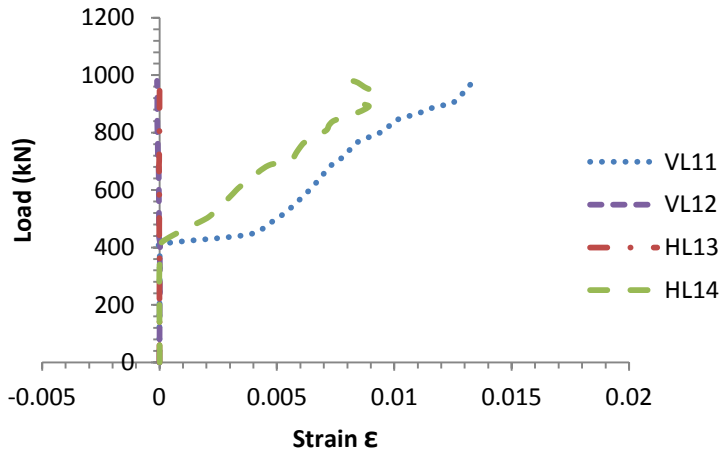

Fig. (5.13) Strain in the vertical and horizontal GFRP web reinforcement left side of specimen A1/50

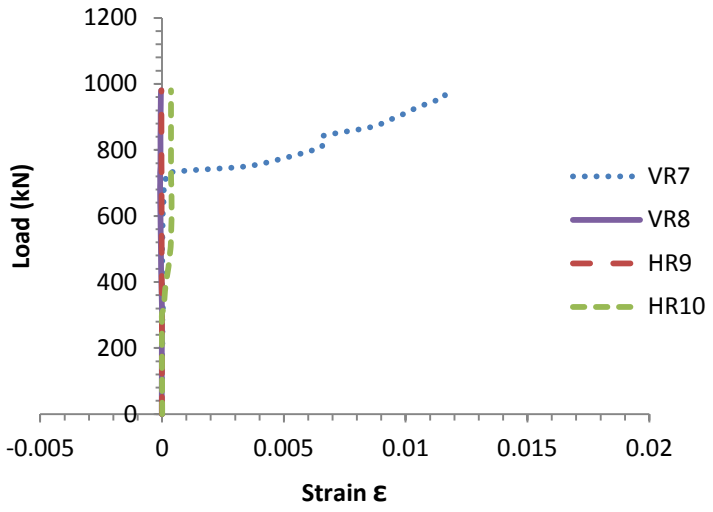

Fig. (5.14) Strain in the vertical and horizontal GFRP web reinforcement right side of specimen A1/50

This level of load (i.e., 373.6 kN) is less than the initial diagonal crack load that was observed from the experimental test. The formation of the rebars of web reinforcement whether horizontally or vertically in the left side were similar to those in the right side. As can be seen from the two figures, the FRP web reinforcement on the left side indicated higher stress than those on the right side because of the different support conditions (i.e., hinge at the left end and roller on the right end). From Figure (5.13), it can be observed that the strain in the GFRP web reinforcements reached about 70.4% of the ultimate tensile strain, ε_{Fu} because of the lower quantity of web reinforcements.

5.3.3. Response of Beam A1/75:

Crack development and failure mode in A1/75:

The formation of the first flexural crack at mid-span appears at 244 kN of loading. The new flexural cracks began to appear and lengthen toward the loading plate as the load increased. The propagation rate of flexural cracks in the specimen A1/75 is much lower

comparing to the two previous specimens. Initial diagonal cracks occurred after 435 kN of load was applied. The initial diagonal cracks formed approximately at the interior edge of the support and propagated towards the loading plate and to a distance less than the mid height of the specimen. On further increase in the load, the formation of the new flexural cracks stopped and the existing ones widened or lengthened toward the compression face of the beam. New diagonal cracks formed and existing ones propagated in the direction towards the loading plate up to a load of approximately 505 kN.

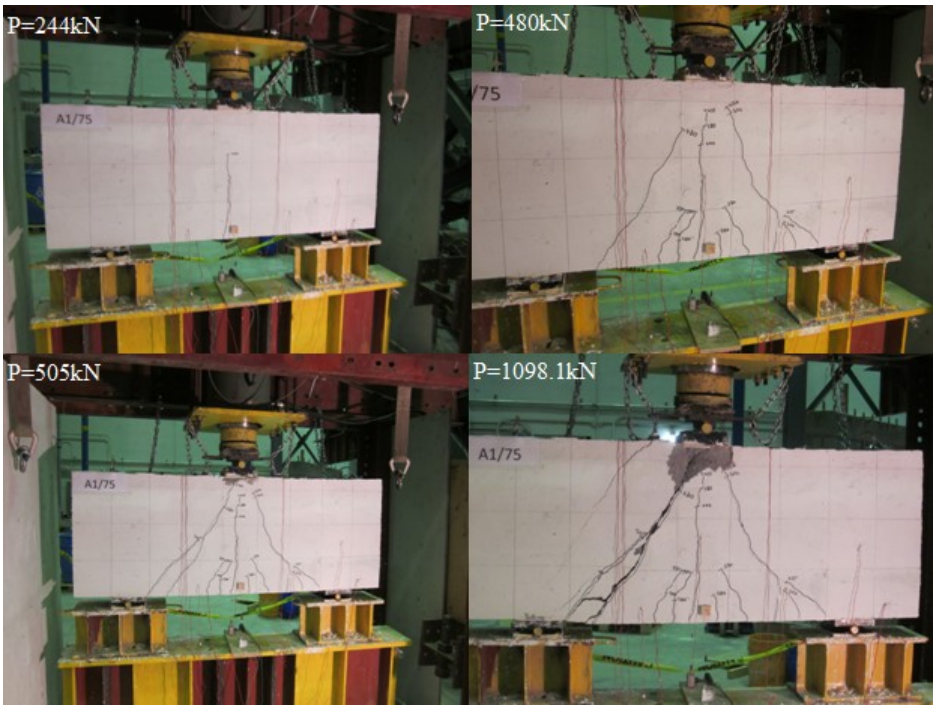

Fig. (5.15) The propagation of the crack patterns in the beam A1/75 at four different loading stages

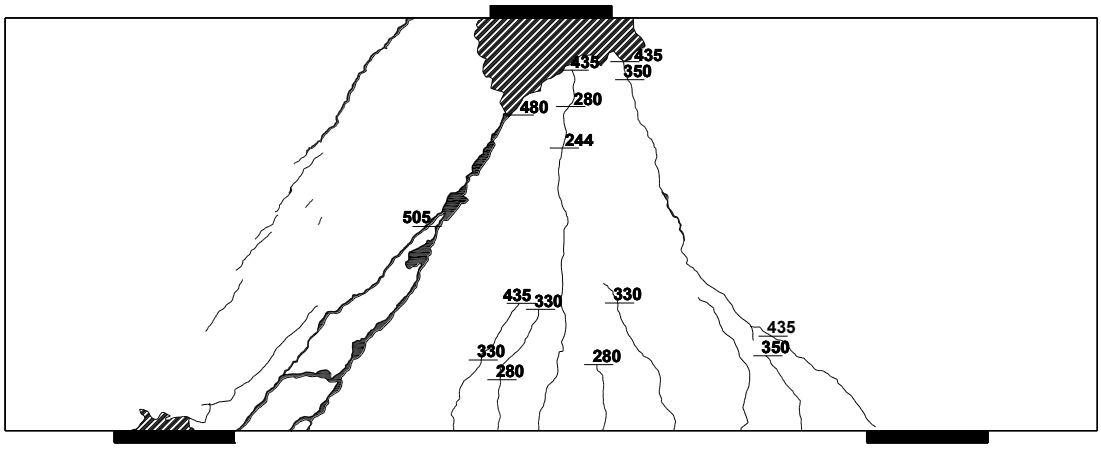

Fig. (5.16) Crack pattern of specimen A1/75

In contrast to the other two previous beams, Specimen A1/75 failed in shear compression failure. When the ultimate load of 1098.1 kN was reached, the concrete at the end of one of the main struts at the loading plate failed by crushing and was accompanied by thunderous sound. The shear compression failure occurred near the loading which is indicated by cross-hatchings in the Figures (5.16). Figure (5.15) shows pictures of the propagation of crack patterns for beam A1/75 at four different loading stages, while Figure (5.16) illustrates the crack patterns at failure with the load level when each crack was first observed. The cracks that caused the failure are marked in bold lines.

Load –Deflection response of A1/75:

The deflection reading was taken at each load increment. When the maximum load was reached, the deflections at mid span were 8.4 mm and 8.6 mm for both sides. After reaching P_{max}, the load started to drop for increased deflection, until failure occurred. The

maximum deflections at mid span were 9.9 mm and 10 mm at the two sides. The load versus mid-span deflection curves of specimen A1/75 is plotted in Figure (5.17).

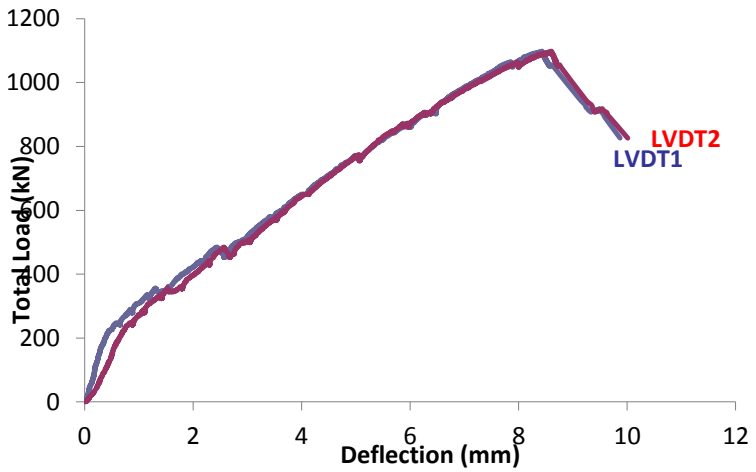

Fig. (5.17) Deflection at mid-span of specimen A1/75

Load –Strain response of the main and web reinforcements in A1/75:

The mid-span strains in the main GFRP longitudinal reinforcements at the upper and the lower faces of the beam at different loading stages are shown in Figure (5.18). At the load of 203.3 kN, the tensile strains began to increase as loading was further increased. This load is less than the load corresponding to the initial flexural crack that appeared in the experimental test. The initial flexural crack appeared to be longer than in the previous two samples that had no or lower amount of web reinforcement. For better accuracy, the initial flexural cracking load and the initial diagonal cracking load recorded from the strain gauges have been used for analyzing all the results of this study. However, in practise, due to economic considerations, most of the structural elements are evaluated and investigated visually by observation of the appearance of the cracks.

Figure (5.19) shows the strain response of a main rebar at the extension edge of the rebar beyond the supporting plate (the nodal zone). It can be observed from Figure (5.19) that the strain in the part of the GFRP main rebar reached only 20.5% of the ultimate strain, which indicates that the anchorage of the rebar was adequate. The strain-load response of the top longitudinal GFRP reinforcement is shown in Figure (5.20).

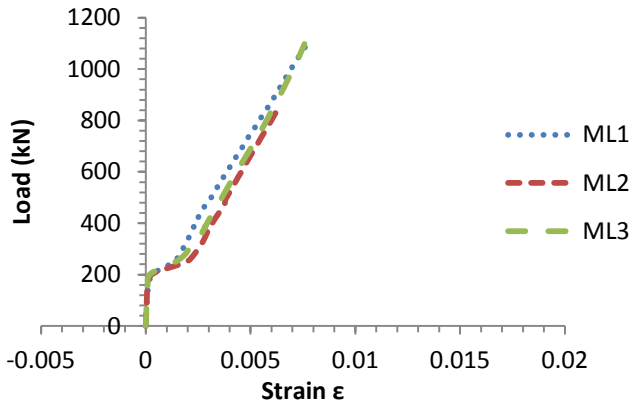

Fig. (5.18) Strain in the middle of the main tension GFRP reinforcement of specimen A1/75

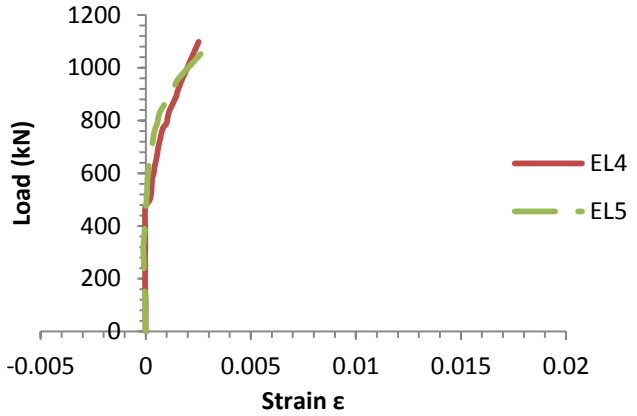

Fig. (5.19) Strain in the end of the main tension GFRP reinforcement of specimen A1/75

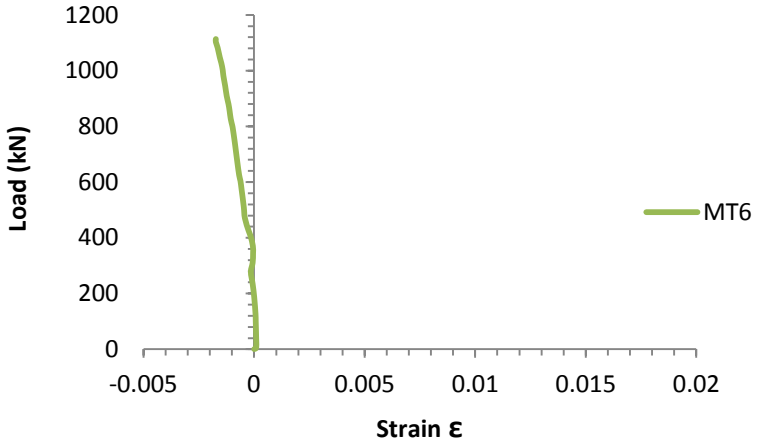

Fig. (5.20) Strain in the middle of the main top GFRP reinforcement of specimen A1/75

The negative strains formed in the rebar at the loading plate in the nodal zone (node) confirmed that this zone was subjected to lateral pressure from the loading plate and the action of the two compression struts. Nevertheless the failure occurred in this zone, but the rebar was still not deformed or damaged yet and only 9.2% of the ultimate strain of GFRP rebar has been reached.

The strains in the vertical and the horizontal GFRP web reinforcement located on the both sides of the beam at different loading stages are shown in Figures (5.21) and (5.22). At the load of 332.4 kN, the tensile strains in the web reinforcement in the left end of the beam at the assumed direction of main struts began to increase as loading was increased. This load level is in approximate agreement with initial diagonal crack that was observed from the experimental test near the left end of the beam. While on the right end, the increase in the strain in the web reinforcement started at 472 kN which approximately corresponds to the appearance of the diagonal crack on that side as observed in the experimental test. It can be observed from Figure (5.21) that the strain in the vertical and

horizontal GFRP reinforcements reached only 52.9% and 49.5% of the ultimate strain, respectively.

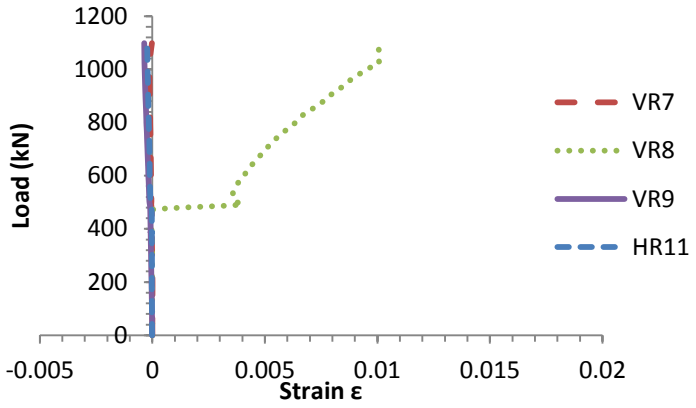

Fig. (5.21) Strain in the vertical and horizontal GFRP web reinforcement right side of specimen A1/75

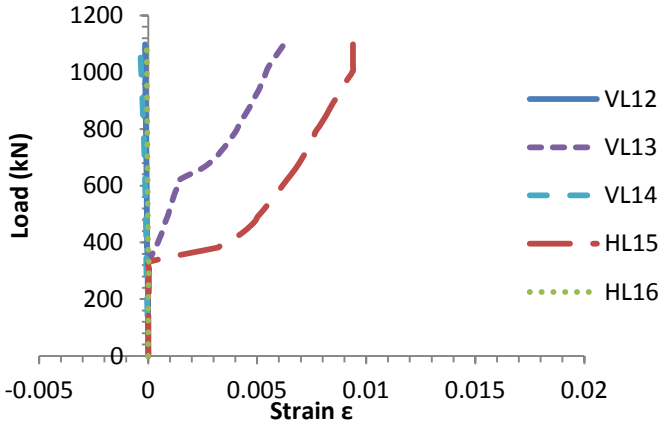

Fig. (5.22) Strain in the vertical and horizontal GFRP web reinforcement left side of specimen A1/75

Before the failure occurred, some of the strain gauges stopped working as their lead wires intersected with the cracks and got damaged or cut. Nevertheless, the big cracks

occurred in the strut and intersected with the web reinforcements, which did not deform much or get damaged as showed in Figure (5.23).

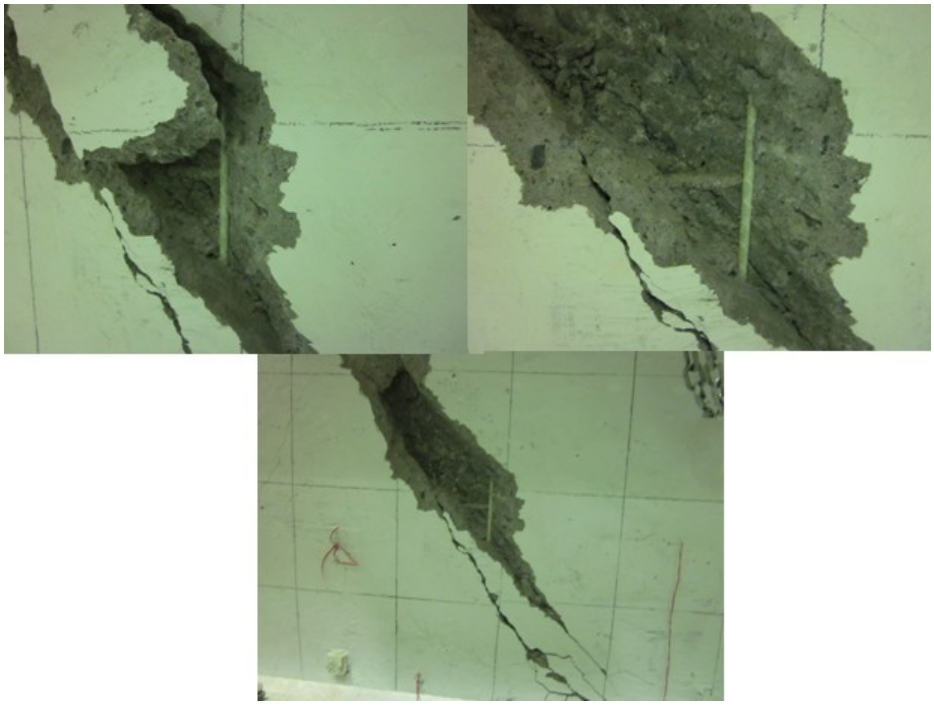

Fig. (5.23) The crack intersects the web reinforcement in specimen A1/75

5.3.4. Response of Beam A1/100:

General response of A1/100:

The formation of the first flexural crack at mid-span was at 205 kN of loading. The new flexural cracks began to appear and lengthened toward the loading plate as the load increased. The formation of new flexural cracks eventually stopped and existing ones became wider, particularly after reaching 360 kN. Initial Diagonal cracks occurred after 405 kN of load was applied. New diagonal cracks formed and existing ones propagated in the direction towards the loading plate up to a load of approximately 800 kN. The beam failed in the same manner as in the case of the previous specimen, A1/75 by shear compression failure.

The shear compression failure (node failure) occurred near the loading which is indicated by cross-hatchings in the Figures (5.25). When the load reached the maximum level, 1113.8 kN, the concrete at the loading plate zone crushed. Figure (5.24) shows pictures of the propagation of crack patterns for beam A1/100 at four different loading stages, while Figure (5.25) illustrates the crack patterns at failure with the load level when each crack was first observed.

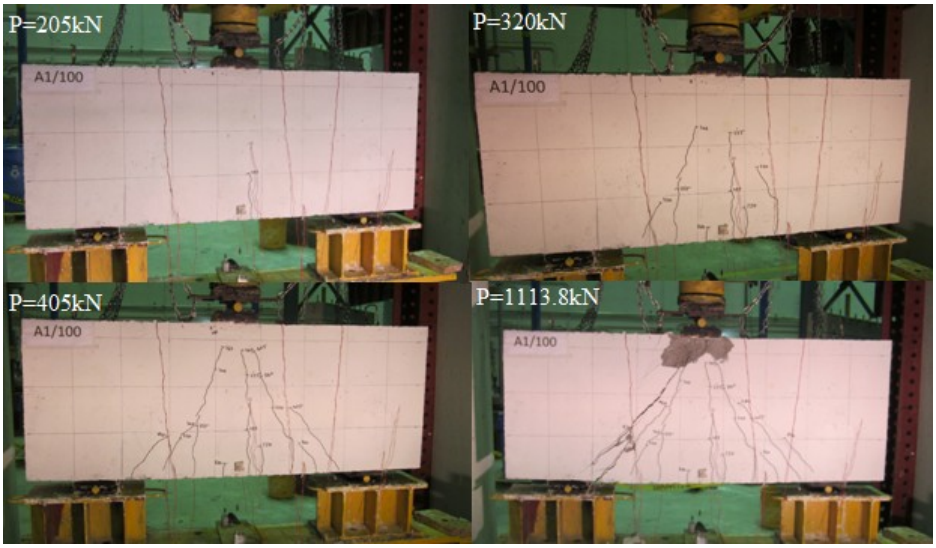

Fig. (5.24) The propagation of the crack patterns in A1/100 at different levels of loading

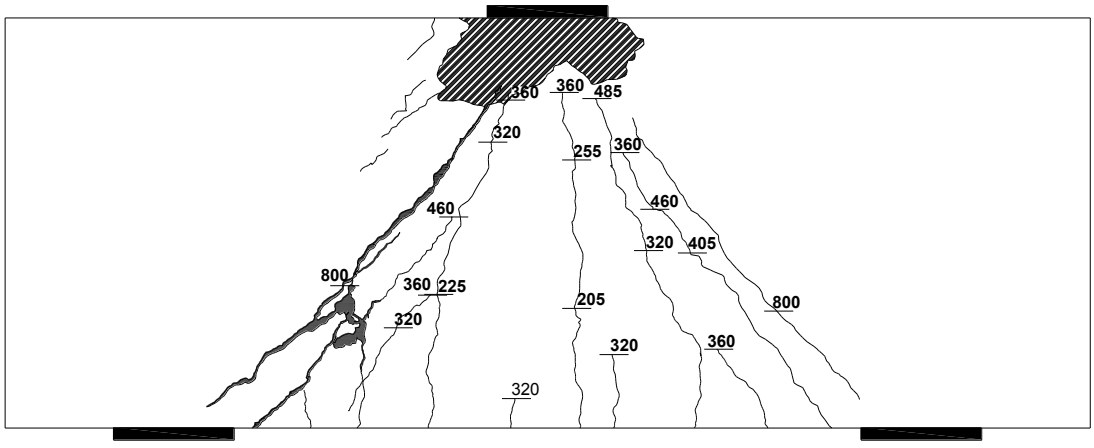

Fig. (5.25) Crack pattern of specimen A1/100

Load –Deflection response of A1/100:

The deflection reading was taken at each load increment. When the maximum load was reached, the deflections at mid span were 8.2 mm and 7.9 mm for both sides. After reaching P_{max}, the load started to drop for increased deflection, until failure occurred. The maximum deflections at mid span were 11.1 mm and 10.7 mm at the two sides. The load versus mid-span deflection curves of specimen A1/100 is plotted in Figure (5.26).

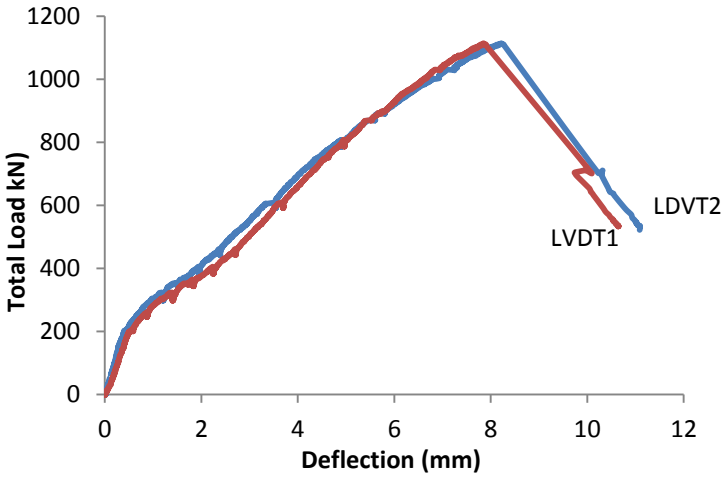

Fig. (5.26) Deflection at the mid-span of specimen A1/100

Load –Strain response of the main and web reinforcements in A1/100:

The mid-span strains in the main GFRP longitudinal reinforcement at the upper and the lower faces of the beam at different loading stages are shown in Figure (5.27). At the load of 187.6 kN, the tensile strains began to increase as loading was further increased. This load is less than the load corresponding to the initial flexural crack that was visually detected in the experimental test. However, strain gauges picked up the formation of the initial micro-cracks much earlier that the cracks became visually detectable. Thus, the variation in the strain gage readings indicates the initiation of a flexural crack more reliably.

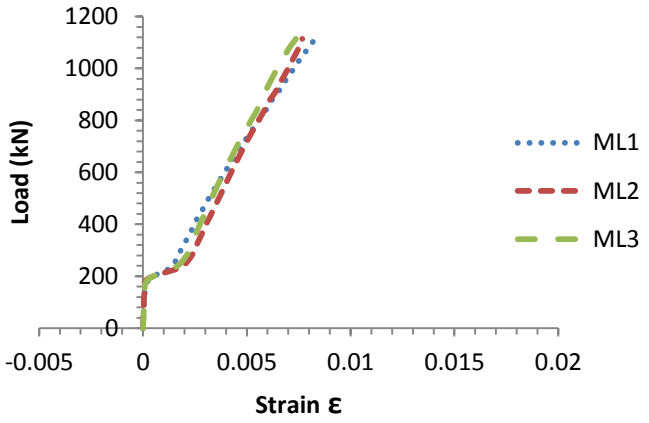

Fig. (5.27) Strain in the middle of the main tension GFRP reinforcement of specimen A1/100

Figure (5.28) shows the strain response of a main rebar at the extension edge of the rebar beyond the supporting plate (the nodal zone). It can be observed from Figure (5.28) that the strain in the end of the GFRP main rebar reached only 15.16% of the ultimate strain, which indicates that the anchorage of the rebar was adequate. The strain-load response of the top longitudinal GFRP reinforcement is shown in Figure (5.29). The negative strains formed in the rebar at the loading plate in the nodal zone (node) confirmed that this zone was subjected to lateral pressure from the loading plate and the action of the two compression struts. Nevertheless the failure occurred in this zone, but the rebar was not found to be deformed yet and only 15.5% of the ultimate strain of GFRP rebar was reached.

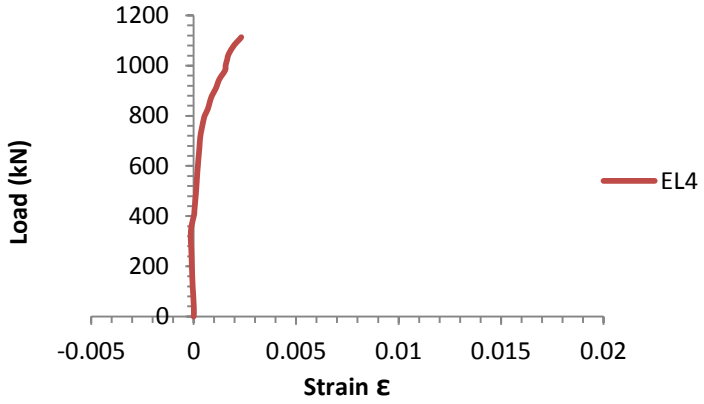

Fig. (5.28) Strain in the end of the main tension GFRP reinforcement of specimen A1/100

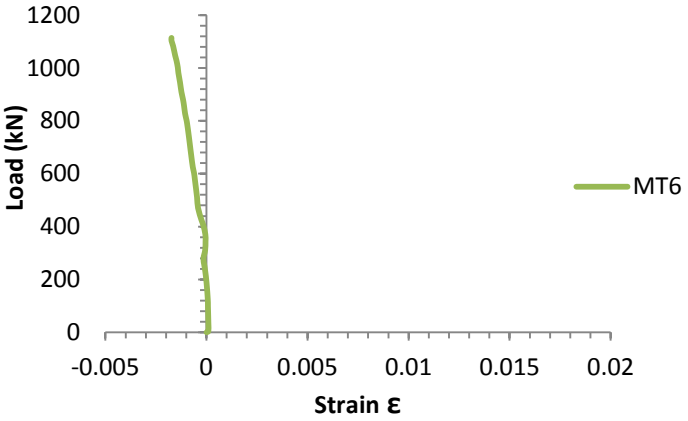

Fig. (5.29) Strain in the middle of the main top GFRP reinforcement of specimen A1/100

The strains in the vertical and the horizontal GFRP web reinforcement located on the both sides of the beam at different loading stages are shown in Figures (5.30) and (5.31). At the load of 370.7 kN, the tensile strains in the web reinforcements in the left and right end of the beam at the assumed direction of main struts began to increase as loading was increased. This load level was less than the load corresponding to the initial diagonal crack that was observed from the experimental test near the left end of the beam. This variation of the results was due to the same reason that was mentioned previously in the

initial flexural cracks. It can be observed from Figure (5.30) that the strain in the vertical and horizontal GFRP reinforcement reached only 26.14% and 14.5% of the ultimate strain, respectively.

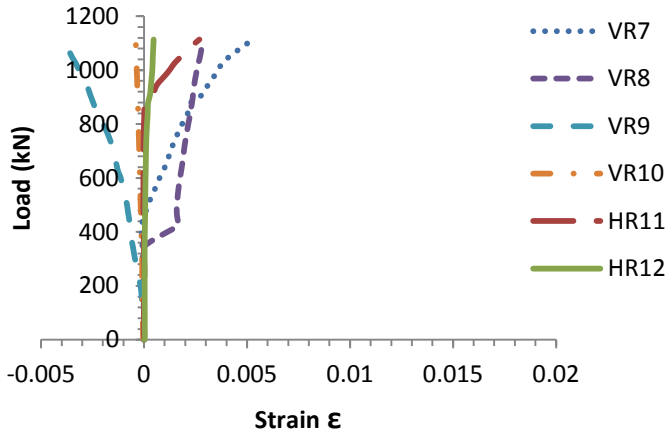

Fig. (5.30) Strain in the vertical and horizontal GFRP web reinforcement right side of specimen A1/100

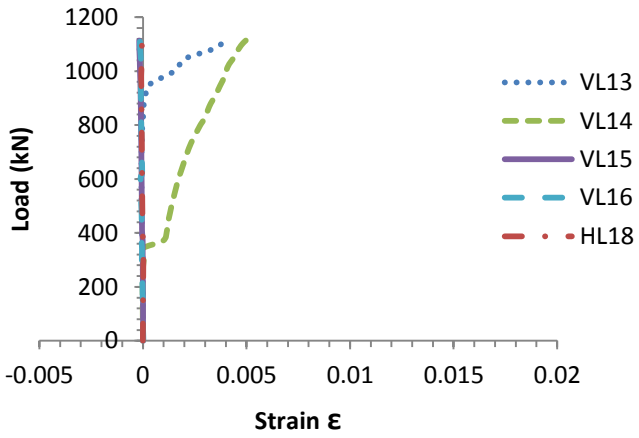

Fig. (5.31) Strain in the vertical and horizontal GFRP web reinforcement left side of specimen A1/100

As can be seen from the results, it is clear that the beam with 100% of web reinforcement A1/100 exhibited quite similar behaviour as of A1/75, but had a slightly higher magnitude of the failure load than that of A1/75 specimen.

Comparison of beam performances within group A:

In the early stages of loading approximately at 24, 22, 19 and 17% of the ultimate load for four specimens: A1/00, A1/50 A1/75 and A1/100, respectively, similar characteristics of crack patterns were observed. Flexural cracks were initiated vertically in the region of pure bending between the two supports where the shear stress is zero. Additional flexural cracks began to appear in the mid-span of the beam and lengthened toward the loading plate as the load increased. After reaching approximately 55, 50, and 44% of the ultimate load in specimens A1/50 A1/75 and A1/100, respectively, the flexural cracks were stabilized, and stopped propagating. While the propagation of flexure cracks in the beam A1/00 continued until they were very close to the failure load. For all beams, diagonal cracking occurred after the flexural cracking.

The first diagonal crack appeared between the loading point and support at 41, 38, 30 and 33% of the maximum loading for four specimens: A1/00, A1/50 A1/75 and A1/100, respectively. Because of the dominance of the shear stresses, the cracks in the region of the shear span were inclined (diagonal) and propagated toward the loading points. As the load increased at approximately 50 to70% of P_{max}, the formation of new diagonal cracks eventually stopped and existing ones widened until failure occurred. In contrast, the propagation of diagonal cracks continued in beam A1/00 until they were very close to the failure load.

In general, the crack patterns of the four beams within group A at failure are quite similar; however, the beams A1/00 and A1/50 were more extensively cracked than the other two beams with higher web reinforcement. The failure mode of all four beams in this group was brittle. Two types of brittle failure (shear compression and diagonal splitting failure) were observed. The beams with less or without web reinforcement showed sudden failure without any caution and failed with diagonal-splitting failure. In beams with web reinforcement of 75% and 100% failure mode was shear compression failure manifested by crushing of concrete at the end of one of the main struts and was accompanied by a thunderous sound. The above observation confirms that sufficient web reinforcement had helped avoiding the sudden shear failure the beams in these cases. Table (5.2) shows comparison between the applied loads at different stages in the four beams. The results of beams in group A indicated that an increase in amount of web reinforcement resulted in an increase in the capacity up to 26%.

Table (5.2) The applied loads at different stages of the four beams in group A.

Specimens	Initial Flexure crack		Initial Diagonal crack		Failure Load (kN)
	Occurred at % of P_{max}	Continued up to % of P_{max}	Occurred at % of P_{max}	Continued up to % of P_{max}	
A1/00	23.7%	Failure	41.1%	Failure	827.1
A1/50	21.6%	54.8%	38.1%	64.7%	980.7
A1/75	18.48%	39.6%	30.0%	50.1%	1098.1
A1/100	17.1%	43.8%	33.3%	71.8%	1113.8

The load versus mid-span deflection curves of the all specimens beams in Group A, are shown in Fig. (5.32). As can be seen from these curves, the failure loads (P_{max}) were 1113.8, 1098.1, 980.7 and 827.1 kN for beams A1/100, A1/75, A1/50 and A1/00,

respectively. After reaching the failure loads (P_{max}) in most of the specimens the load started to drop. When the maximum load was reached, the deflections at mid span were 8.22, 8.43, 10.33and 8.91 mm for beams A1/100, A1/75, A1/50 and A1/00, respectively. In general, the mid-span deflection at the maximum load for beams with web reinforcement is lower than that with less or without web reinforcement.

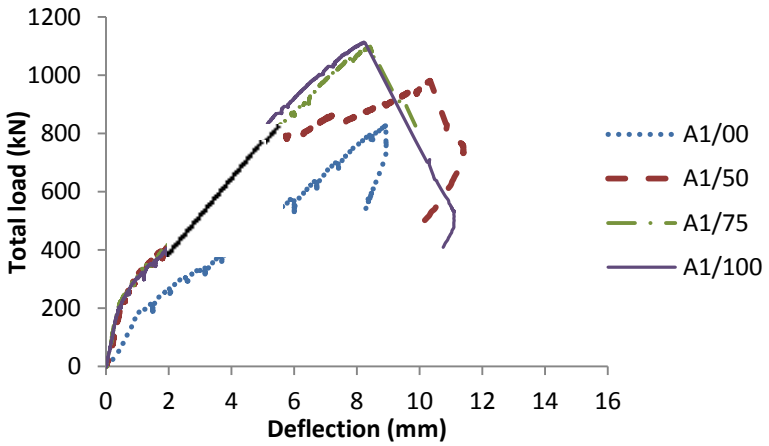

Fig.(5.32) Load- Deflection response for all beams in Group A

The serviceability limitations for deflection were determined by CSA standard A23.3 and expressed as fraction of the clear span. In this study, the applied loading corresponding to the permissible deflection of *l/360* and *l/180* were analyzed and compared. The deflection limit of *l/360* was reached at percentage between 43 to 54% of $P_{max,}$ while the second limit of *l/180* was reached at larger percentage of P_{max} from 78 to 90%. Table (5.3) compared between the deflection at maximum loads and at permissible deflection limits of beams in group A.

Table (5.3) The deflection at different stages of load for all beams in Group A.

Specimens	Δ at *Pmax* at mid-span (mm)	Load at permissible deflection (kN)		% of *Pmax* (kN)	
		l/360	*l/180*	*l/360*	*l/180*
A1/00	8.22	605.4	1002.46	54%	90%
A1/50	8.43	579.2	974.6	52%	88%
A1/75	10.33	584.1	842.3	59%	85%
A1/100	8.91	363.2	648.2	43%	78%

5.4. Response of the beam in Group B:

In Group B with *a/d* ratio of 1.5, only specimen, B1.5/100 was constructed with ρ_w equal of 100%. The main focus of the present study was to cover the boundary cases of the deep beam with a low *a/d* (i.e., Beams in Group A with *a/d* = 1) and high a/d (i.e., Beams in Group C with *a/d* = 2). Beam B1.5/100 serves to verify the behaviour of FRP-RC beep beams with web reinforcements, with an intermediate value of *a/d* ratio.

Crack development and failure mode in B1.5/100:

The first flexural crack at mid-span appeared at 130 kN of loading. The new flexural cracks began to appear and lengthened toward the loading plate as the load increased. Initial Diagonal cracks occurred after 230 kN of load was applied. The Initial Diagonal cracks formed approximately at the interior edge of the support, propagating toward the loading plate, and to a distance less than the mid-height of the specimen. The formation of new flexural cracks eventually stopped and existing ones become wider, particularly after reaching 260 kN.

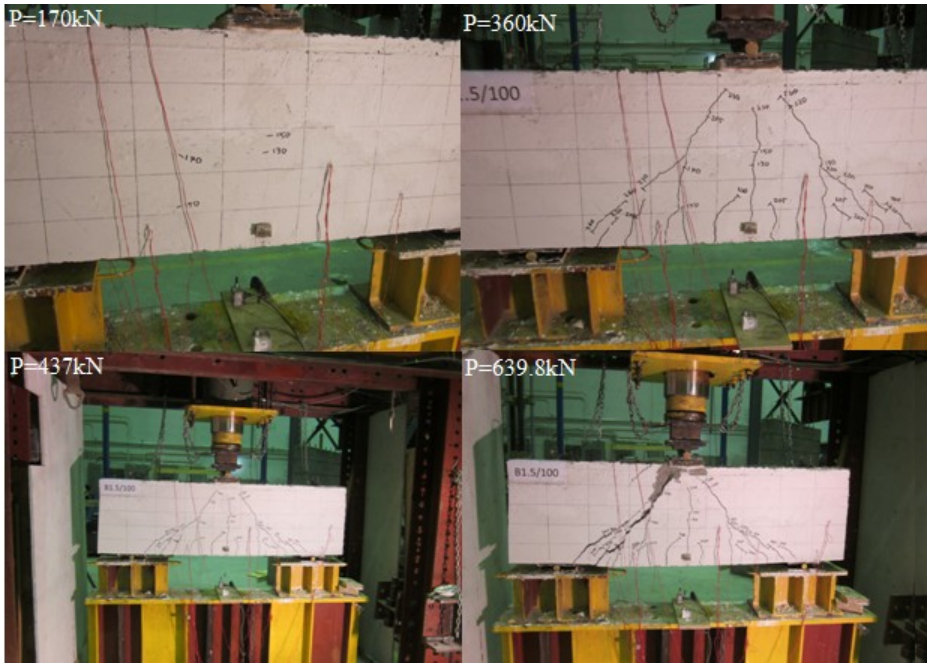

Fig. (5.33) The crack patterns in beam B1.5/100 at four different loading.

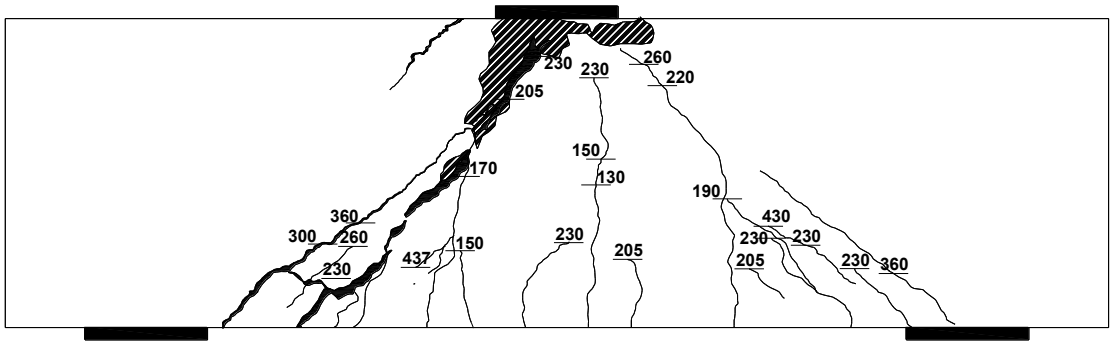

Fig. (5.34) Crack pattern of specimen B1.5/100

A new diagonal cracks formed and existing ones propagated in the direction towards the loading plate up to a load of approximately 430 kN. By increasing the load, a sudden thunderous sound was heard at 82.2% of P_{max}. When the ultimate load 639.8 kN was reached, the concrete at the loading plate zone crushed (shear compression failure). At

the same time, the main concrete strut failed followed by several diagonal cracks. Specimen B1.5/100 exhibited a similar pattern of failure as Specimen A1/75, but had a slightly less magnitude of the failure load. Figure (5.33) shows pictures of the crack patterns for beam B1.5/100 at four different loading stages, while Figure (5.34) illustrates the crack patterns at failure with the load level when each crack was first observed. The cracks that caused the failure are marked in bold lines in Figure (5.34).

Load –Deflection response of B1.5/100:

When the maximum load was reached, the deflections at mid span were 11.9 mm and 12.5 mm for both sides. After reaching P_{max}, the load started to drop with increased deflection, until failure occurred. The maximum deflections at mid span were 13.7 mm and 14.5 mm at the two sides. The load versus mid-span deflection curves of specimen B1.5/100 are plotted in Figure (5.35).

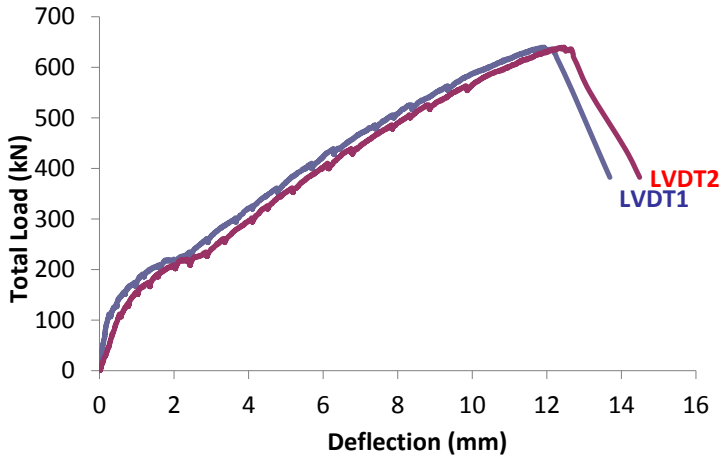

Fig. (5.35) Deflection at mid-span of specimen B1.5/100

Load –Strain response of the main and web reinforcements in B1.5/100:

The mid-span strains in the main GFRP longitudinal reinforcements at the upper and the lower faces of the beam at different loading stages are shown in Figure (5.36). At the load level of 96 kN, the tensile strains began to increase as loading was increased. Also it can be noted from the figure that the average strain increased at a higher rate at the loads of 96 to 171kN and the strain rate stabilized. The opening of the cracks occurred at that level of loads which lead to the elongation in the rebar resulting in a higher strain rate.

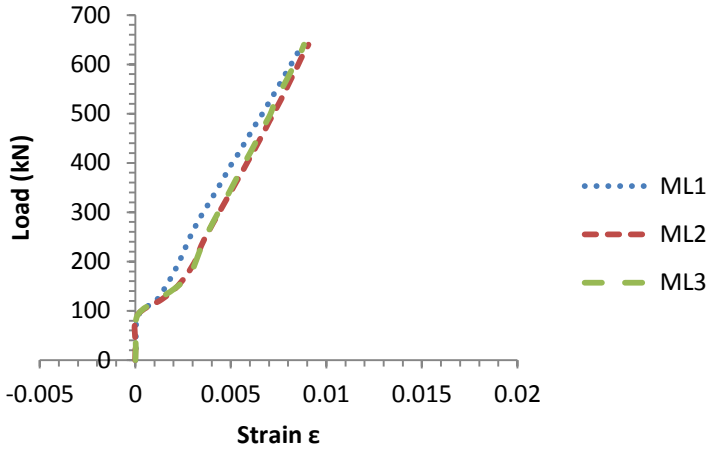

Fig. (5.36) Strain in the middle of the main tension GFRP reinforcement of specimen B1.5/100

Figure (5.37) shows the strain response of the rebar at the extension edge of beyond the supporting plate (the nodal zone). From the Figure (5.37) it can be observed that the strain in the GFRP rebars at this region reached only 46.7% of the ultimate strain, indicating that the anchorage of the rebar was sufficient. The strain gauge installed on the top longitudinal GFRP reinforcement did not work in this case.

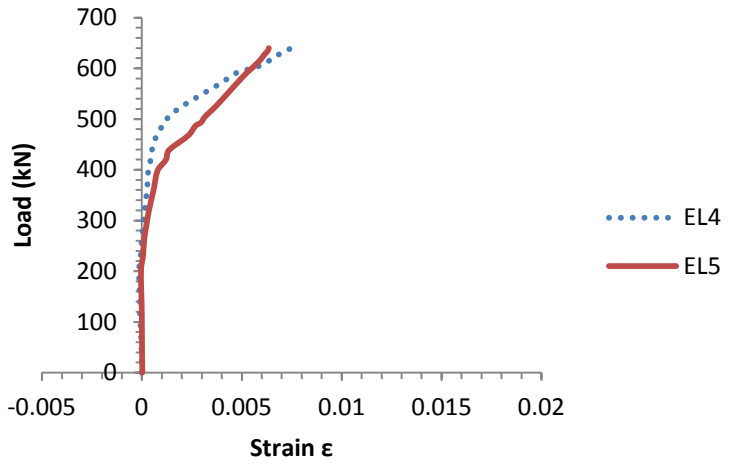

Fig. (5.37) Strain in the end of the main tension GFRP reinforcement of specimen B1.5/100

The strains in the vertical and the horizontal GFRP web reinforcements located on the both sides of the beam for different loading stages are shown in Figures (5.38) and (5.39). At the load of 144.5 kN, the tensile strain in gauge VR8 (Fig. 5.38) in a stirrup located near the right support but crossing a main strut, began to increase as the loading was increased. On the other hand, the strain gauge VR9, which is located on a stirrup left of strain gage VR8 recorded the strain increase later at 205.7 kN. The diagonal crack in the region appeared between the two load levels. The strain gage VR9 is located clearly within the assumed direction of main strut. Therefore, the convergence between the experimental observation and the reading of strain gage VR9 is consistent. From the Figure (5.38) can be observed that the strain in the vertical GFRP reinforcement reached only 66.82% of the ultimate strain, while in the horizontal web reinforcements, it reached only 25.07% of ε_{Fu}.

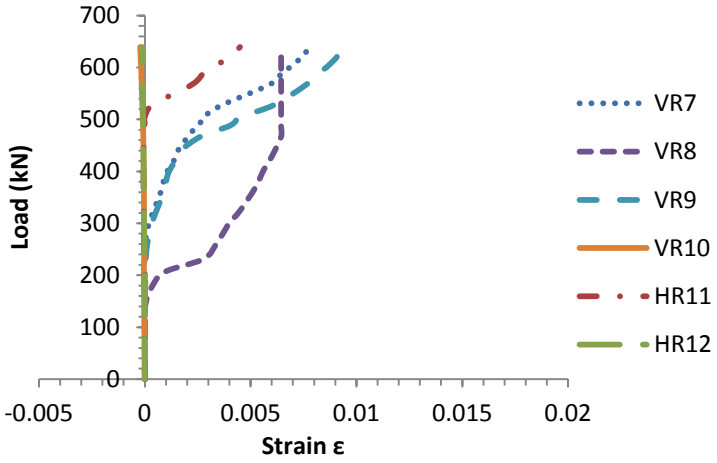

Fig. (5.38) Strain in the vertical and horizontal GFRP web reinforcement right side of specimen B1.5/100

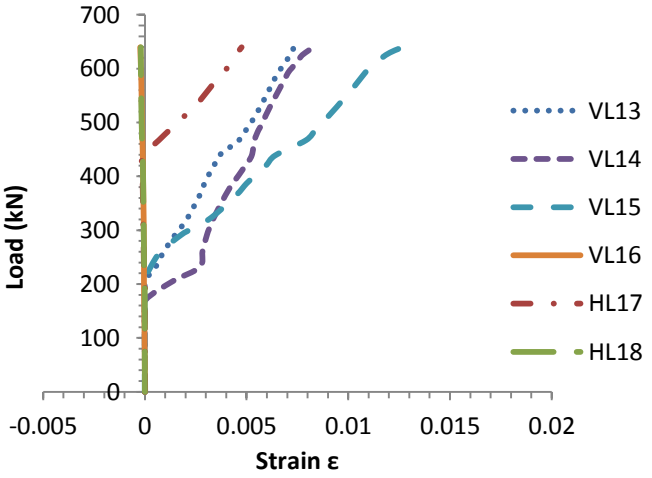

Fig. (5.39) Strain in the vertical and horizontal GFRP web reinforcement left side of specimen B1.5/100

5.5. Response of Beams in Group C

The beams in this group had *a/d* ratio of 2, and except for the amount of web reinforcement, all four specimens in this group are identical. The amount of web reinforcements, ρ_w provided in C2/00, C2/50, C2/75 and C2/100 are 0, 38, 60, and 100 %, respectively; where, 100% indicates the minimum web reinforcements required for crack control.

5.5.1. Response of Beam C2/00:

Crack development and failure mode in C2/00:

The formation of the first flexural crack at the bottom of the mid-span appears at 30% of maximum loading. The new flexural cracks began to appear and lengthened toward the loading plate as the load increased. Initial Diagonal cracks occurred after approximately 53% of the maximum load was applied. The initial diagonal cracks formed close to the interior edge of the support, propagating toward the loading plate to the mid-height of the specimen. New diagonal cracks formed in the general direction between the supports and the load point, at the mid-depth of the beam. The formation of new flexural cracks eventually stopped after reaching 57.3% of P_{max}.

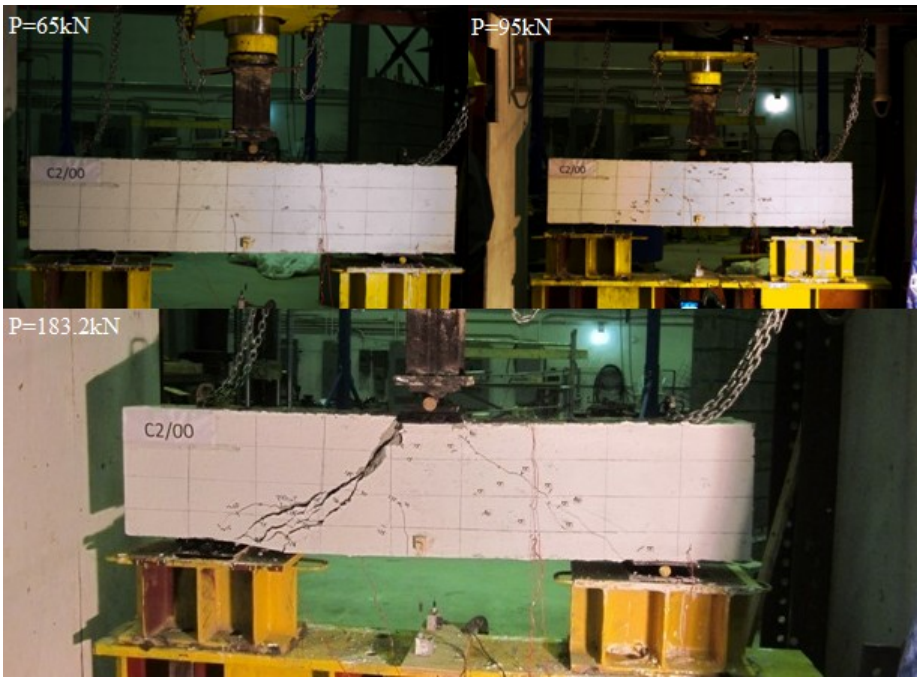

Fig. (5.40) The crack patterns in beam C2/00 at three different loading.

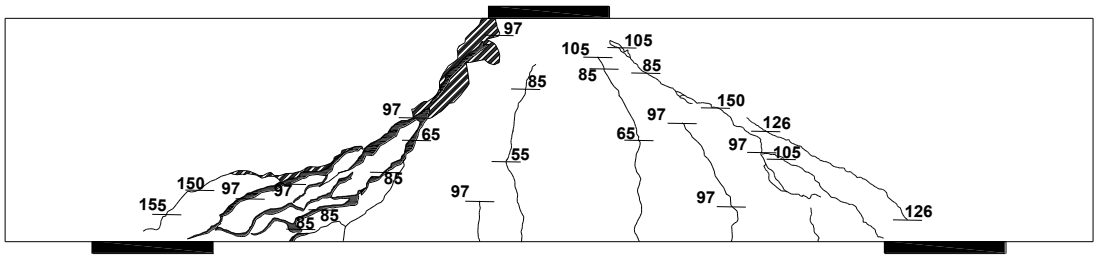

Fig. (5.41) Crack pattern of specimen C2/00

By increasing the load, more diagonal cracks were developed in the directions parallel to the axes of the strut. Developing a new diagonal cracks was stopped after reaching 84.6% of P_{max} and the existing ones widened or lengthened until the failure occurred.

The beam failed by crushing of strut when the load reached maximum level of 183.2 kN. The failure occurred at the mid-depth of the beam, longitudinally between the end of the loading plate and the beginning of a strut, following the formation of several diagonal cracks. This type of failure (strut crushing failure) occurred since there was no web reinforcement provided in the beam. Figure (5.40) shows the pictures of the crack patterns for beam C2/00 at four different loading stages, while, Figure (5.41) illustrates the crack patterns at failure with the loads at each crack marked when first observed. The cracks that caused the failure are marked in bold lines in Figure (5-40).

Load –Deflection response of C2/00:

When the maximum load was reached, the deflections at mid span were 10.4 mm and 10.2 mm at the two sides. As can be seen from Figure (5.42), the maximum deflection

coincided with P_{max} which is in contrast with specimens in group A. The load versus mid-span deflection curves of specimen C2/00 are plotted in Figure (5.42).

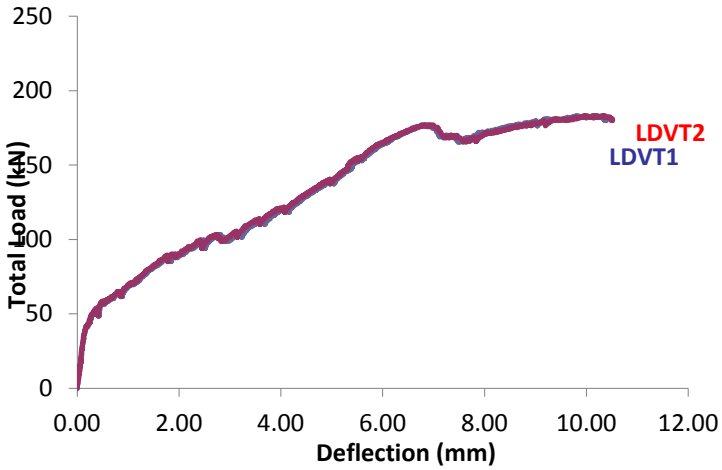

Fig. (5.42) Deflection at mid-span of specimen C2/00

Load –Strain response of the main reinforcement in C2/00:

The mid-span strains in the upper and the lower main GFRP longitudinal reinforcement at different loading stages are shown in Figure (5.43). At the load of 43.4 kN, the tensile strain began to increase as loading was increased. This load level is in approximate agreement with initial flexural crack that was observed from the experimental test. Figure (5.44) shows the strain response of a bottom rebars at the extension edge beyond the supporting plate (the nodal zone). From Figure (5.44) it can be observed that the strain of the rebar in that region reached 26.5% of the ultimate strain of GFRP rebar, indicating that the anchorage of the rebar was satisfactory. The strain-load response located at the top longitudinal GFRP reinforcement is shown in Figure (5.45).

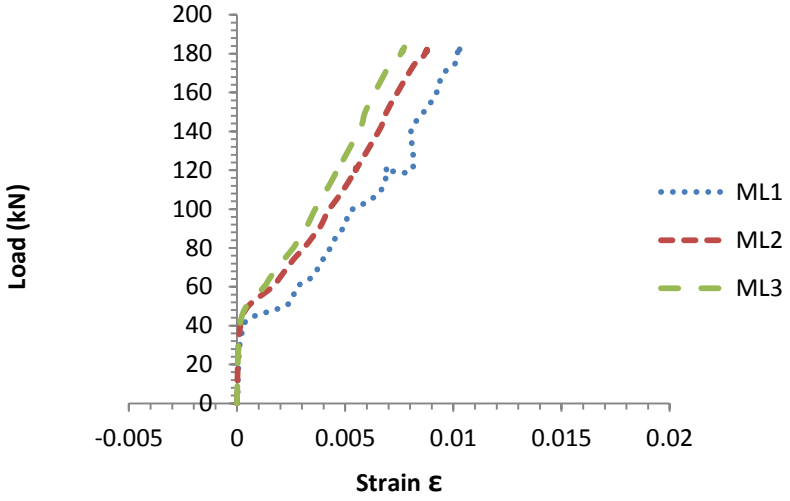

Fig. (5.43) Strain in the middle of the main tension GFRP reinforcement of specimen C2/00

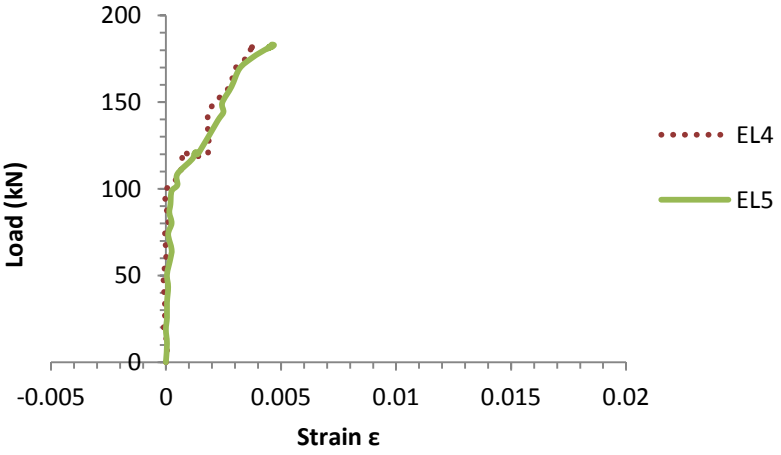

Fig. (5.44) Strain in the end of the main tension GFRP reinforcement of specimen C2/00

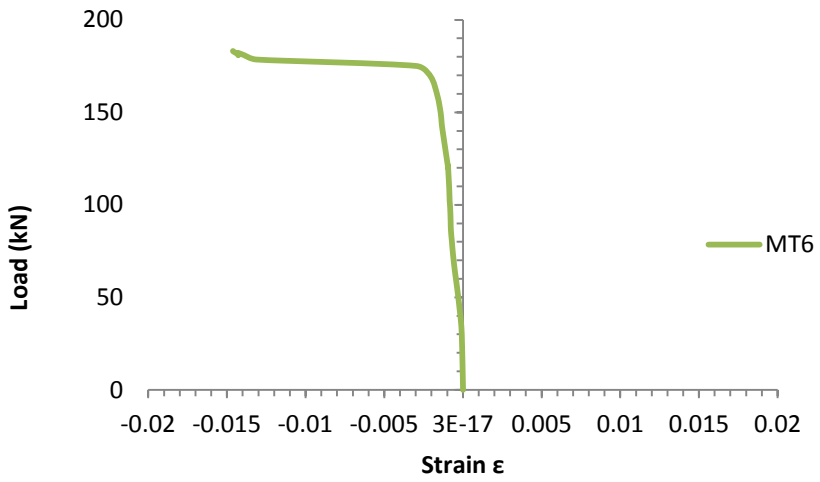

Fig. (5.45) Strain in the middle of the main top GFRP reinforcement of specimen C2/00

5.5.2. Response of Beam C2/50:

General response of C2/50:

The crack pattern, load-deflection response, and the strain-load response of the beam C2/50 are illustrated in Figures (5. 46, 47, 48, 49, 50 and 51). As can be seen from the results, it is clear that the beam with 38 % of web reinforcement C2/50 exhibits relatively similar behaviour and has higher loads than that observed from the previous beam C2/00. The propagation rate of flexural cracks of this beam is higher than that observed in the previous beam. Although beam C2/50 failed in the same manner as C2/00, the pre-failure damage appears to be less severe than that in C2/00.

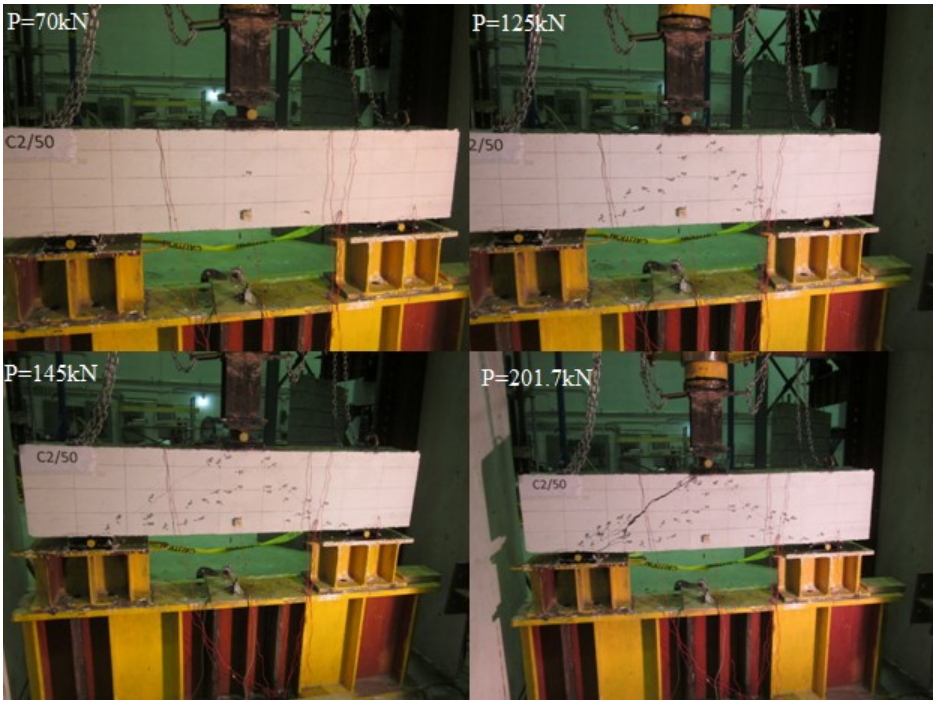

Fig. (5.46) The crack patterns in beam C2/50 at four different loading.

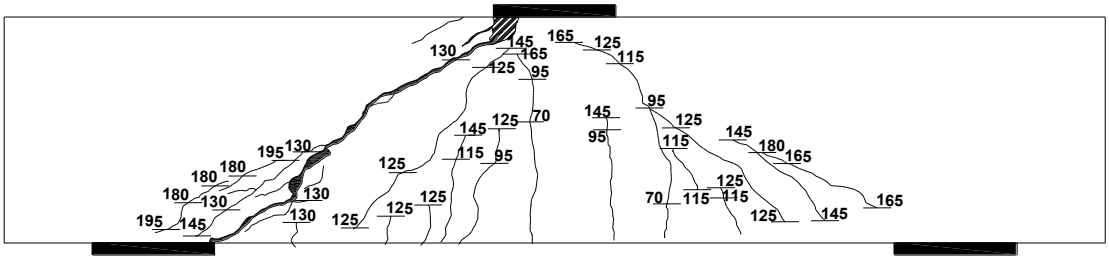

Fig. (5.47) Crack pattern of specimen C2/50

Load –Deflection response of C2/50:

The deflection reading was taken at each load increment. When the maximum load was reached, the deflections at mid span were 9.03 mm and 9.04 mm for both sides. After reaching P_{max}, the load started to drop for increased deflection, until failure occurred. The

maximum deflections at mid span were 10.5 mm and 10.4 mm at the two sides. The load versus mid-span deflection curves of specimen A1/75 are plotted in Figure (5.48).

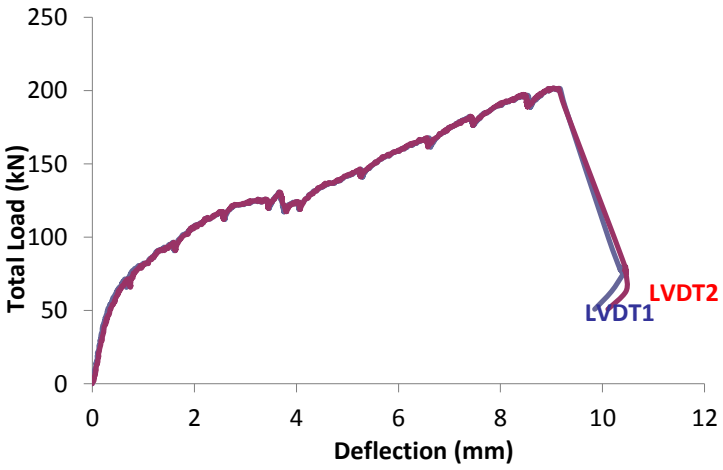

Fig. (5.48) Deflection at mid-span of specimen C2/50

Load –Strain response of the main and web reinforcements in C2/50:

The mid-span strains in the upper and the lower main GFRP longitudinal reinforcement at different loading stages are shown in Figure (5.49). At the load of 46.79 kN, the tensile strain began to increase as loading was increased. This load level is less than that corresponding to the initial flexural crack that was observed from the experimental test. Figure (5.50) shows the strain response of a bottom rebars at the extension edge beyond the supporting plate (the nodal zone). From Figure (5.50) it can be observed that the strain of the rebar in that region reached 10% of the ultimate strain of GFRP rebar, indicating that the anchorage of the rebar was satisfactory. The strain-load response located at the top longitudinal GFRP reinforcement is shown in Figure (5.51).

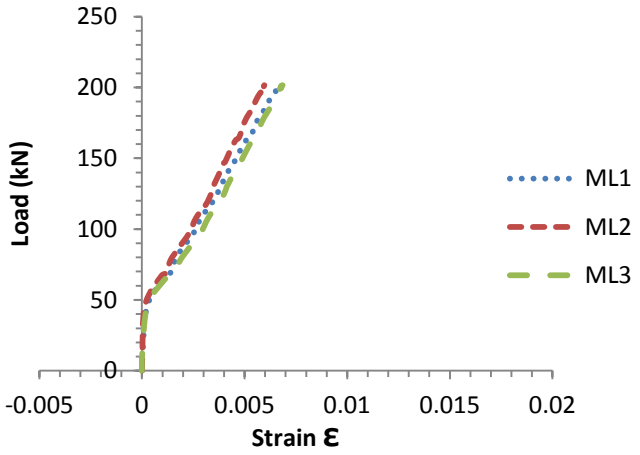

Fig. (5.49) Strain in the middle of the main tension GFRP reinforcement of specimen C2/50

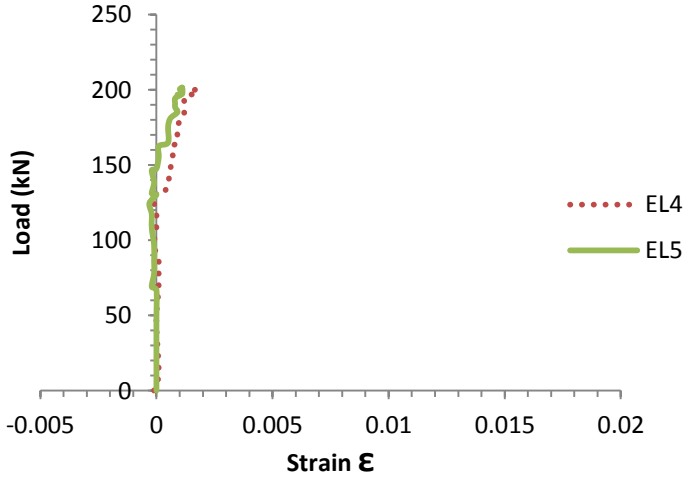

Fig. (5.50) Strain in the end of the main tension GFRP reinforcement of specimen C2/50

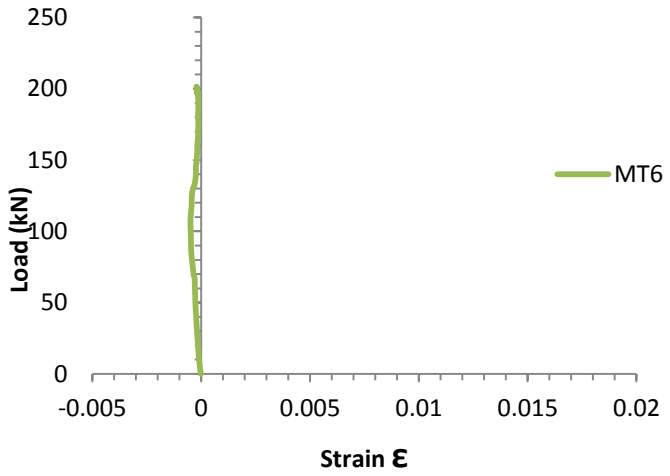

Fig. (5.51) Strain in the middle of the main top GFRP reinforcement of specimen C2/50

The strains in the vertical and horizontal GFRP web reinforcement on the both sides of the beam at different loading stages are shown in Figures (5.52) and (5.53). At the load of 131.1 kN, the tensile strains recorded by gauges VL7 and VL8 located in the region in of the assumed direction of main struts began to increase as loading was increased. This load approximately corresponds to the diagonal crack observed from the experimental test. From the Figures (5.52) and (5.53) we can see that level of strain in the vertical GFRP reinforcement was limited to 67% of the ultimate strain.

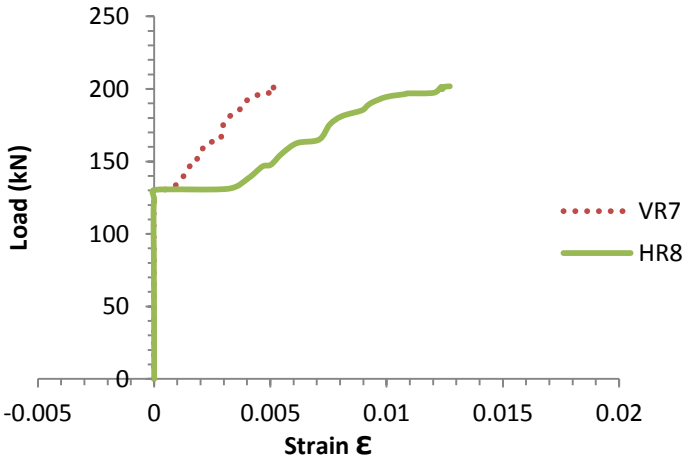

Fig. (5.52) Strain in the vertical GFRP web reinforcement left side of specimen C2/50

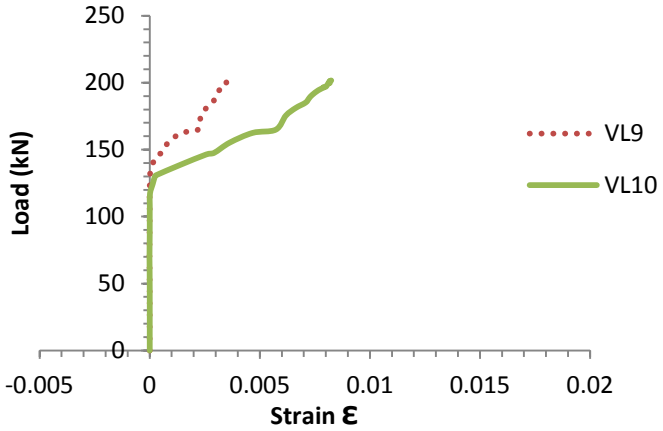

Fig. (5.53) Strain in the vertical GFRP web reinforcement right side of specimen C2/50

5.6. Response of Beam C2/75:

Crack development and failure mode in C2/75:

The first flexural crack at mid-span appeared at 80 kN of loading. New flexural cracks began to appear and lengthened toward the loading plate as the load increased. The propagation rate of flexural cracks in specimen C2/75 is much lower compared to the two previous specimens. Initial diagonal cracks occurred after 115 kN of load was applied. The initial diagonal cracks formed between the support and load point at the mid-depth of the beam. The formation of new flexural cracks eventually stopped after reaching 67.1% of P_{max}.

By increasing the load, more diagonal cracks were developed in the directions parallel to the axes of the strut. New diagonal cracks formed and existing ones propagated in the directions parallel to the axes of the strut up to the failure. When the ultimate load 193.6 kN was reached, the beam C2/75 failed by crushing of strut. Figure (5.54) shows the pictures of the crack patterns for beam C2/75 at four different loading

stages, while Figure (5.55) illustrates the crack patterns at failure with the loads at each crack marked when first observed. The cracks that caused the failure are marked in bold lines in Figure (5.55).

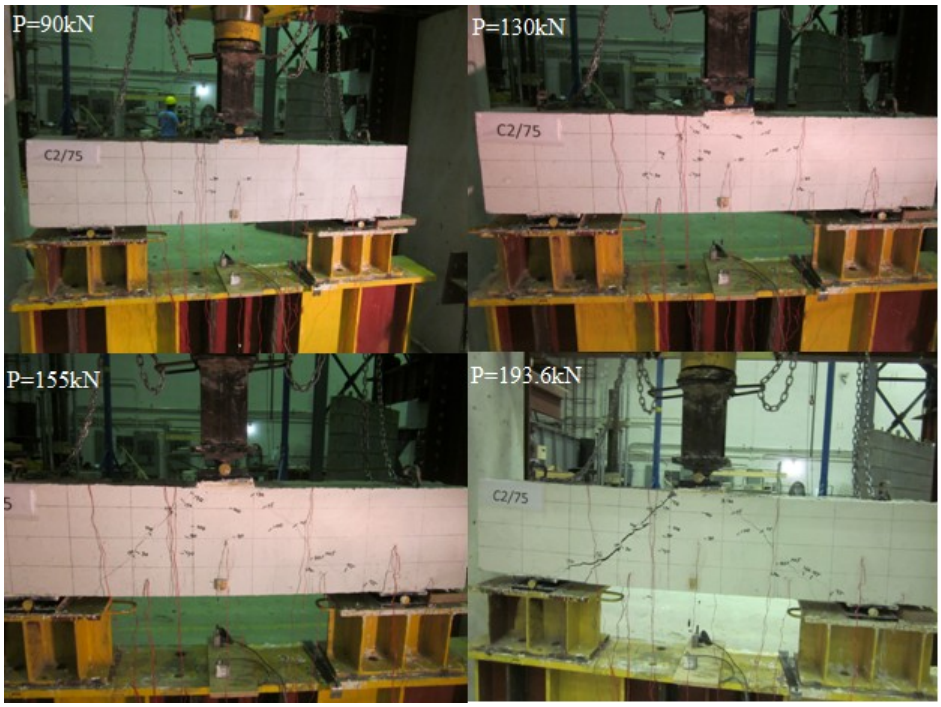

Fig. (5.54) The propagation of the crack patterns in the beam C2/75 at four different loading.

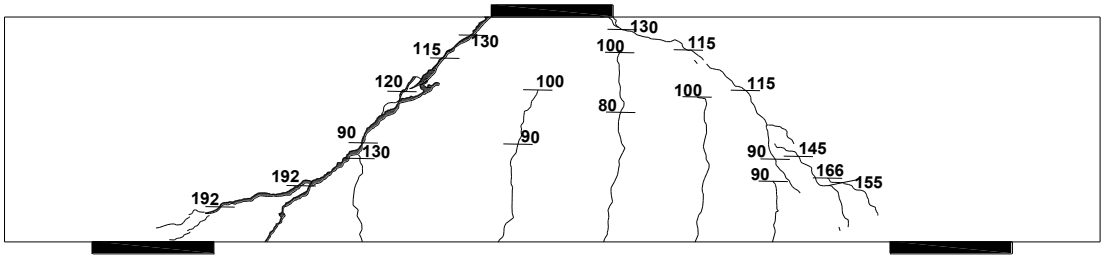

Fig. (5.55) Crack pattern of specimen C2-75

Load –Deflection response of C2/75:

When the maximum load was reached, the deflections at mid span were 8.12 mm and 8.96 mm on both sides. After reaching P_{max}, the load started to drop for increased deflection, until failure occurred. The maximum deflections at mid span were 9.18 mm and 10.3 mm at the two sides. The load versus mid-span deflection curves of specimen C2/75 are plotted in Figure (5.56).

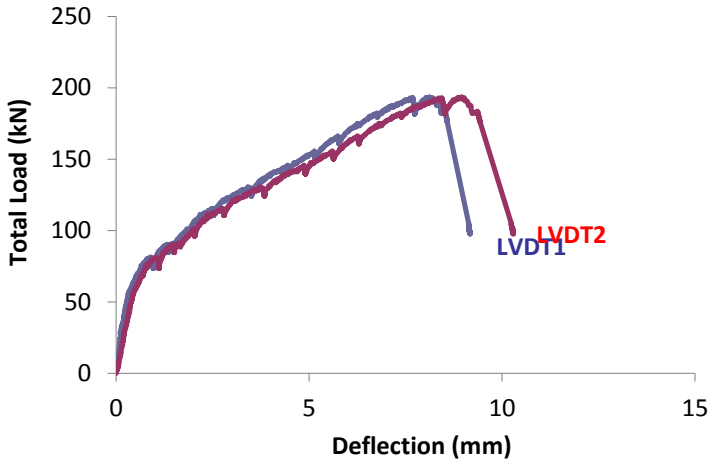

Fig. (5.56) Deflection at mid-span of specimen C2/75

Load –Strain response of the main and web reinforcements in C2/75:

The mid-span strains in the upper and the lower main GFRP longitudinal reinforcement at different loading stages are shown in Figure (5.57). At the load of 36.71 kN, the tensile strains in these bars (gauges ML2 and ML3) began to increase as loading was increased. While the tensile strain recorded by ML1 began to increase after applying 58.39 kN of load. These loads are less than that corresponding to the initial flexural crack that was observed from the experimental test.

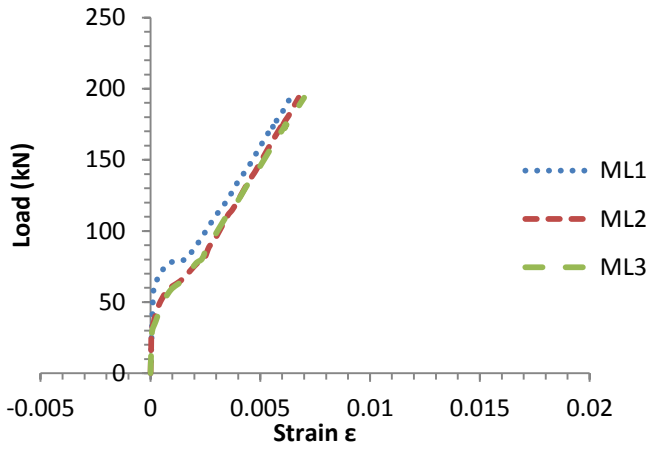

Fig. (5.57) Strain in the middle of the main tension GFRP reinforcement of specimen C2/75

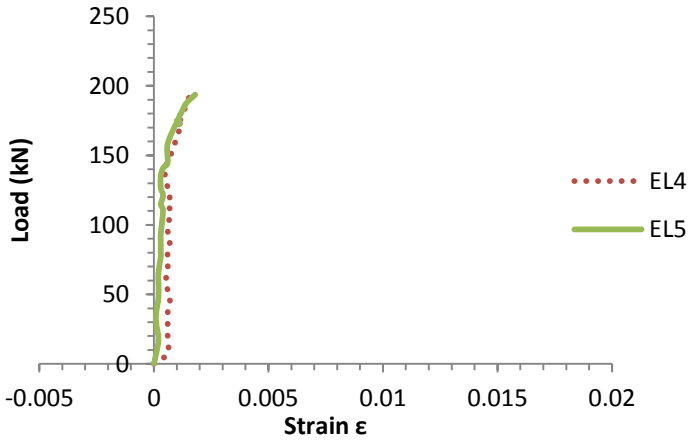

Fig. (5.58) Strain in the end of the main tension GFRP reinforcement of specimen C2/75

Figure (5.58) shows the strain response of a tensile rebar at the extension edge beyond the supporting plate (the nodal zone). From the results it can be observed that strain in the GFRP rebar in this region reached up to 10.6% of the ultimate strain, indicating that the anchorage of the rebar was satisfactory. The strain-load response of the top longitudinal GFRP reinforcement is shown in Figure (5.59). The lateral pressure from the loading

plate and the action of the two loading compression strut at the nodal zone (node) make strain in the top rebar very small.

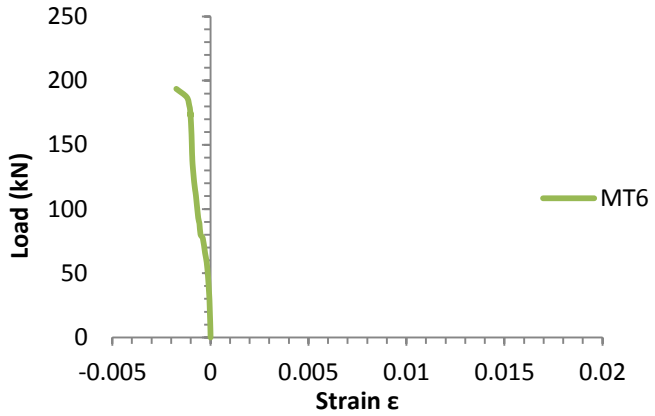

Fig. (5.59) Strain in the middle of the main top GFRP reinforcement of specimen C2/75

The strains in the vertical and the horizontal GFRP web reinforcement on both sides of the beam at different loading stages are shown in Figures (5.60) and (5.61). At the load of 80.3 and 93.2 kN, the tensile strains in the web reinforcement near the left and the right support region and crossing the main struts in the assumed direction, began to increase as the loading was increased.

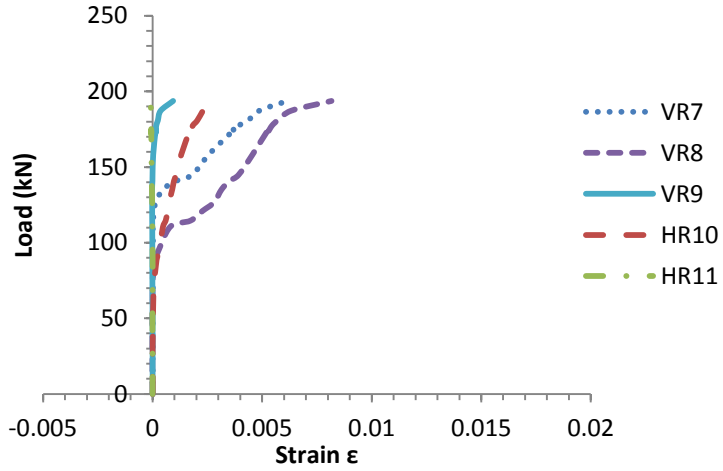

Fig. (5.60) Strain in the vertical and horizontal GFRP web reinforcement right side of specimen C2/75

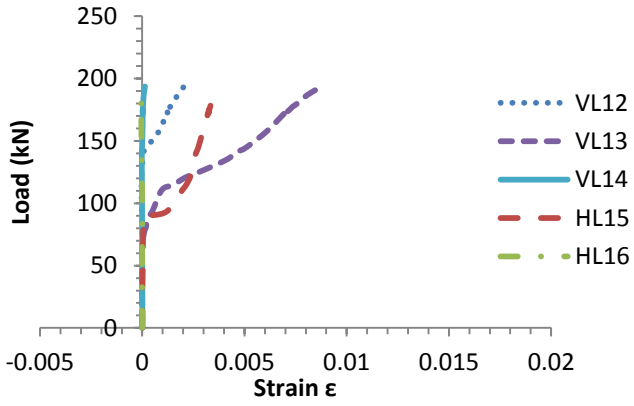

Fig. (5.61) Strain in the vertical and horizontal GFRP web reinforcement left side of specimen C2/75

These loads are less than that for the first diagonal crack as observed from the experimental test. From the Figures (5.60) and (5.61) it can be observed that the strain in the vertical and horizontal web reinforcement reached only 42.9% and 19.0% of the ultimate strain of GFRP, respectively.

5.7. Response of Beam C2/100:

General response of C2/100:

The first flexural crack at mid-span appeared at 80 kN of loading. The new flexural cracks began to appear and lengthened toward the loading plate as the load increased. Initial diagonal cracks occurred after 140 kN of load was applied. The initial diagonal cracks formed approximately at the interior edge of the support propagated towards the loading plate. The propagation rate of flexural cracks in Specimen C2/100 was found to be similar to that of Specimen C2/75, but much lower compared to the other two specimens with less or without web reinforcement. On further increase in the load up to 74.6% of P_{max}, both the formation of the new flexural cracks and the new diagonal cracks

stopped and the existing ones widened up to the failure. Contrary to the other three previous beams of group C, Specimen C2/100 failed in shear compression failure.

When the ultimate load of 248.1 kN was reached, the concrete at the end of one of the main struts at the loading plate failed by crushing. Figure (5.62) shows pictures of the propagation of crack patterns for beam C2/100 at four different loading stages. The shear compression failure occurred near the loading plate which is indicated by cross-hatchings in Figure (5.63). Figure (5.63) illustrates the crack patterns at failure with the loads at each crack marked when first observed.

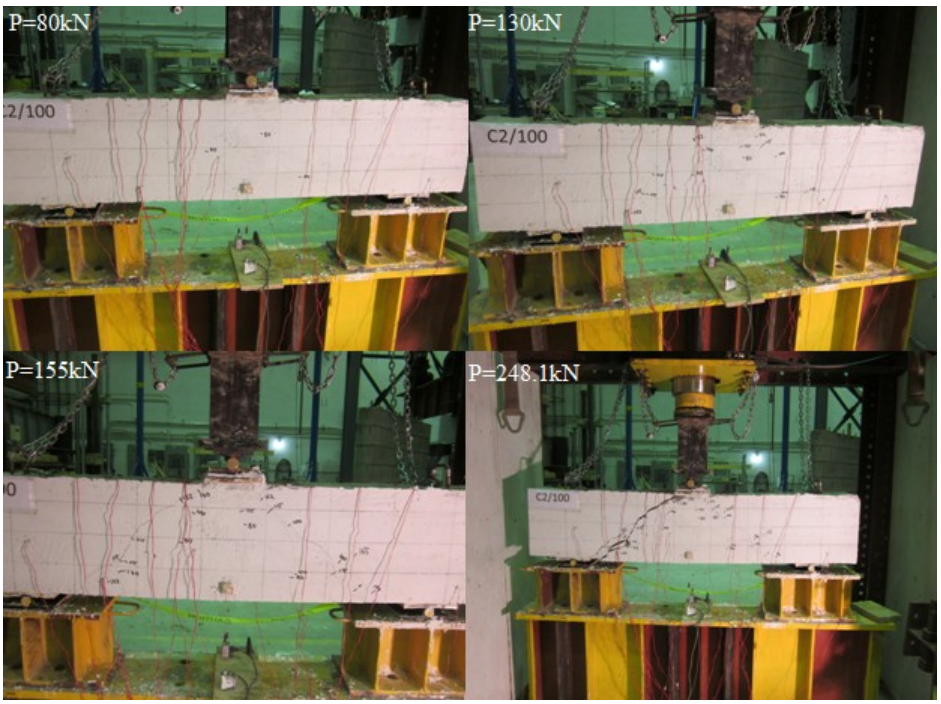

Fig. (5.62) The propagation of the crack patterns in the beam C2/100 at four different loading.

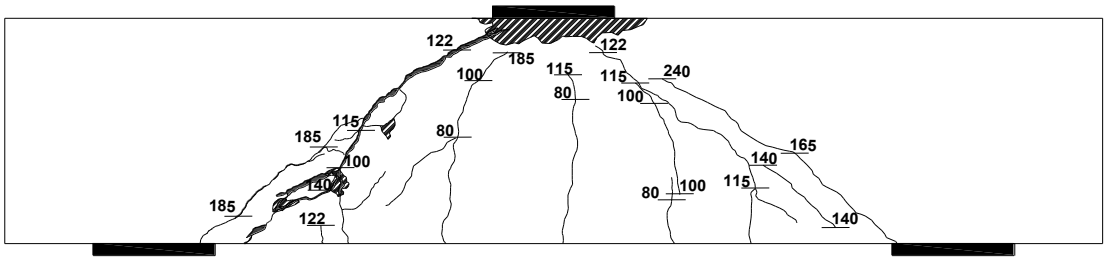

Fig. (5.63) Crack pattern of specimen C2/100

Load –Deflection response of C2/100:

When the maximum load was reached, the deflections at mid span were 12.04 mm and 12.23 mm on both sides. After reaching P_{max}, the load started to drop for increased deflection, until failure occurred. The maximum deflections at mid span were 14.31 mm and 14.51 mm at the two sides. The load versus mid-span deflection curves of specimen C2/75 are plotted in Figure (5.64).

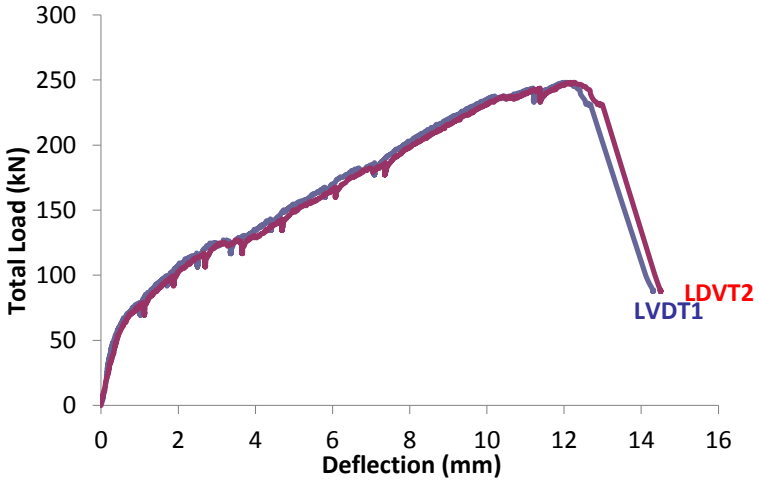

Fig. (5.64) Deflection at mid-span of specimen C2/100

Load –Strain response of the main reinforcements in C2/100:

The mid-span strains in the upper and the lower GFRP longitudinal reinforcement at different loading stages are shown in Figure (5.65). At the load of 48.0 kN, the tensile strain began to increase as loading was increased. This load is less than that corresponding to the first flexural crack as observed from the experimental test. Figure (5.66) shows the strain response of a bottom rebars at the extension edge beyond the supporting plate (the nodal zone). From Figure (5.66) it can be observed that the strain of the rebar in that region reached 11.76% of the ultimate strain of GFRP rebar, indicating that the anchorage of the rebar was satisfactory. The strain-load response for top longitudinal GFRP reinforcement at the mid-span is shown in Figure (5.67). While the failure occurred in this zone, the rebar was not found to be deformed yet, and only 19.83% of the ultimate strain of GFRP rebar has been reached.

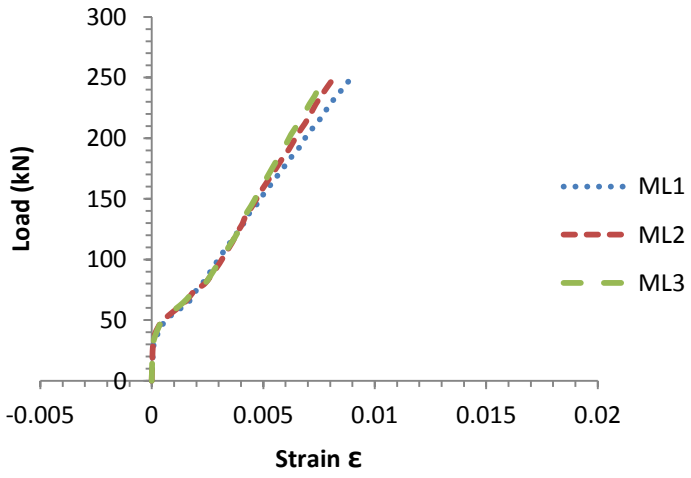

Fig. (5.65) Strain in the middle of the main tension GFRP reinforcement of specimen C2/100

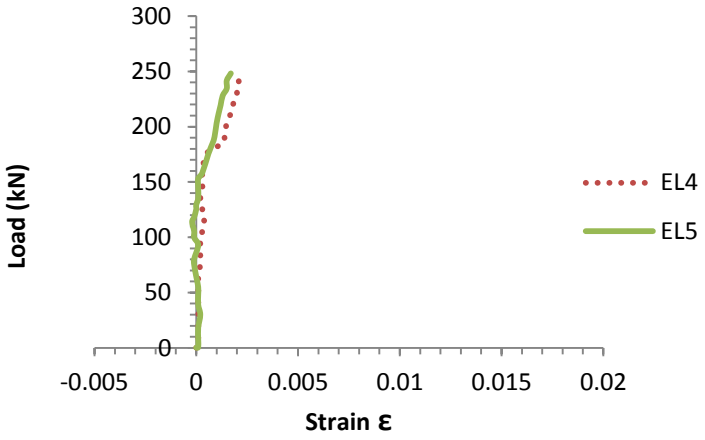

Fig. (5.66) Strain in the end of the main tension GFRP reinforcement of specimen C2/100

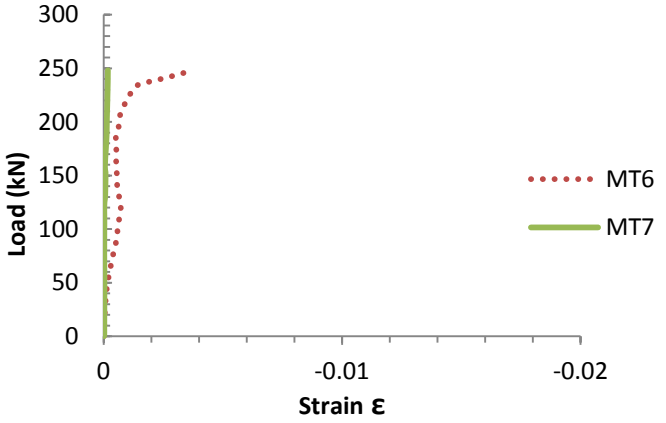

Fig. (5.67) Strain in the middle of the main top GFRP reinforcement of specimen C2/100

The strains in the vertical and the horizontal GFRP web reinforcements on both sides of the beam at different loading stages are shown in Figures (5.68) and (5.69). At the load of 113.8 and 125.1 kN, the tensile strains in the web reinforcement near the left and the right support regions and at the crossing the main struts in the assumed direction, began to increase as the loading was increased. These loads were found to be less than that for the first diagonal crack as observed from the experimental test. From Figures (5.68) and (5.69) it can be observed that the strain in the vertical and horizontal web reinforcement reached only 52.6% and 55.6% of the ultimate strain of GFRP, respectively.

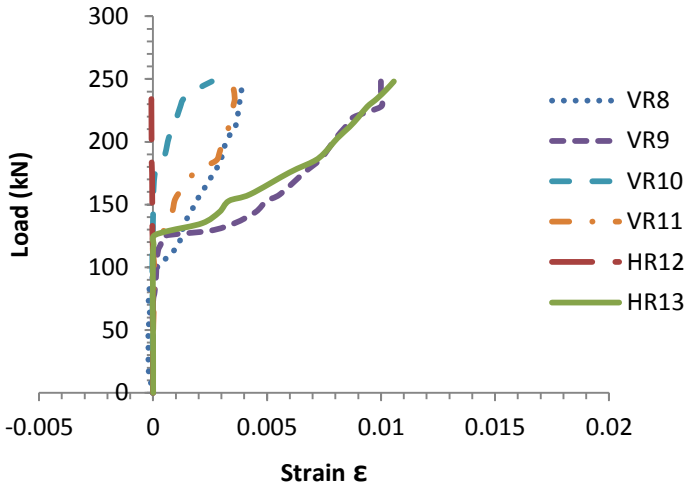

Fig. (5.68) Strain in the vertical and horizontal GFRP web reinforcement right side of specimen C2/100

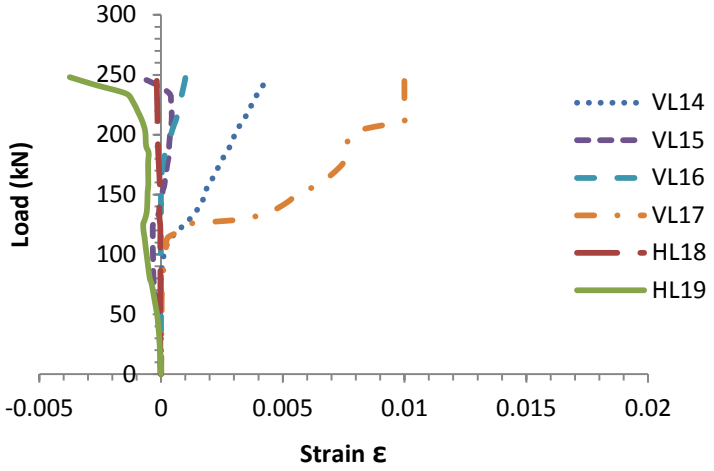

Fig. (5.69) Strain in the vertical and horizontal GFRP web reinforcement left side of specimen C2/100

Figure (5.70) shows the crack intersects the web reinforcement in specimen C2/100 after failure. Similar to the beam A1/75, big cracks occurred in the strut and at the node and intersected with the web reinforcement; the rebars did not been deformed or damaged yet.

Fig. (5.70) The crack intersects the web reinforcement specimen C2/100

Comparison of beam performances within group C:

In the early stages of loading approximately at 24, 13, 30 and 19% of the ultimate load for four specimens: C2/00, C2/50 C2/75 and C2/100, respectively, similar characteristics of crack patterns were observed. Flexural cracks were initiated vertically in the region of pure bending between the two supports where the shear stress is zero. Additional flexural cracks began to appear in the mid-span of the beam and lengthened toward the loading plate as the load increased. After reaching approximately 52, 64, 48 and 50% of the ultimate load in specimens C2/00, C2/50, C2/75 and C2/100, respectively, the flexural cracks were stabilized, and stopped propagating.

The first diagonal crack between the loading point and support appeared at 57, 85, 67 and 75% of maximum loading for four specimens: C2/00, C2/50 C2/75 and C2/100,

respectively. Because of the dominance of the shear stresses, the cracks in the region of the shear span were observed to be inclined and propagated toward the loading point. After reaching approximately 62 and 75% of the ultimate load in specimens C2/00 and C2/100, respectively, the diagonal cracks were stabilized, and stopped propagating. While the propagation of flexure cracks in the beam C2/50 and C2/75 continued until they were very close to the failure load. Generally, the failure crack patterns of the four beams within group C were almost similar; however, Beams C2/00 and C2/50 were more extensively cracked than the other two beams with higher web reinforcement.

The failure mode of all four beams in this group was brittle. Two types of brittle failure (strut crushing and shear compression) were observed. The beams C2/00, C2/50, and C2/75 failed by crushing of the strut since there were no sufficient web reinforcements provided in the beams. On the other hand, the beam specimen with 100% of web reinforcement failed in shear compression mode of failure.

Table (5.4) shows a comparison among the specimens in Group C at different stages of the applied loads. It is noted that an increase in the amount of web reinforcement resulted in an increase in the capacity up to 26%.

Table (5.4) The applied loads at different stages of the four beams in Group C.

Specimens	Initial Flexure crack		Initial Digonal crack		Failure Load (kN)
	Occurred at % of P_{max}	Continued up to % of P_{max}	Occurred at % of P_{max}	Continued up to % of P_{max}	
C2/00	23.70%	53.00%	57.3%	62%	183.2
C2/50	23.00%	65.00%	85.2%	Failure	201.7
C2/75	30.20%	48.10%	67.1%	Failure	193.6
C2/100	19.40%	50.40%	74.6%	74.6%	248.1

The load versus mid-span deflection curves of the all specimens in Group C are shown in Fig. (5.71). As can be seen from these curves, the failure loads (P_{max}) were 183.2, 201.7, 193.6and 248.1 kN for beams C2/00, C2/50, C2/75 and C2/100, respectively. After reaching the failure loads (P_{max}) in most of the specimens, the load started to drop. When the maximum load was reached, the deflections at mid span were 10.36, 9.12, 8.12 and 12.04 mm for beams C2/00, C2/50, C2/75 and C2/100, respectively. In general, the mid-span deflection at the maximum load for beams with web reinforcement was lower than that with less or no web reinforcement.

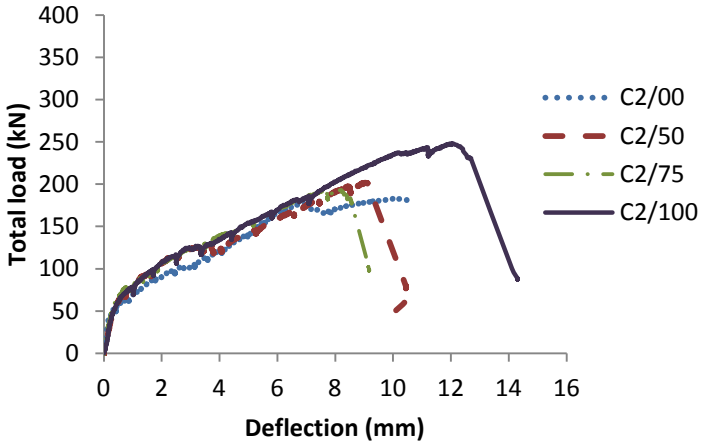

Fig.(5.71) Load- Deflection response for specimens in Group C

The applied loading corresponding to the permissible deflection limits *l/360* and *l/180* were analyzed and compared. The deflection limit of *l/360* was reached at percentage between 53 to 68% of P_{max}, while the second limit of *l/180* was reached at larger percentage of P_{max} from 76 to 97%. These results coincided with the results of the beams in Group A. Table (5.5) shows the comparison of the deflection at maximum loads and at permissible deflection limits for all beams in Group C.

Table (5.5) The deflection at different stages of load for all beams in Group C.

Specimens	Δ at *Pmax* at mid-span (mm)	Load at permissible deflection (kN)		% of *Pmax* (kN)	
		l/360	*l/180*	*l/360*	*l/180*
C2/00	10.36	113.2	169.4	62%	93%
C2/50	9.12	130.7	179.5	65%	89%
C2/75	8.12	131.9	188.0	68%	97%
C2/100	12.04	130.3	187.6	53%	76%

5.8. Summary:

The beams exhibit three types of shear failure mode: shear-compression failure, diagonal-splitting failure, and strut crushing failure. The failure mode of these three types is brittle failure. For Group A specimens, Beams A1/00 and A1/50 failed with diagonal-splitting failure. This failure was observed because there was insufficient web reinforcement to resist the tensile stresses in cracked concrete. The concrete at the end of one of the main struts of specimen A1/75 failed in a shear compression failure by crushing and was accompanied by a thunderous sound. Beam A1/100, exhibits relatively similar failure mode and accommodated higher loads than that observed from beam A1/75. In contrast to the beams in Groups A, three beams in group C, C1/00, C1/50 and C1/75 failed by strut crushing failure. While the beam C2/100 failed by crushing of the concrete at the end of one of the main struts (shear compression failure). Although the beam with 100% of web reinforcement C2/100 exhibited relatively similar crack propagation and had higher loads than that observed from the beam C2/75, the beam C2/100 failed by crushing of the concrete at the end of one of the main struts (shear compression failure).

Chapter 6: Effect of the Key Factors and Validation of the Design Provisions

6.1. Introduction:

A synthesis of the experimental results has been provided in this chapter to highlight the effects of the key factors such as, the shear span to depth ratio and the amount of web reinforcement on the behavior of the FRP-RC deep beams. As shown in Chapter 3 for conventional RC deep beams, the shear-span to depth ratio and the amount of web reinforcement is the key factors governing the behaviour of a deep beam. These two parameters are expected to be important for FRP-RC deep beams as well. The experimental plan was thus developed to understand the effects of these two parameters in the behaviour of FRP-RC deep beams. This chapter also presents the comparison of the test results with the design procedure developed for designing FRP-RC deep beam in the context of Canadian (CSA) and (ACI) codes.

Two design procedures in the CAN/CSA-S806-12[2012] code are compared in this chapter to assess their safety and accuracy to estimate the ultimate shear strengths of 13 specimens. These specimens include the nine beams in this research and another four specimens that were tested by Farghaly and Benmokrane [2013]. The procedures included here are the STM model and the shear design procedure in flexural regions in the CAN/CSA-S806-12[2012] code. Also an STM design procedure for FRP-reinforced concrete deep beams is developed in this chapter since the ACI 440.1 R-06[2006] standard does not provide a procedure for designing deep beams reinforced with FRP bars. The design procedure for FRP-reinforced concrete deep beams is similar to the STM approach for conventional beams with some adjustments that account for the

properties of FRP. The suitability of these modified STM design procedures in predicting the ultimate strength of RC deep beams has been verified with the results of the experimental study. The ultimate shear capacity of each specimen as determined experimentally was compared to that estimated using the modified STM provided in ACI 318-08[2008] with adjustment for FRP. They are also compared with the shear capacities calculated using the procedures given in ACI 440.1 R-06 [2006] for normal beams.

6.2. The effect of shear span-depth ratio *a/d*:

A number of experimental studies have been conducted on steel reinforced concrete deep beams to study the effect the span/depth ratio on their behaviour. As mentioned in this thesis, these studies have indicated that the shear span depth ratio and has played a big role on effecting their behaviour. The effect of the shear span-to-depth ratio on the behaviour of concrete deep beams reinforced by FRP has been investigated according to the experimental results. The effect of the shears pan-to-depth ratio *a/d* on the behavior of the beams was assessed by comparing the load-deflection response, cracking pattern, and failure mode of the current experimental specimens.

6.2.1. On the load-deflection behavior:

In general, the mid-span deflection at the maximum load in group A is lower than that of the specimens in group C. For easy comparison and to study the effect of the variables, the ultimate mid-span deflection over the effective depth, Δ/d versus the percentage of the ratio of web reinforcement is plotted in Fig. (6.1). Generally, the group C beams with *a/d*=2 sustained greater ultimate mid-span deflection over the effective depth Δ/d ratio

as compared to the group A beams, i.e., the beams become more flexible with an increase in the shear span-to-depth ratio *a/d*.

The load versus the mid-span deflection curves of the three beams A1/100, B1.5/100 and C2/100 are plotted in Fig (6.2). The mid-span deflection at the maximum load of specimen A1/100 is much lower than the two other specimens. After reaching P_{max} and failure, the load started to drop, with a simultaneous increase of the deflection in all samples.

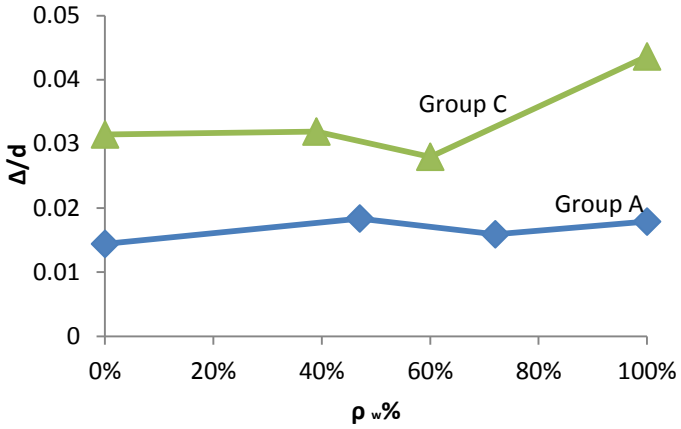

Fig. (6.1) Ultimate mid-span deflection over the active depth Δ/d versus the percentage of the ratio of web reinforcement

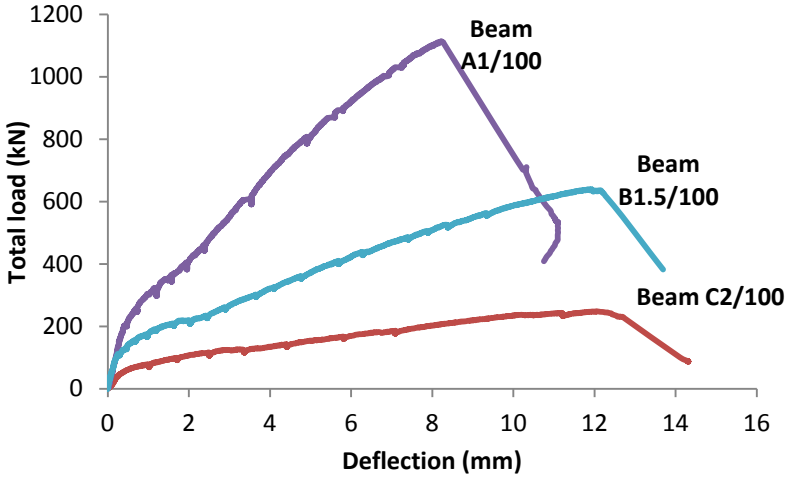

Fig.(6.2) Load deflection response of A1/100,B1.5/100 and C2/100 beams.

As can be seen from the Figure (6.2), beam A1/100 exhibited the steepest load–deflection curve while beam C2/100 had the curve with the shallowest slope. Generally, beams with a higher shear span-to-depth ratio *a/d* had a gentler load deflection curve.

For the three beams, the ultimate mid-span deflection over the effective depth *Δ/d* versus the dimensionless load $2V/f_c`b_wd$ is plotted in Fig. (6.3).The deflection gradually increased for beams with higher shear-span to depth ratio, i.e., with increasing *a/d* ratio, the beam becomes more flexible. These results are in agreement with the experimental investigation by Tan and Lu [1997a] on steel reinforced concrete deep beams. Tan and Lu [1997a] indicated that the stress-deflection curve was gentler in the beams that had a higher *a/d*, and they also observed that the beam becomes more flexible with an increase in the *a/d* ratio.

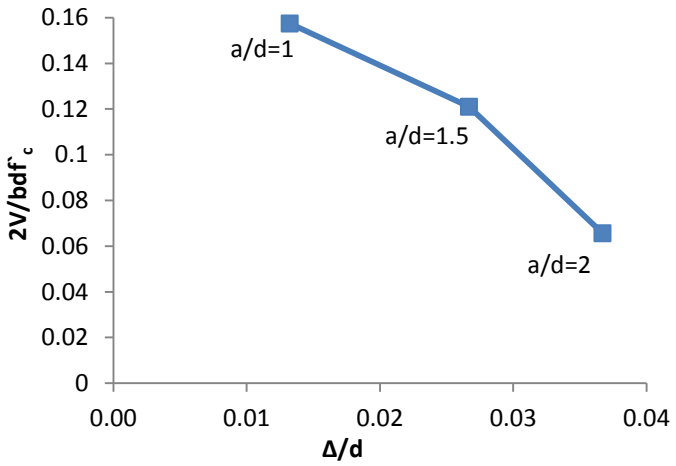

Fig.(6.3) Ultimate shear stress versus *Δ/d* for A1/100,B1.5/100 and C2/100 beams.

6.2.2. On the crack developments:

The formation of the first flexural crack at the bottom of the mid-span appears at 18, 20 and 30% of maximum loading for the three specimens: A1/100, B1.5/100 and C2/100, respectively. The propagation rate of flexural cracks is very similar for the three beams.

Initial diagonal cracks in beams A1and B1.5 occurred after approximately 35% of the maximum load was applied, while it appeared at 56% of P_{max} in specimen C2/100.

Comparing the behaviour of the two groups A and C, the formation of the first flexural crack at mid-span for group A appears at approximately of 20% of the ultimate load, while for group C, the first flexural crack at mid-span appears at approximately 30% of the ultimate load. For all of the specimens, new formation of flexural cracks began to appear and lengthened towards the loading plate as the load increased. After varying durations in the two groups, an initial diagonal crack occurred, approximately at the interior edge of the support propagating toward the loading plate. More flexural cracks and diagonal cracks developed as the load increased. In general, the failure crack patterns of the four beams within each group are similar; however, the beams without web reinforcement are more extensively cracked than the beams with web reinforcement.

In general, the propagation rates of the flexural cracks in group A are much higher than those of the beams in group C, indicating the effect of the shear span-to-depth ratio *a/d* on the crack propagation. By increasing the load, more flexural cracks and diagonal cracks were developed and the existing ones widened or lengthened toward the compression face of the beams. Especially in group A, after reaching approximately 65% of (P_{max}), the formation of new cracks eventually stopped and existing ones widened until failure occurred. In contrast, the propagation of cracks continued in the group C beams until they were very close to the failure load.

The dimensionless initial cracking load, diagonal cracking load and failure load ($2V/f_c`b_wd$) are plotted against a/d for three beams in Fig. (6.4). As can be seen from the graph, all of the beams exhibit the flexural behavior under almost the same dimensionless

load $2V/f_c`b_wd$. The dimensionless load in large-sized beams, especially at the failure stage, is higher than for smaller beams.

It can also be observed that the load-resisting capacity after the first diagonal crack increases whenever the shear-span to depth ratio is smaller. In other words, beams with smaller (a/d) have more reserve strength. The reserve strength is the load-bearing capacity developed in deep beams after diagonal cracking occurred.

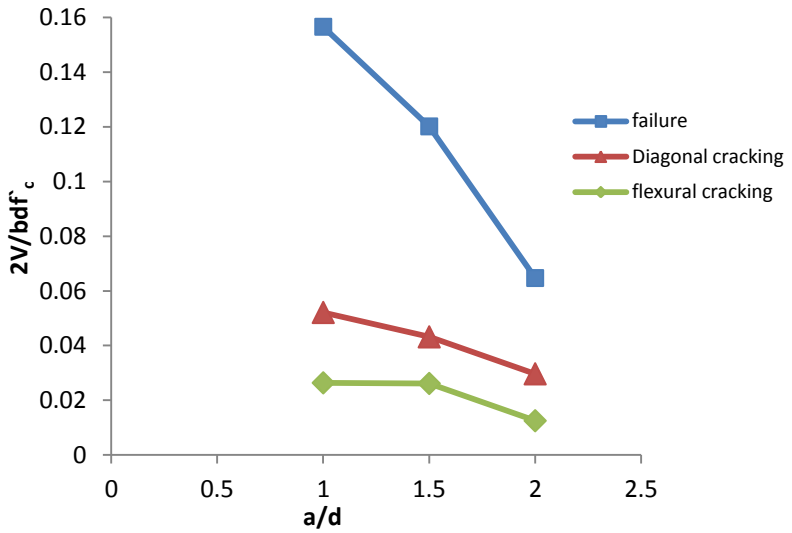

Fig. (6.4) Flexural, diagonal and ultimate shear stress versus shear span-depth ratio (a/d).

6.2.3. On the failure modes:

Figures (6.5) and (6.6) show the load levels corresponding to the initial flexural crack, initial diagonal crack and the failure for the tested beams (Groups A and C) with different percentages of web reinforcement. The ultimate load in the beams Group A, especially at the failure stage, is higher than the maximum load for the beams in Beam C because of their relative section sizes, which also can be observed for the beams in the same group where the ultimate load of the beams with web reinforcement is higher than for the un-reinforced beams.

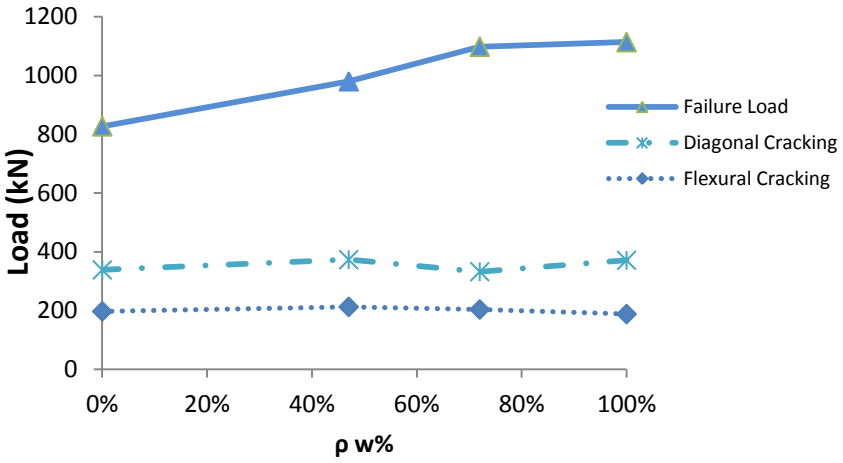

Fig. (6.5) Flexural, diagonal and ultimate load versus the percentage of the ratio of web reinforcement for beams in Group A.

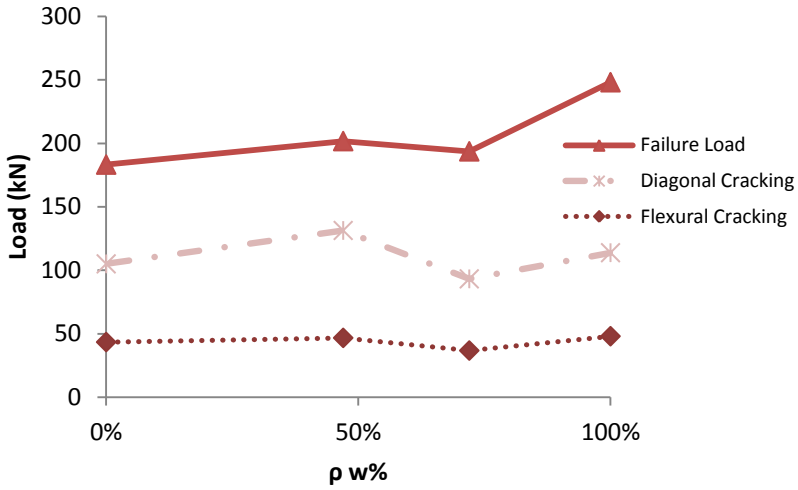

Fig. (6.6) Flexural, diagonal and ultimate load versus the percentage of the ratio of web reinforcement for beams in Group C.

It can also be observed from Figures (6.4), (6.5) and (6.6) that the load-resisting capacity after the first diagonal crack increases whenever the shear span-depth to ratio decreases. In other words, beams with smaller *a/d* ratios have more reserve strength. It should also be noted that the load levels in Group A beams corresponding to the flexural cracking and the diagonal cracking exhibited approximately the same level of load, While

the load level corresponding to failure increases with the increasing amount of web reinforcement.

The last column of Table (5.1) indicates the failure modes of all the specimens. As can be observed from (cracks pattern figures in chapter 5), shear failure was the common failure mode in all specimens, with varying severity in the type and level of damage. The beams exhibit three types of brittle failure mode: shear-compression failure, diagonal-splitting failure, and strut crushing failure. For group A specimens, Beams A1/00 and A1/50 failed with diagonal-splitting failure. The concrete at the end of one of the main struts of specimen A1/75 and A1/100 failed by crushing and was accompanied by a loud noise. In contrast to the beams in Groups A, three beams in group C, C1/00, C1/50 and C1/75 failed by strut crushing. Shear compression failure was the failure mode of beam C1/100, with a level of damage that was less severe than that of the two beams A1/75 and A1/100.

By comparing the failure modes within two groups, it can be observed that each group exhibits different type of failure mode, indicating the effect of the shear span depth ratio *a/d* in beams' failure modes. The load levels in Group C beams were corresponding to flexural exhibited approximately the same level of load, while the load levels corresponding to diagonal cracking decreases with the amount of 75 % web reinforcement which is unexpected and the load starts increasing with the amount of 100 % web reinforcement. However, the failure load levels increase with the amount of increase in web reinforcement.

6.3. The effect of web reinforcements:

Earlier works by Smith and Vantsiotis [1983], Tan et al [1997a], Shin et al[1999], Kong et al [1970] and Rogowsky et al[1986] on the effect of web reinforcement on the various aspects of deep-beam (conventional) behaviour showed that web reinforcement have a significant effect on the mid-span deflection, crack-width, failure modes and ultimate strengths. Many researchers have observed that web reinforcement increases beam stiffness, and that this influence becomes significant according to the arrangement and amount of web reinforcement, and on the *L/d* and *a/d* ratios. Despite the divergent views in determining the effect of web reinforcements on crack control, the majority has concluded that the effect of web reinforcements on crack width and crack control is akin to its effect on beam stiffness. Most of the researchers clarified that beams with web reinforcement exhibit the same modes of failure as compared to the beams without web reinforcement. For beams with web reinforcement the ultimate shear strength of deep beams is slightly increased as compared to those without; this contribution of shear reinforcement has not yet been determined as it has in conventional deep beams.

The effect of FRP shear reinforcement on the behavior of the beams was assessed by comparing the load-deflection response, load-strain response cracking pattern, and failure mode of specimens within A and C groups.

6.3.1. On the load-deflection behavior:

As can be observed from Figure (6.1), the ultimate deflection gradually increased for beams with web reinforcement in two groups A and C. It is mainly due to increased capacity of the beams with higher amount of web reinforcement. These results show that the web reinforcement has played significant role on affecting the beam stiffness.

6.3.2. On the crack development and failure mode:

By comparing crack patterns of the two groups, the formation of the first flexural crack at mid-span for group A appears at approximately 17 to 24% of the ultimate load according to the amount of the web reinforcement, while for group C, the first flexural crack at mid-span appears at approximately 13 to 24% of the ultimate load. The failure crack patterns of the four beams within each group are similar; however, the beams without web reinforcement are more extensively cracked than the beams with web reinforcement. The mid-span strain response of the main GFRP longitudinal reinforcements at different loading stages for specimens in group A and C are shown in Figs (6.7).

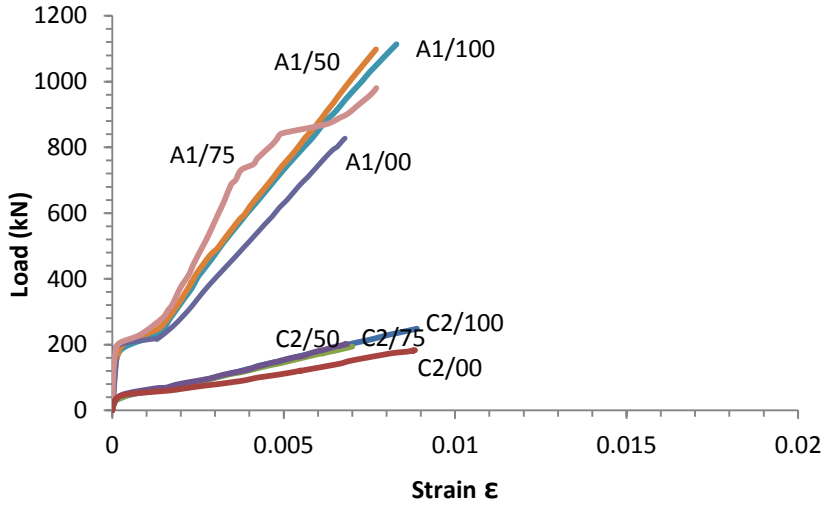

Fig. (6.7) Load –Strain response in the middle of the main tension GFRP reinforcement of specimens in Group A and C

When the flexural crack initiated, the tensile strains began to increase as the loading was increased. The initial flexural crack for the beams with more web reinforcement appeared to be longer than that observed in other cases; this is because the effect of the

web reinforcements in increasing the beams stiffness (the beam rigidity). And the beam rigidity is expressed here in the study as the resistance of the deformation that produced from the applied loads.

The results of beams A1/100, A1/75, A1/50 and A1/00 indicated that the strain in the tensile rebars reached only 54.2%, 50.3% 50.4 % and 44.4% of the ultimate strain, respectively. For group C, the results of beams C2/100, C2/75, C2/50 and C2/00 indicated that the strain in the tensile rebars reached only 52.3%, 41.2% 40.3% and 52.0% of the ultimate strain, respectively. According to clause 8.5.3.1 of the CAN/CSA-S806-12[2012], the ultimate tensile strength F_u should be reduced by about 65% to calculate the tie strength. Compared to the experimental results, this reduction suggested by the code is reliable.

The splitting failure was observed in beam A1/00 and A1/50 because there was not sufficient web reinforcement to resist tensile stresses in cracked concrete. While in group C, the beam C2/100 exhibited shear compression failure but the other three beams failed by crushing of the strut. This difference of the failure modes of the beams in group A and C indicates that the failure mode is affected by both the web reinforcement and *a/d* ratio.

6.3.3. On the Ultimate shear capacity:

Beams in a group which had 100% of FRP web reinforcement had the highest ultimate shear capacity. The ultimate shear capacities of the specimens with and without web reinforcement were compared to calculate the contribution of the FRP web reinforcement on the ultimate shear capacity of a beam. The contribution of the FRP web reinforcement in the two groups A & C is equal to 143.4 kN and 32.4 kN, respectively. The results show that FRP web reinforcement increase the ultimate shear capacity of FRP reinforced

concrete deep beams by about 26% as compared to the beams without web reinforcement. This contribution of the web reinforcement can be expressed as a function of the geometry, web reinforcement details and the shear span-to-depth ratio, as proposed below.

$$V_{web\ contr} = \frac{\phi_F A_{FV} f_{FU} d}{s(\frac{a}{d})} \qquad (6.1)$$

Where the Φ_F FRP strength reduction factor, A_{fv} is the amount of FRP shear reinforcement within spacing s, d is the effective depth, f_{fu} is the design tensile strength of FRP and s is the stirrup spacing.

By using this equation (Eq (6.1)), the contribution of the web reinforcements was found to be 131.7 kN and 39.0 kN for specimens A1/100 and C2/100, respectively. These values are consistent with the experimental results. On the other hand, the contribution calculated by using the provisions of CAN/CSA-S806-12[2012] for specimens A1/100 and C2/100 are 47.40 kN and 56.07 kN, respectively. Clearly, these values are lower than that obtained based on the test results.

Table (6.1) The predictions for contribution of the FRP web reinforcement on the ultimate shear capacity

Specimens	$V_{web\ contrcalc}/\ V_{web\ contr}^{TEST}$ Proposed equation	$V_{web\ contrcalc}/\ V_{web\ contr}^{TEST}$ Equation (8-22) of the CAN/CSA-S806-12 code
Beam A1	0.92	0.33
Beam C2	1.20	1.73
Mean	1.06	1.03
SD	0.20	0.99
COV	0.19	0.96

Table (6.1) shows the comparison between the prediction of the contribution of the FRP web reinforcement on the ultimate shear capacity $V_{web\ contr}{}^{TEST}$ by using Eq [9] that proposed here and the equation (8-22) of the CAN/CSA-S806-123 code. From Table (6.1), the contribution $V_{web\ contrcalc}/\ V_{web\ contr}{}^{TEST}$ by using the proposed equation are 0.92 and 1.20 for beams A1 and C2, respectively. As for the equation (8-22) of the CAN/CSA-S806-123 code, the contribution $V_{web\ contrcalc}/\ V_{web\ contr}{}^{TEST}$ are 0.33 and 1.73 for beams A1 and C2, respectively. The equation (8-22) of the CAN/CSA-S806-12[2012] code gives unconservative estimation for the contribution of the web reinforcements when compared to the test results especially when *a/d* equal to one. And with decreasing *a/d*, the contribution is overestimated by using the CAN/CSA-S806-12[2012] code. In general, the mean value of $V_{web\ contrcalc}/\ V_{web\ contr}{}^{TEST}$ by using the code equation is 1.03, with a standard deviation (*SD*) equal to 0.99 and a coefficient of variation (*COV*) of 0.96. While the proposed equation gives a mean value of 1.06, the lowest standard derivation of 0.20 and the lowest coefficient of variation of 0.19, indicating that the equation gives the reliable and acceptable results for the contribution of FRP web reinforcement.

6.4. Comparison of test results with predicted values by design provisions:

Table (6.2) shows the ultimate shear strength predictions for the nine beams and Farghaly and Benmokrane [2013] beams according to the two design procedures and compared to the actual shear capacity. The ultimate shear capacity of the eight specimens was determined by using the STM provisions in CAN/CSA-S806-12[2012].

Table (6.2) Summary of the predictions for ultimate shear strength.

Reference	Specimen No	V_{calc}/V_u^{TEST} STM S806-12	V_{calc}/V_u^{TEST} Sectional Model S806-12
Current study	A1/100	0.45	0.29
	A1/75	0.46	0.29
	A1/50	0.51	0.30
	A1/00	0.61	0.32
	B1.5/100	0.82	0.48
	C2/100	0.55	1.07
	C2/75	0.70	1.17
	C2/50	0.67	1.02
	C2/00	0.74	0.92
Farghaly and Benmokrane[12]	G8N6	0.94	0.28
	G8N8	0.93	0.21
	C12N3	0.94	0.39
	C12N4	0.93	0.31
Mean		0.71	0.54
SD		0.19	0.36
COV		0.262	0.660

The ultimate shear capacity of an STM was determined by using the capacity of the weakest element of a simple assumed truss. The prediction of ultimate shear strength calculated by using the procedure of shear design in flexural regions in CAN/CSA-S806-12[2012] is obtained from equations 6 and 8 for normal beams, which represents the contribution of two parts: concrete, V_c and FRP shear reinforcement, V_{cf}.

Table (6.2) also shows the mean, the standard deviation (SD) and the coefficient of variation (COV) for shear capacity predicted using the code provisions. The results show that the prediction of the procedure of shear design considering a shallow beam is quite conservative, especially for beams with lower (*a/d*) ratios, while for beams with (*a/d*) ratios equal to two, the procedure overestimates the capacity.

The prediction of the ultimate shear strength for specimens without web reinforcement was reliable, while for the specimens with web reinforcement the shear capacity was overestimated. These overestimated predictions were due to the way the contribution of

the shear reinforcements is calculated for shallow beams using CAN/CSA-S806-12[2] provisions. Compared to the predictions for the beams in the current study, the predictions of the beams tested by Farghaly and Benmokrane [2013] were slightly more conservative.

For easy comparison between the STM Model and the sectional model, the dimensionless shear stress capacity ν as computed using Equation (6.2) below has been plotted against the shear span-to-depth *a/d* ratio as shown in Fig (6.8).

$$v = V_{calc}/bd\,f'_c \qquad (6.2)$$

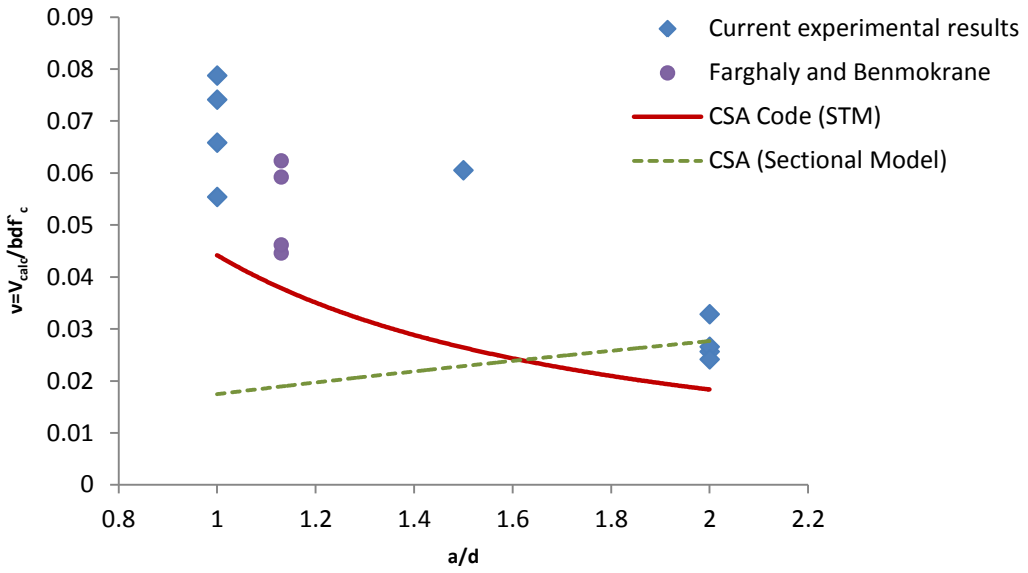

Fig. (6.8). Use of strut and tie model and sectional mode to predict the strengths of a series of beams

The STM model provides a very good estimate of the capacity when compared to the experimental results, while the sectional model (i.e., the procedure of shear design of shallow beams) does not provide an accurate estimate of capacity as expected. The results shown in Figure (6.8) and Table (6.2) confirm that the STM model procedure in the

CAN/CSA-S806-12[2012] code provides a conservative and convenient design method for FRP-reinforced concrete deep beams.

6.5. Comparison of experimental results with predicted capacity by the proposed design procedure for deep beams based on ACI code:

Table (6.3) shows the comparison of the ultimate shear strength and the nominal design strength of the three beams using the thin beam theory of ACI 440.1R-06[2006] and the proposed design procedure for deep beams based on the modification to ACI 318.08[2008] procedure. In ACI 440.1R-06[2006], the ultimate shear strength of thin FRP-reinforced beams has the contribution of two parts, shear strength provided by concrete V_c, and by FRP shear reinforcement V_f. For the STM model a simple truss was assumed to calculate the capacity. All the possibilities of the applied loads and the resulting forces in each element were calculated by using the modified provision of STM in ACI318.08 [2008] using both uniform and bottle shaped struts. The ultimate shear capacity was determined by using the capacity of the weakest element. The results show that the ACI 440.1R-06[2006] code prediction using the traditional thin beam theory is very conservative for each of the beams, as expected.

Table (6.3) Summary of the predictions for ultimate shear strength.

Specimen No	V_n / V_n^{TEST} ACI 440.1R-06	V_n / V_n^{TEST} Mod-ACI 318-08 (Uniform cross section strut)	V_n / V_n^{TEST} Mod-ACI 318-08 (bottle shaped strut)
A1/100	0.16	0.74	0.5
B1.5/100	0.21	0.64	0.64
C2/100	0.21	0.86	0.86
Mean	0.19	0.75	0.67
SD	0.03	0.11	0.18
COV	0.15	0.15	0.27

The predictions using the STM of ACI 318[2008] with the proposed modification for FRP-reinforcements show acceptable and conservative results for both uniform and bottle shaped struts. The STM model provided in the Canadian code, which is not discussed here, was also found to provide acceptable and conservative results. The nominal capacity of Specimen A1/100 was slightly more conservative than that of B1.5/100 and C2/100. These results are encouraging while considering the possibility of adopting the STM procedure for FRP reinforced concrete deep beams in the ACI code. The STM procedure as provided in ACI 318.08[2008] code can be adapted to design FRP-reinforced concrete deep beams, taking into consideration the properties of the FRP. To that end, further tests with different ratios of the key variables that affect deep beam behavior would be required.

6.6. Summary:

The experimental results of FRP reinforced concrete deep beams are summarized in this chapter. Based on the comparison of the experimental results of different FRP reinforced concrete deep beam groups, the influence of critical variables on the behaviour of FRP reinforced concrete deep beams have been studied. The experimental results are also used for validating the current and proposed design procedures for FRP-RC deep beams. It is found that the Canadian provisions are generally adequate, while there are scopes for improvement. The proposed procedure for designing FRP-RC deep beams adapted from the ACI code provisions for conventional deep beam is also found to work well. These aspects are discussed below in more details.

6.6.1. Effect of the key factors:

The behavior of the beams with higher shear span-to-depth ratio *a/d* becomes more flexible. The rigidity of the three beams A1/100, B1.5/100 and C2/100 was gradually increased respectively, whenever the shear span depth ratio decreased. Also the beam stiffness is affected by the web reinforcement where the rigidity of the tested beams was increased due to the web reinforcement in the two groups of beams A and C. It has been found that the influence of shear behavior becomes dominant when the shears span-to-depth ratio *a/d* decreases. In addition, the load-resisting capacity is increased after the first diagonal crack in the specimens with a small shear span-to-depth ratio. The experimental results also indicate that the web reinforcement significantly influences the behavior of the FRP reinforced concrete deep beams. This influence can be seen on the beam stiffness where the deflection gradually increased for beams with web reinforcement in the two groups of beams studied in detail (i.e., A and C).

The pre-failure damage appears to be more severe in beams without or with less web reinforcement indicating the influence of the web reinforcement on controlling crack propagation. Also the ultimate shear strength is affected by web reinforcement where the capacity of the tested beams was increased due to the web reinforcement. Based on the experimental results, an equation has been proposed to calculate the contribution of the FRP web reinforcement to the ultimate shear capacity of FRP-reinforced concrete deep beams. When compared to the test results, the equation gives the reliable and acceptable results compared to that calculated by using Equation (8-22) of the CAN/CSA-S806-12 [2012]. As for the failure modes of the beams, it is mainly affected by the shear span-to-depth ratio *a/d* and by the web reinforcement. The experimental study also indicates that

the reduction of the ultimate tensile strength F_u according to clause 8.5.3.1 of the CAN/CSA-S806-12[2012] code was sufficient when compared to the experimental results.

6.6.2. Comparison with the design provisions:

The study shows that the STM design procedure in the CAN/CSA-S806-12 code [2012] provides a conservative and convenient design method for FRP-reinforced concrete deep beams. There are some aspects of the provisions that are inconsistent, for example, the way strut capacity is calculated, and the stress limit in a straight FRP bar is defined. Also there is a concern about the required minimum quantity of web reinforcements specified in the standard, which seems quite conservative and may lead to very close spacing. In general, the predictions of the capacity using the Modified STM procedure for the ACI code showed acceptable and conservative results. After modifying the tie strength according to FRP properties, the STM design procedures in Appendix A of the ACI 318-08 code [2008] constitute a practical design method for FRP-reinforced concrete deep beams. The code provisions of ACI 440.1R-06[2006] produce very conservative results to predict the ultimate shear strength as compared to the experimental studies. The investigation reveals that adopting the procedure in the ACI 318-08 Code [2008] and taking into consideration the properties of FRP reinforcement provides a reliable design procedure for FRP reinforced concrete deep beams.

Chapter 7: Summary and Conclusions

7.1. Summary

There are many studies available in the literature that demonstrate the effectiveness of FRP bars as internal reinforcement in concrete structural elements. However, there are not many studies available on the use of internal FRP reinforcement in concrete deep beams. Therefore, a set of nine FRP-RC deep beam specimens have been tested in the present study to understand their behaviour and assess the effect of the key parameters.

The increasing use of this material in construction led to the development of standards for the design and construction of building components with Fiber-Reinforced Polymers. The CAN/CSA-S806-02[2002], the ACI 440.1 R-06[2006] and the CAN/CSA-S806-12[2012] standards provide requirements for the design and evaluation of building components made of fiber-reinforced polymers (FRP) in buildings, as well as for building components reinforced with FRP materials. A design manual has been issued by the ISIS Canada Research Network to provide guidelines and design equations that can be used for the design of FRP-reinforced concrete structures. Neither the CAN/CSA-S806-02[2002] nor the ACI 440.1 R-06[2006] standards provided a procedure for designing deep beams reinforced with FRP bars. In the newer edition, the CAN/CSA-S806-12[2012] does adopt the STM approach for conventional beams with some adjustments to account for the properties of FRP. Such an approach has not been adopted in the ACI 440.1 R-06[2006] for deep beams as yet. A design procedure for FRP-reinforced concrete deep beams similar to the STM-based procedure for conventional deep beams still

remains to be developed. This test program seeks to assess the suitability of the adaptation of the STM design procedures provided in ACI 318-08 [2008] code for designing FRP reinforced concrete deep beams after modifying the tie strength according to FRP properties.

In the beginning of this research, a parametric study has been conducted on the behaviour of conventional concrete deep beams based on the available experimental data collected from the literature review. The objective of this part of the research was to understand the behaviour of the conventional deep beams, relevant code provisions and key factor in order to develop similar design procedures for FRP-RC deep beams. At that time (prior to 2012) no design procedure was available for such beams in Canada and elsewhere. This study reviews and compares the design provisions for concrete deep beams provided in the three prominent design codes for reinforced concrete using the Strut-and-Tie Model. The effectiveness of the STM provisions of different codes in predicting the capacity and failure modes of concrete deep beams has been studied in a large number of available experimental studies. The influence of key variables on the capacity of deep beams predicted by Strut-and-Tie Model (STM) provisions in codes, such as the shear span-to-depth ratio, the web reinforcement, and the compressive strength of concrete, has also been studied. The findings of the present study are expected to be useful to both design practitioners and to code-development authorities.

Based on the above study and review of the code provisions for conventional deep beams and FRP-reinforced ordinary beams, a design procedure for FRP-reinforced concrete deep beams was developed and a set of nine beams was designed and constructed for experimental evaluation of their behaviour. The above design procedure

was developed for the Canadian jurisdiction based on the provisions of CSA A23.3-04 standard applicable for conventional deep beams and the provisions of CSA-S806-02 applicable for FRP-RC ordinary beams. The CSA S806-12 provisions that were available later had a similar procedure except for the amount of the web reinforcement. The results of the present experimental study and those reported in Farghaly and Benmokrane [2013] were used for studying the effect of key factors on the behaviour of FRP-RC deep beams, and validating the effectiveness of the STM design procedures in the CSA-S806-12 [2012] code for designing FRP reinforced concrete deep beams. In addition, a design procedure for FRP-RC deep beams similar to that provided in ACI 318-08 was also proposed for possible adoption in a future version of ACI 440. The results of the present and available experimental studies were used for validating the effectiveness of that procedure as well.

7.2. Conclusions:

A total of nine full-scale concrete deep beam specimens with shear span to depth ratios *a/d* of 1, 1.5 and 2 were constructed and tested under three-point loading to failure. The studied variables were the shear span to depth ratio and the quantity of web shear reinforcement. The behaviour of deep beams is indicated by their levels of ultimate shear strength, mid deflection, FRP reinforcement strain, crack propagation, and by their type of failure. The test results are also compared to predictions based on the design procedures of the ACI and the CSA design and construction code for building structures with fibre-reinforced polymers. Based on the review of available experimental studies and comparison of code provisions for conventional deep beams, and the experimental study conducted on FRP-RC deep beams, the following conclusions were drawn.

7.2.1. Conclusions based on the behaviour of conventional deep beams and relevant code provisions:

- The Strut and Tie Models as provided in three prominent codes, namely ACI-318-08 [2008], CSA-A23.3-04 [2004], and Eurocode EN1992-1-1 [2004], are generally found to be appropriate methods for the design and evaluation of the shear strength capacity of concrete deep beams with a shear–span to depth ratio less than or equal to two.
- Although the effect of web reinforcement is not accounted for in some of the code provisions, experimental studies show that such reinforcements improve the capacity of concrete deep beams.
- The code provisions may not produce accurate results in the prediction of the mode and location of failure as observed in the experimental studies.
- The provisions of the Canadian Code appear to be the most conservative in estimating the capacity of concrete deep beams.
- When the Eurocode method is modified by multiplying the ultimate load by a factor β as provided in the code, it provides a reasonable and conservative estimate of capacity similar to that obtained by using the provisions of the Canadian code.
- The procedure of ACI improves significantly when bottled-shaped struts are used instead of uniform cross-section struts, and shows conservative results. However, the code does not provide guidance on when to use the bottle-shaped or the uniform strut sections.
- The STM design procedures in Appendix A of the ACI 318-085 codes, after modifying the efficiency factors of bottled shape struts and calculated as function

of shear span-to-depth ratio as proposed in the present work, provides an improvement in the conservative estimate of the capacity of a concrete deep beam.

7.2.2. Conclusions based on the present experimental study of FRP-RC deep beams and relevant design provisions:

- The deflection gradually increases for beams with higher shear span-to-depth ratio *a/d*, i.e. the behavior of beams with higher shear span-to-depth ratio *a/d* becomes more flexible.
- When the shear-span to depth ratio *a/d* decreases, the influence of the shear behavior becomes dominant.
- The higher load-resisting capacity was observed after the first diagonal crack for beams with the smaller shear span depth ratio.
- Although the three specimens A1, B1.5and C2 with 100% of web reinforcement failed in shear-compression mode, the effect of the *a/d* ratio was reflected in the severity of the pre-failure damage.
- Web reinforcement has a significant effect on controlling the crack propagation, and the pre-failure damage appears to be more severe for beams without or with less web reinforcement.
- The ultimate shear strength of the tested beams was increased due to the web reinforcement.
- Web reinforcement has a significant effect on the beam stiffness, where the deflection gradually increased for beams with web reinforcement in two groups (A and C).

- The beams' failure modes are mainly affected by the shear span-to-depth ratio *a/d* and by the web reinforcement.
- The code provisions of ACI 440.1R-06 [2006] produce very conservative results to predict the ultimate shear strength compared to the experimental studies, as expected.
- The reduction of the ultimate tensile strength F_u according to clause 8.5.3.1 of the CAN/CSA-S806-12 code [2012] appears sufficient when compared to the experimental results.
- The STM design procedures in Appendix A of the ACI 318-08 code [2008], after modifying the tie strength according to FRP properties, constitute a conservative and convenient design method for FRP-reinforced concrete deep beams.
- The significant increase in the tensile strain in web reinforcements the region of the assumed direction of the main struts and in the main longitudinal FRP rebars indicates that the Strut-and-Tie Model (STM) is the appropriate method for the design of FRP reinforced concrete deep beams with (*a/d*) less than or equal to two.
- It was also observed that the strain in the both layers of the longitudinal rebars were similar in a given specimen, indicating that the longitudinal rebars acted in a group as the tie in the STM model.
- The STM design procedure in the CAN/CSA-S806-12 [2012] code provides a practical and reliable design method for FRP-reinforced concrete deep beams. However, there are some aspects of the provisions that are inconsistent. For example, the way strut capacity is calculated, and the stress limit in a straight FRP bar is defined. Also there is concern about the required minimum quantity of web

reinforcements specified in the standard, which seems quite conservative and may lead to very close spacing.

- Based on the work presented in this thesis an equation has been proposed to calculate the contribution of the FRP web reinforcement to the ultimate shear capacity of FRP-reinforced concrete deep beams.

7.3. Research Contributions:

The contributions of the current research include the following:

- The code provisions have been evaluated by using a database of available experimental results of more than three hundred test specimens compiled in the present study.
- The effectiveness of the STM provisions of the codes in predicting the capacity and failure modes of deep beams has been studied.
- In addition, the effects on the capacity of deep beams of various parameters, such as the web reinforcement, shear-span to depth ratio, and the strength of concrete, have been investigated using the results of the experimental studies.
- The behavior and strength of FRP reinforced concrete deep beams are investigated in an experimental study.
- This investigation reveals that adopting the procedure in the ACI 318-08 Code [2008] and taking into consideration the properties of FRP reinforcement provides a conservative and convenient design procedure for FRP reinforced concrete deep beams.

- The shear design procedures of the ACI 440.1R-06 Code [2006] and of the modified Strut and Tie model (STM) from Appendix A of the ACI 318-08 Code [2008] were compared based on their test results.
- A new equation is presented in this study to calculate the contribution of the FRP web reinforcement to the ultimate shear capacity of FRP-reinforced concrete deep beams.
- The test results are also compared to predictions based on the current CSA design and construction code for building structures with fibre-reinforced polymers.
- This investigation reveals that the Strut and Tie model procedure in the CSA-S806-12 code [2012] provides a conservative and convenient design procedure for FRP-reinforced concrete deep beams.

7.4. Limitations of the Current Research and Potential for Future Research:

The present study provides and extensive review of literature and available experimental studies with a comparison of code provisions for the design of conventional RC deep beams, and an experimental study on FRP-RC deep beams to understand their behavior and validate the current and proposed design procedures. However, there are some limitations in the present work that should be considered for future research.

- The test specimens were designed and constructed prior to the publication of current CSA standard (CSA S806-12) and thus could not its provisions. However, the design method developed for these specimens were very similar to the current provisions except in the ways how web reinforcements are provided and the strut strength is calculated. Further experimental studies are required with specimens adhering to the current code provisions.

- All the beam specimens were tested in three-point loading since the available experimental studies on conventional deep beams indicate similar behaviour in beams tested in three-point or four-point loading tests. However, further experimental studies are required for FRP-RC deep beams tested in four-point loading.

Additional experimental work, analytical studies and finite element analysis are needed to enhance the reliability and suitability of the STM model both in the CSA code and the proposed provisions intended for ACI code to design the FRP-reinforced concrete deep beams.

- The current research could be expanded by changing the horizontal and vertical web reinforcement patterns and higher quantity.
- Investigating the structural behaviour of FRP-reinforced concrete deep beams with shear spans to depth ratios less than one.
- Studying the effect of other variables that not included in this study such as: longitudinal FRP reinforcement ratio (ρ) and concrete compressive strength (f'_c).
- Investigating the effect of presence of opening on the behaviour of FRP-reinforced concrete deep beams.
- Conducting numerical analyses on the FRP reinforced concrete deep beams to assist performing parametric study using the calibrated numerical models.

References

ACI Committee 318,[2002] "Building Code Requirements for Structural Concrete," *American Concrete Institute, Farmington Hills*, MI, 443 pgs.

ACI Committee 318, [2008]"Building Code Requirements for Structural Concrete (ACI 318-08) and Commentary (318R-08), *American Concrete Institute, Farmington Hills*, MI, 430 pp.

ACI Committee 440 [2006] "Guide for the Design and Construction of Concrete Reinforced with FRP Bars (ACI 440.1R-06)."), *American Concrete Institute, Farmington Hills,* MI, 44 pp.

Aguilar, G.; Matamoros, A.; Parra-Montesinos, G.; Ramirez, J.; and Wight, J. K.,[2002] "Experimental Evaluation of Design Procedures for Shear Strength of Deep Reinforced Concrete Beams", *ACI Structural Journal*, V. 99, No. 4, pp. 539-548.

ASTM Standard section 4[2013] "ASTM Book of Standards - Section 4 – Construction," *American Society for Testing and Materials book*, V. 04.02, 1068 pp.

CSA Standard A23.3-84, [1984] "Design of Concrete Structures," *Canadian Standards Association,* Rexdale, ON,Canada.

CAN/CSA Standard A23.3-04, [2004], "Design of Concrete Structures for Buildings with Explanatory Notes," *Canadian Standards Association,* Rexdale, ON, Canada.

CAN/CSA-S806-02, [2002] "Design and Construction of Building Components with Fibre-Reinforced Polymers", *Canadian Standards Association,* Toronto, Ontario, Canada.

CAN/CSA S806-12, [2012] "Design and construction of building components with fiber-reinforced polymers." *Canadian Standards Association*, Mississauga, Ontario, Canada, 208 pp.

CAN/CSA Standard A23.1-09/A23.2-09, [2009] "Concrete materials and methods of concrete construction/Test methods and standard practices for concrete" Canadian Standards Association, Rexdale, ON, Canada, 647 pp.

Carlos, G. Q. F., Gustavo, P. M., and James, k. W., [2006] "Strength of Struts in Deep Concrete Members Designed Using Strut-and-Tie Method," *ACI Structural Journal*, V. 103, No. 4, pp. 577-586.

Collins, M.P. and Mitchell, D."Prestressed Concrete Structures." *Prentice-Hall,* 5th edition, 2001,766 pp.

ACI Committee 318, “Building Code Requirements for Structural Concrete (ACI 318-02) and Commentary (318R-02), *American Concrete Institute*, Farmington Hills, MI, 2002, 443 pp.

Edward .G. Nawy., [2005]“Reinforced Concrete: A Fundamental Approach.” ACI 318-05 code 6th edition, *Prentice Hall*, 824 pp.

El-Sayed A. K., El-Salakawy. E. F., and Benmokrane.B., [2006a] “ Shear Strength of FRP Reinforced Concrete Beams without Transverse Reinforcement,” *ACI Structural Journal*, V. 103, No. 2, pp. 235-243.

El-Sayed A. K., El-Salakawy. E. F., and Benmokrane.B., [2006b] “Shear Capacity of High-Strength Concrete Beams Reinforced with FRP Bars,” *ACI Structural Journal*, V. 103, No. 3, pp. 383-389.

European Standard DD ENV 1992-1-1,[1992] “Design of Concrete Structures General Rules for Buildings (together with United Kingdom National Application Document),” *European Committee for Standardization,* CEN. 274 pgs.

European Standard EN1992-1-1, [2004] “Euro code 2: Design of Concrete Structures – Part 1-1: General Rules and Rules for Buildings,” *European Committee for Standardization*, CEN.

[12] Farghaly, A., Benmokrane, B., “Shear Behavior of FRP-Reinforced Concrete Deep Beams without Web Reinforcement,” *Journal of Composites for Construction*, V. 17, Issue. 6, Dec 2013, pp. 04013015-1to10.

Foster, S. J., and Gilbert, R. I., [1998] “Experimental studies on high strength concrete deep beams", *ACI Structural Journal*, V.95, No. 4, pp. 382-390.

Foster, S.J and R. Malik, A.R.,[2002] “Evaluation of Efficiency Factor Models used in Strut-and-Tie Modeling of Nonflexural Members,” *Journal of Structural Engineering,* V.128, Issue 5, pp. 569–577

Kong, F. K., Robins, P. J., Cole, D. F., [1970] “Web Reinforcement Effects on Deep Beams", *ACI Structural Journal*, V.67, No. 12, pp. 1010-1018.

Garay-Moran, J. D., and Lubell, A. S., [2008] “Behaviour of Concrete Deep Beams with High-Strength Reinforcement,” Structural Engineering Report No.277, Department of Civil and Environmental Engineering, *University of Alberta,* Edmonton, AB, Canada, 283 pp.

ISIS Canada Corporation, [2007] “Design Manual No. 3: reinforcing concrete structures with fibre-reinforced polymers”, *University of Manitoba*, Winnipeg, MB, Canada, V.2, 151 pp.

Jung-Keun Oh, Sung-Woo Shin, [2001] "Shear strength of reinforced high-strength concrete deep beams", *ACI Structural Journal*,. Vol.98, No.2, pp.164-173.

Kani, G. N. J., "How Safe Are Our Large Reinforced Concrete beams," *ACI Journal*, Proceedings V. 64, No.3, Mar.1967, pp. 128–141.

Keun-Hyeok Yang, Heon-Soo Chung,Eun-Taik Lee, Hee-Chang Eun, [2003] "Shear characteristics of high-strength concrete deep beams without shear reinforcements", *Engineering Structures*, Vol.25,pp.1343-1352.

Kong, P. Y. L., and Rangan, B.V., [1998] "Shear strength of high performance concrete beams", *ACI Structural Journal*, V. 95, No. 6, pp.677–688.

Kotosoves, M. D., and Pavlovic, M. N., [2004] "Size Effects in Beams with Small Shear Span-to-Depth Ratios," *Computer & Structures*, V. 82, Issues 2-3, pp.143-156.

MacGregor, J. G., [2000] "Reinforced Concrete, Mechanics and Design." 2nd Edition, *Prentice Hall*, ,848 pp.

Matamoros, A., and Wong, K. H., [2003] "Design of Simply Supported Deep Beams Using Strut-and-Tie Models," *ACI Structural Journal*, V. 100, No. 6, pp. 704-712.

Michael, D. Brown, and Oguzhan, B., [2008] "Design of Deep Beams Using Strut-and-Tie Model _ Part I: Evaluating U.S Provisions," *ACI Structural Journal*, V. 105, No.4, pp. 395–404.

Michael, D. B., Cameron, L. S., Oguzhan, B., James, O. J., John, E. B., Sharon. L. W., "Design for Shear in Reinforced Concrete Using Strut-and-Tie Models," *Center for Transportation Research ,* University of Texas at Austin, Report. 0-4371-2, Jan-Apr. 2006, 330 pp.

Nathan, C. R., and Sergio, F. B., [2008] "Behaviour of Deep Beams with Short Longitudinal Bar Anchorages," *ACI Structural Journal*, V.105, No.4, pp.460-470.

Park. JW, Kuchma. D, [2007] "Strut-and-Tie Model Analysis for Strength Prediction of Deep Beams," *ACI Structural Journal*, V. 104, No.6, pp. 657–666.

Park, S., and Aboutaha, R. S., [2009] "Strut-and-Tie Method for CFRP Strengthened Deep RC Members," *Journal of Structural Engineering*, V. 135, No.6, pp. 632–643.

Rigotti, M., [2002]"Diagonal cracking in reinforced concrete deep beams: an experimental investigation". *Concordia University*, PhD thesis , 235pp .

Rogowsky, D. M., MacGregor, J. G., and Ong. S. Y., [1986]"Tests of Reinforced Concrete Deep Beams," *ACI Structural Journal*, V. 83, No. 4, pp. 614-623.

Shin, S. W., Lee, K. S., Moon, J., and Ghosh, S. K., [1999] “Shear strength of reinforced high-strength concrete beams with shear span-to-depth ratios between 1.5 and 2.5”, *ACI Structural Journal*, V. 96, No. 4, pp. 549-556.

Smith, K. N., and Vantsiotis, A. S., [1983] “Shear strength of deep beams, ” *ACI Structural Journal*, V. 79, No. 3, pp. 201–213.

Tan, K. H., and Lu, H.Y., [1999] “Shear behaviour of large reinforced concrete deep beams and code comparisons,” *ACI Structural Journal*, V. 96, No. 5, pp. 836–845

Tan, K. H., Kong, F. K., Teng, S., and Weng, L. W., [1997a] “Effect of Web Reinforcement on High Strength Concrete Deep Beams ", *ACI Structural Journal*, V. 94, No. 5, pp. 572-581.

Tan, K.H., Teng, S., Kong, F.K. and Lu, H.Y., [1997b] “Main tension steel in high strength concrete deep and short beams", *ACI Structural Journal*, V. 94, No. 6, pp. 752-768.

Tan, K.H., Kong, F. K., Teng, S., and Guan, L., [1995] "High-Strength Concrete Deep Beams with Effective Span and Shear Span Variations." *ACI Structural Journal*, V. 92, No. 4, pp. 395 – 405.

Walraven, J., and Lehwalter, N., [1994] “Size effects in short beams loaded in shear, ” *ACI Structural Journa*l, V. 91, No. 5, pp. 585–593.

Zhang, N., and Tan, K. H., [2007] “Size effect in RC deep beams: Experimental investigation and STM verification,” Engineering Structures, V.29, pp.3241-3254.

Kani, G. N. J., “How Safe Are Our Large Reinforced Concrete beams,” *ACI Journal*, Proceedings V. 64, No.3, Mar.1967, pp. 128–141.

Appendix A:

Reference	No	deep beam ID	$f`_c$ (Mpa)	h (mm)	d (mm)	b (mm)	l_e (mm)	a/d	P (%)	ρ_{sv} (%)	ρ_{sh} (%)	V_u on each load	failure mode
Zhang and Tan	1	1DB35bw	25.9	350	313	80	1050	1.10	1.250	0.400	0.000	100	Shear Compression
	2	1DB50bw	27.4	500	454	115	1500	1.10	1.280	0.390	0.000	187	Shear Compression
	3	1DB70bw	28.3	700	642	160	2100	1.10	1.220	0.450	0.000	427	Shear Compression
	4	1DB100bw	28.7	1000	904	230	3000	1.10	1.200	0.410	0.000	775	Shear Compression
	5	2DB35	27.4	350	314	80	1050	1.10	1.250	0.000	0.000	85	Shear Compression
	6	2DB50	32.4	500	459	80	1500	1.10	1.150	0.000	0.000	136	Shear Compression
	7	2DB70	24.8	700	650	80	2100	1.10	1.280	0.000	0.000	156	Shear Compression
	8	2DB100	30.6	1000	926	80	3000	1.10	1.260	0.000	0.000	242	Shear Compression
	9	3DB35b	27.4	350	314	80	1050	1.10	1.250	0.000	0.000	85	Shear Compression
	10	3DB50b	28.3	500	454	115	1500	1.10	1.280	0.000	0.000	167	Shear Compression
	11	3DB70b	28.7	700	642	160	2100	1.10	1.220	0.000	0.000	361	Shear Compression
	12	3DB100b	29.3	1000	904	230	3000	1.10	1.200	0.000	0.000	672	Shear Compression
Nathan and Breña	13	DB 1.0-1.00	33.3	635	581	152	1220	1.00	0.453	0.080	0.058	339	Crushing of strut
	14	DB 1.0-0.75	31.7	635	581	152	1220	1.00	0.453	0.080	0.058	372	Crushing of strut
	15	DB 1.0-0.50	30.6	635	581	152	1220	1.00	0.453	0.080	0.058	365	Crushing of strut
	16	DB 1.0-0.32	27.0	635	581	152	1220	1.00	0.453	0.080	0.058	334	Crushing of strut
	17	DB 1.0-0.75L	29.9	635	581	152	1220	1.00	0.643	0.080	0.058	371	Crushing of strut
	18	DB 1.0-0.28L	29.4	635	581	152	1220	1.00	0.643	0.080	0.058	321	Anchorage failure
	19	DB 1.5-0.75	32.7	457	405	152	1220	1.50	0.650	0.111	0.084	230	Crushing of strut
	20	DB 1.5-0.50	34.1	457	405	152	1220	1.50	0.650	0.111	0.084	212	Crushing of strut
	21	DB 1.5-0.38	33.8	457	405	152	1220	1.50	0.650	0.111	0.084	214	Anchorage failure
	22	DB 2.0-0.75	34.7	356	303	152	1220	2.00	0.869	0.142	0.134	157	Crushing of strut
	23	DB 2.0-0.50	33.0	356	303	152	1220	2.00	0.869	0.142	0.134	149	Crushing of strut
	24	DB 2.0-0.43	35.6	356	303	152	1220	2.00	0.869	0.142	0.134	133	Anchorage failure
Tan and Lu	25	1-500/0.5	49.1	500	444	140	1500	0.56	2.600	0.000	0.000	850	Crushing of strut
	26	1-500/0.75	42.5	500	444	140	1750	0.84	2.600	0.000	0.000	700	Crushing of strut
	27	1-500/1.00	37.4	500	444	140	2000	1.13	2.600	0.000	0.000	570	Crushing of strut
	28	2-1000/0.5	31.2	1000	884	140	2000	0.56	2.600	0.120	0.120	875	Shear Compression
	29	2-1000/0.75	32.7	1000	884	140	2480	0.84	2.600	0.120	0.120	650	Shear Compression
	30	2-1000/1.00	30.8	1000	884	140	3000	1.13	2.600	0.120	0.120	435	Shear Compression
	31	3-1400/0.5	32.8	1500	1251	140	2410	0.56	2.600	0.120	0.120	1175	Diagonal splitting
	32	3-1400/0.75	36.2	1500	1251	140	3100	0.84	2.600	0.120	0.120	950	Diagonal splitting
	33	3-1400/1.00	35.3	1500	1251	140	3840	1.13	2.600	0.120	0.120	800	Diagonal splitting
	34	4-1750/0.5	42.6	2000	1559	140	2760	0.56	2.600	0.120	0.120	1636	Crushing of strut
	35	4-1750/0.75	40.4	2000	1559	140	3640	0.84	2.600	0.120	0.120	1240	Shear Compression
	36	4-1750/1.00	44.8	2000	1559	140	4520	1.13	2.600	0.120	0.120	1000	Diagonal splitting
Oh and Shin	37	N4200	23.72	560	500	130	2000	0.85	1.560	0.000	0.000	297	Shear Compression
	38	N42A2	23.72	560	500	130	2000	0.85	1.560	0.120	0.430	318	Crushing of strut
	39	N42B2	23.72	560	500	130	2000	0.85	1.560	0.220	0.430	422	Crushing of strut
	40	N42C2	23.72	560	500	130	2000	0.85	1.560	0.340	0.430	400	Crushing of strut
	41	H4100	49.1	560	500	130	2000	0.50	1.560	0.000	0.000	719	Shear Compression
	42	H41A2(1)*	49.1	560	500	130	2000	0.50	1.560	0.120	0.430	799	Shear Compression
	43	H41B2	49.1	560	500	130	2000	0.50	1.560	0.220	0.430	791	Shear Compression

Reference	No	deep beam ID	$f`_c$ (Mpa)	h (mm)	d (mm)	b (mm)	l_e (mm)	a/d	P (%)	ρ_{sv} (%)	ρ_{sh} (%)	V_u on each load	failure mode
	44	H41C2	49.1	560	500	130	2000	0.50	1.560	0.340	0.430	794	Shear Compression
	45	H4200	49.1	560	500	130	2000	0.85	1.560	0.000	0.000	449	Shear Compression
	46	H42A2(1)	49.1	560	500	130	2000	0.85	1.560	0.120	0.430	547	Crushing of strut
	47	H42B2(1)	49.1	560	500	130	2000	0.85	1.560	0.220	0.430	511	Crushing of strut
	48	H42C2(1)	49.1	560	500	130	2000	0.85	1.560	0.340	0.430	471	Crushing of strut
	49	H4300	49.1	560	500	130	2000	1.25	1.560	0.000	0.000	378	Crushing of strut
	50	H43A2(1)	49.1	560	500	130	2000	1.25	1.560	0.120	0.430	389	Crushing of strut
	51	H43B2	49.1	560	500	130	2000	1.25	1.560	0.220	0.430	427	Crushing of strut
	52	H43C2	49.1	560	500	130	2000	1.25	1.560	0.340	0.430	451	Crushing of strut
	53	H4500	49.1	560	500	130	2000	2.00	1.560	0.000	0.000	126	Crushing of strut
	54	H45A2	49.1	560	500	130	2000	2.00	1.560	0.120	0.430	236	Crushing of strut
	55	H45B2	49.1	560	500	130	2000	2.00	1.560	0.220	0.430	266	Crushing of strut
	56	H45C2	49.1	560	500	130	2000	2.00	1.560	0.340	0.430	264	Crushing of strut
	57	H41A0	50.67	560	500	120	2000	0.50	1.290	0.130	0.000	389	Shear Compression
	58	H41A1	50.67	560	500	120	2000	0.50	1.290	0.130	0.230	446	Shear Compression
	59	H41A2(2)	50.67	560	500	120	2000	0.50	1.290	0.130	0.130	549	Shear Compression
	60	H41A3	50.67	560	500	120	2000	0.50	1.290	0.130	0.130	509	Shear Compression
	61	H42A2(2)	50.67	560	500	120	2000	0.85	1.290	0.130	0.130	439	Crushing of strut
	62	H42B2(2)	50.67	560	500	120	2000	0.85	1.290	0.240	0.240	404	Crushing of strut
	63	H42C2(2)	50.67	560	500	120	2000	0.85	1.290	0.370	0.370	419	Crushing of strut
	64	H43A0	50.67	560	500	120	2000	1.25	1.290	0.130	0.130	239	Crushing of strut
	65	H43A1	50.67	560	500	120	2000	1.25	1.290	0.130	0.130	292	Crushing of strut
	66	H43A2(2)	50.67	560	500	120	2000	1.25	1.290	0.130	0.130	310	Crushing of strut
	67	H43A3	50.67	560	500	120	2000	1.25	1.290	0.130	0.130	326	flexure failure
	68	H45A2(2)	50.67	560	500	120	2000	2.00	1.290	0.130	0.130	185	flexure failure
	69	U41A0	73.6	560	500	120	2000	0.50	1.290	0.130	0.130	491	Shear Compression
	70	U41A1	73.6	560	500	120	2000	0.50	1.290	0.130	0.130	625	Shear Compression
	71	U41A2	73.6	560	500	120	2000	0.50	1.290	0.130	0.130	614	Shear Compression
	72	U41A3	73.6	560	500	120	2000	0.50	1.290	0.130	0.130	612	Shear Compression
	73	U42A2	73.6	560	500	120	2000	0.85	1.290	0.130	0.130	468	Crushing of strut
	74	U42B2	73.6	560	500	120	2000	0.85	1.290	0.240	0.240	460	Crushing of strut
	75	U42C2	73.6	560	500	120	2000	0.85	1.290	0.370	0.370	457	Crushing of strut
	76	U43A0	73.6	560	500	120	2000	1.25	1.290	0.130	0.130	326	Crushing of strut
	77	U43A1	73.6	560	500	120	2000	1.25	1.290	0.130	0.130	347	Crushing of strut
	78	U43A2	73.6	560	500	120	2000	1.25	1.290	0.130	0.130	379	Crushing of strut
	79	U43A3	73.6	560	500	120	2000	1.25	1.290	0.130	0.130	373	flexure failure
	80	U45A2	73.6	560	500	120	2000	2.00	1.290	0.130	0.130	239	flexure failure
	81	N33A2	23.72	560	500	120	1500	1.25	1.560	0.120	0.120	236	Crushing of strut
	82	N43A2	23.72	560	500	120	2000	1.25	1.560	0.120	0.120	263	Crushing of strut
	83	N53A2	23.72	560	500	120	2500	1.25	1.560	0.120	0.120	214	Crushing of strut
	84	H31A2	49.1	560	500	120	1500	0.50	1.560	0.120	0.120	771	Shear Compression
	85	H32A2	49.1	560	500	120	1500	0.85	1.560	0.120	0.120	548	Crushing of strut
	86	H33A2	49.1	560	500	120	1500	1.25	1.560	0.120	0.120	390	Crushing of strut
	87	H51A2	49.1	560	500	120	2500	0.50	1.560	0.120	0.120	726	Shear Compression
	88	H52A2	49.1	560	500	120	2500	0.85	1.560	0.120	0.120	587	Crushing of strut
	89	H53A2	49.1	560	500	120	2500	1.25	1.560	0.120	0.120	375	Crushing of strut
Smith and Vantsiotis	90	0A0-44	20.5	356	305	102	813	0.77	1.490	0.000	0.000	140	Crushing of strut
	91	0A0-48	21	356	305	102	813	0.77	1.490	0.000	0.000	136	Crushing of strut
	92	1A1-10	18.7	356	305	102	813	0.77	1.490	0.003	0.002	161	Crushing of strut
	93	1A3-11	18.1	356	305	102	813	0.77	1.490	0.003	0.005	148	Crushing of strut
	94	1A4-12	16.1	356	305	102	813	0.77	1.490	0.003	0.007	141	Crushing of strut
	95	1A4-51	20.6	356	305	102	813	0.77	1.490	0.003	0.007	171	Crushing of strut
	96	1A6-37	21.1	356	305	102	813	0.77	1.490	0.003	0.009	184	Crushing of strut
	97	2A1-38	21.7	356	305	102	813	0.77	1.490	0.006	0.002	175	Crushing of strut
	98	2A3-39	19.8	356	305	102	813	0.77	1.490	0.006	0.005	171	Crushing of strut
	99	2A4-40	20.3	356	305	102	813	0.77	1.490	0.006	0.007	172	Crushing of strut
	100	2A6-41	19.1	356	305	102	813	0.77	1.490	0.006	0.009	162	Crushing of strut
	101	3A1-42	18.5	356	305	102	813	0.77	1.490	0.013	0.003	161	Crushing of strut
	102	3A3-43	19.2	356	305	102	813	0.77	1.490	0.013	0.005	173	Crushing of strut

Reference	No	deep beam ID	$f`_c$ (Mpa)	h (mm)	d (mm)	b (mm)	l_e (mm)	a/d	P (%)	ρ_{sv} (%)	ρ_{sh} (%)	V_u on each load	failure mode
	103	3A4-45	20.8	356	305	102	813	0.77	1.490	0.013	0.007	179	Crushing of strut
	104	3A6-46	19.9	356	305	102	813	0.77	1.490	0.013	0.009	168	Crushing of strut
	105	0B0-49	21.7	356	305	102	940	1.01	1.490	0.000	0.000	149	Crushing of strut
	106	1B1-01	22.1	356	305	102	940	1.01	1.490	0.002	0.002	147	Crushing of strut
	107	1B3-29	20.1	356	305	102	940	1.01	1.490	0.002	0.005	144	Crushing of strut
	108	1B4-30	20.8	356	305	102	940	1.01	1.490	0.002	0.007	140	Crushing of strut
	109	1B6-31	19.5	356	305	102	940	1.01	1.490	0.002	0.009	153	Crushing of strut
	110	2B1-05	19.2	356	305	102	940	1.01	1.490	0.004	0.002	129	Crushing of strut
	111	2B3-06	19	356	305	102	940	1.01	1.490	0.004	0.005	131	Crushing of strut
	112	2B4-07	17.5	356	305	102	940	1.01	1.490	0.004	0.007	126	Crushing of strut
	113	2B4-52	21.8	356	305	102	940	1.01	1.490	0.004	0.007	150	Crushing of strut
	114	2B6-32	19.8	356	305	102	940	1.01	1.490	0.004	0.009	145	Crushing of strut
	115	3B1-08	16.2	356	305	102	940	1.01	1.490	0.006	0.002	131	Crushing of strut
	116	3B1-36	20.4	356	305	102	940	1.01	1.490	0.008	0.002	159	Crushing of strut
	117	3B3-33	19	356	305	102	940	1.01	1.490	0.008	0.005	158	Crushing of strut
	118	3B4-34	19.2	356	305	102	940	1.01	1.490	0.008	0.007	155	Crushing of strut
	119	3B6-35	20.7	356	305	102	940	1.01	1.490	0.008	0.009	166	Crushing of strut
	120	4B1-09	17.1	356	305	102	940	1.01	1.490	0.013	0.002	153	Crushing of strut
	121	0C0-50	20.7	356	305	102	1118	1.34	1.490	0.000	0.000	116	Crushing of strut
	122	1C1-14	19.2	356	305	102	1118	1.34	1.490	0.002	0.002	119	Crushing of strut
	123	1C3-02	21.9	356	305	102	1118	1.34	1.490	0.002	0.005	123	Crushing of strut
	124	1C4-15	22.7	356	305	102	1118	1.34	1.490	0.002	0.007	131	Crushing of strut
	125	1C6-16	21.8	356	305	102	1118	1.34	1.490	0.002	0.009	122	Crushing of strut
	126	2C1-17	19.9	356	305	102	1118	1.34	1.490	0.003	0.002	124	Crushing of strut
	127	2C3-03	19.2	356	305	102	1118	1.34	1.490	0.003	0.005	104	Crushing of strut
	128	2C3-27	19.3	356	305	102	1118	1.34	1.490	0.003	0.005	115	Crushing of strut
	129	2C4-18	20.44	356	305	102	1118	1.34	1.490	0.003	0.007	125	Crushing of strut
	130	2C6-19	20.8	356	305	102	1118	1.34	1.490	0.003	0.009	124	Crushing of strut
	131	3C1-20	21	356	305	102	1118	1.34	1.490	0.006	0.002	141	Crushing of strut
	132	3C3-21	16.5	356	305	102	1118	1.34	1.490	0.006	0.005	125	Crushing of strut
	133	3C4-22	18.3	356	305	102	1118	1.34	1.490	0.006	0.007	128	Crushing of strut
	134	3C6-23	19	356	305	102	1118	1.34	1.490	0.006	0.009	137	Crushing of strut
	135	4C1-24	19.6	356	305	102	1118	1.34	1.490	0.008	0.002	147	Crushing of strut
	136	4C3-04	18.5	356	305	102	1118	1.34	1.490	0.006	0.005	129	Crushing of strut
	137	4C3-28	19.2	356	305	102	1118	1.34	1.490	0.008	0.005	152	Crushing of strut
	138	4C4-25	18.5	356	305	102	1118	1.34	1.490	0.008	0.007	153	Crushing of strut
	139	4C6-26	21.2	356	305	102	1118	1.34	1.490	0.008	0.009	159	Crushing of strut
	140	0D0-47	19.5	356	305	102	1473	2.01	1.490	0.000	0.000	73	Crushing of strut
	141	4D1-13	16.1	356	305	102	1473	2.01	1.490	0.004	0.002	87	Crushing of strut
Walraven and Lehwalter	142	V711	18.1	200	160	250	680	1.00	1.100	0.000	0.000	165	flexure failure
	143	V022	19.9	400	360	250	1030	1.00	1.100	0.000	0.000	270	Crushing of strut
	144	V511	19.8	600	560	250	1380	1.00	1.100	0.000	0.000	350	Crushing of strut
	145	V411	19.4	800	740	250	1780	1.00	1.100	0.000	0.000	365	Crushing of strut
	146	V711/4	19.5	200	160	250	680	1.00	1.100	0.150	0.000	207	flexure failure
	147	V022/4	18.2	400	360	250	1030	1.00	1.100	0.150	0.000	317	Crushing of strut
	148	V511/4	18.7	600	560	250	1380	1.00	1.100	0.150	0.000	465	Crushing of strut
	149	V411/4	17	800	740	250	1780	1.00	1.100	0.150	0.000	467	Crushing of strut
	150	V711/3	19.6	200	160	250	680	1.00	1.100	0.300	0.000	380	flexure failure
	151	V022/3	19.6	400	360	250	1030	1.00	1.100	0.300	0.000	380	Crushing of strut
	152	V511/3	21.3	600	560	250	1380	1.00	1.100	0.300	0.000	580	Crushing of strut
	153	V411/3	19.8	800	740	250	1780	1.00	1.100	0.300	0.000	665	Crushing of strut

Reference	No	deep beam ID	$f`_c$ (Mpa)	h (mm)	d (mm)	b (mm)	l_e (mm)	a/d	P (%)	ρ_{sv} (%)	ρ_{sh} (%)	V_u on each load	failure mode
Tan et all	154	I-1/0.75	56.3	500	442.5	110	1750	0.85	2.580	0.000	0.000	500	Diagonal splitting
	155	I-2N/0.75	56.2	500	442.5	110	1750	0.85	2.580	2.860	0.000	760	Crushing of strut
	156	I-3/0.75	59.2	500	442.5	110	1750	0.85	2.580	0.000	1.590	560	Crushing of strut
	157	I-4/0.75	63.8	500	442.5	110	1750	0.85	2.580	0.000	1.590	580	Shear Compression
	158	I-5/0.75	57.6	500	442.5	110	1750	0.85	2.580	0.000	3.170	775	Crushing of strut
	159	I-6S/0.75	59.7	500	442.5	110	1750	0.85	2.580	2.860	1.590	775	Diagonal splitting
	160	II-1/1.00	77.6	500	442.5	110	2000	1.13	2.580	0.000	0.000	255	Diagonal splitting
	161	II-2N/1.0	77.6	500	442.5	110	2000	1.13	2.580	1.430	0.000	520	Diagonal splitting
	162	II-3/1.00	78	500	442.5	110	2000	1.13	2.580	0.000	1.590	390	Diagonal splitting
	163	II-4/1.00	86.3	500	442.5	110	2000	1.13	2.580	0.000	1.590	330	Diagonal splitting
	164	II-5/1.00	86.3	500	442.5	110	2000	1.13	2.580	0.000	3.170	470	Diagonal splitting
	165	II-6N/1.00	75.3	500	442.5	110	2000	1.13	2.580	1.430	1.590	670	Crushing of strut
	166	III-1/1.50	77.6	500	442.5	110	2500	1.69	2.580	0.000	0.000	185	Diagonal splitting
	167	III-2N/1.50	77.6	500	442.5	110	2500	1.69	2.580	1.430	0.000	335	Diagonal splitting
	168	III-2S/1.50	77.6	500	442.5	110	2500	1.69	2.580	1.430	0.000	400	Shear Compression
	169	III-3/1.50	78	500	442.5	110	2500	1.69	2.580	0.000	1.590	200	Diagonal splitting
	170	III-4/1.50	86.3	500	442.5	110	2500	1.69	2.580	0.000	1.590	190	Diagonal splitting
	171	III-5/1.50	86.3	500	442.5	110	2500	1.69	2.580	0.000	3.170	265	Diagonal splitting
	172	III-6N/1.50	78.9	500	442.5	110	2500	1.69	2.580	1.430	1.590	460	Shear Compression
	165	II-6N/1.00	75.3	500	442.5	110	2000	1.13	2.580	1.430	1.590	670	Crushing of strut
	166	III-1/1.50	77.6	500	442.5	110	2500	1.69	2.580	0.000	0.000	185	Diagonal splitting
	167	III-2N/1.50	77.6	500	442.5	110	2500	1.69	2.580	1.430	0.000	335	Diagonal splitting
	168	III-2S/1.50	77.6	500	442.5	110	2500	1.69	2.580	1.430	0.000	400	Shear Compression
	169	III-3/1.50	78	500	442.5	110	2500	1.69	2.580	0.000	1.590	200	Diagonal splitting
	170	III-4/1.50	86.3	500	442.5	110	2500	1.69	2.580	0.000	1.590	190	Diagonal splitting
	171	III-5/1.50	86.3	500	442.5	110	2500	1.69	2.580	0.000	3.170	265	Diagonal splitting
	172	III-6N/1.50	78.9	500	442.5	110	2500	1.69	2.580	1.430	1.590	460	Shear Compression
	165	II-6N/1.00	75.3	500	442.5	110	2000	1.13	2.580	1.430	1.590	670	Crushing of strut
	166	III-1/1.50	77.6	500	442.5	110	2500	1.69	2.580	0.000	0.000	185	Diagonal splitting
	167	III-2N/1.50	77.6	500	442.5	110	2500	1.69	2.580	1.430	0.000	335	Diagonal splitting
	168	III-2S/1.50	77.6	500	442.5	110	2500	1.69	2.580	1.430	0.000	400	Shear Compression
	169	III-3/1.50	78	500	442.5	110	2500	1.69	2.580	0.000	1.590	200	Diagonal splitting
	170	III-4/1.50	86.3	500	442.5	110	2500	1.69	2.580	0.000	1.590	190	Diagonal splitting
	171	III-5/1.50	86.3	500	442.5	110	2500	1.69	2.580	0.000	3.170	265	Diagonal splitting
	172	III-6N/1.50	78.9	500	442.5	110	2500	1.69	2.580	1.430	1.590	460	Shear Compression
Tan et all	173	1-2.00/0.75	71.2	500	448.2	110	1750	0.84	2.000	0.480	0.000	545	Shear Compression
	174	1-2.00/1.00	71.2	500	448.2	110	2000	1.12	2.000	0.480	0.000	500	Shear Compression
	175	1-2.00/1.50	72.1	500	448.2	110	2500	1.67	2.000	0.480	0.000	250	Diagonal splitting
	176	1-2.00/2.50	74.1	500	448.2	110	3500	2.79	2.000	0.480	0.000	195	flexure failure
	177	2-2.58/0.25	69.9	500	442.5	110	1250	0.28	2.580	0.480	0.000	835	Shear Compression
	178	2-2.58/0.50	64.6	500	442.5	110	1500	0.56	2.580	0.480	0.000	740	Shear Compression
	179	2-2.58/0.75	64.6	500	442.5	110	1750	0.85	2.580	0.480	0.000	530	Shear Compression
	180	2-2.58/1.00	68.1	500	442.5	110	2000	1.13	2.580	0.480	0.000	250	Diagonal splitting
	181	2-2.58/1.50	68.1	500	442.5	110	2500	1.69	2.580	0.480	0.000	150	Diagonal splitting
	182	2-2.58/2.00	69.9	500	442.5	110	3000	2.26	2.580	0.480	0.000	130	Diagonal splitting
	183	2-2.58/2.50	54.7	500	442.5	110	3500	2.82	2.580	0.480	0.000	155	flexure failure
	184	3-4.08/0.25	69.9	500	420	110	1250	0.30	4.080	0.480	0.000	925	Shear Compression
	185	3-4.08/0.50	64.6	500	420	110	1500	0.60	4.080	0.480	0.000	720	Shear Compression
	186	3-4.08/0.75	64.6	500	420	110	1750	0.89	4.080	0.480	0.000	670	Shear Compression
	187	3-4.08/1.00	68.1	500	420	110	2000	1.19	4.080	0.480	0.000	520	Crushing of strut
	188	3-4.08/1.50	68.1	500	420	110	2500	1.79	4.080	0.480	0.000	150	Diagonal splitting
	189	3-4.08/2.00	69.9	500	420	110	3000	2.38	4.080	0.480	0.000	190	Diagonal splitting
	190	3-4.08/2.50	54.8	500	420	110	3500	2.98	4.080	0.480	0.000	135	flexure failure
	191	4-5.80/0.75	71.2	500	397.5	110	1750	0.94	5.800	0.480	0.000	700	Crushing of strut
	192	4-5.80/1.00	71.2	500	397.5	110	2000	1.26	5.800	0.480	0.000	530	Shear Compression
	193	4-5.80/1.50	72.1	500	397.5	110	2500	1.89	5.800	0.480	0.000	390	Diagonal splitting
	194	4-5.80/2.50	74.1	500	397.5	110	3500	3.14	5.800	0.480	0.000	265	flexure failure

Reference	No	deep beam ID	$f`_c$ (Mpa)	h (mm)	d (mm)	b (mm)	l_e (mm)	a/d	P (%)	ρ_{sv} (%)	ρ_{sh} (%)	V_u on each load	failure mode
Foster and Gilbert	195	B1.2-1	91	1200	1124	125	1450	0.76	1.281	0.604	0.259	1000	Crushing of strut
	196	B1.2-2	96	1200	1124	125	1450	0.76	1.281	0.604	0.259	1000	Crushing of strut
	197	B1.2-3	80	1200	1124	125	1450	0.76	1.281	0.604	0.259	1300	shear-flexure failure
	198	B1.2-4	80	1200	1124	125	1450	0.76	1.281	0.604	0.259	1050	Crushing of strut
	199	B2.0-1	83	700	624	125	1400	1.32	2.308	0.604	0.340	795	shear-flexure failure
	200	B2.0-2	120	700	624	125	1400	1.32	2.308	0.604	0.340	825	flexure failure
	201	B2.0-3	78	700	624	125	1400	1.32	2.308	0.604	0.340	700	flexure failure
	202	B2.0A-4	86	700	624	125	1400	0.88	2.308	0.604	0.340	950	flexure failure
	203	B2.0B-5	89	700	624	125	1400	1.32	2.308	0.000	0.000	585	flexure failure
	204	B2.0C-6	93	700	624	125	1400	1.32	2.308	0.906	0.000	730	flexure failure
	205	B2.0D-7	104	700	624	125	1400	1.32	2.308	0.604	0.000	720	flexure failure
	206	B3.0-1	80	700	624	125	2100	1.88	2.308	0.604	0.340	510	flexure failure
	207	B3.0-2	120	700	624	125	2100	1.88	2.308	0.604	0.340	525	flexure failure
	208	B3.0-3	77	700	624	125	2100	1.88	2.308	0.604	0.340	525	flexure failure
	209	B3.0A-4	88	700	624	125	2100	1.28	2.308	0.604	0.340	775	flexure failure
	210	B3.0B-5	89	700	624	125	2100	1.88	2.308	0.000	0.000	435	flexure failure
Shin et all	211	MHB1.5-0	52	250	215	125	645	1.50	3.770	0.000	0.000	131	flexure failure
	212	MHB1.5-25	52	250	215	125	645	1.50	3.770	0.450	0.000	182	Diagonal splitting
	213	MHB1.5-50	52	250	215	125	645	1.50	3.770	0.910	0.000	242	Diagonal splitting
	214	MHB1.5-75	52	250	215	125	645	1.50	3.770	1.360	0.000	279	Shear Compression
	215	MHB1.5-100	52	250	215	125	645	1.50	3.770	1.810	0.000	299	Shear Compression
	216	MHB2.0-0	52	250	215	125	645	2.00	3.770	0.000	0.000	102	flexure failure
	217	MHB2.0-25	52	250	215	125	645	2.00	3.770	0.450	0.000	129	Diagonal splitting
	218	MHB2.0-50	52	250	215	125	645	2.00	3.770	0.910	0.000	202	Diagonal splitting
	219	MHB2.0-75	52	250	215	125	645	2.00	3.770	1.360	0.000	216	Shear Compression
	220	MHB2.0-100	52	250	215	125	645	2.00	3.770	1.810	0.000	225	Shear Compression
	221	MHB2.5-0	52	250	215	125	645	2.50	3.770	0.000	0.000	66	flexure failure
	222	MHB2.5-25	52	250	215	125	645	2.50	3.770	0.450	0.000	115	Diagonal splitting
	223	MHB2.5-50	52	250	215	125	645	2.50	3.770	0.910	0.000	161	Diagonal splitting
	224	MHB2.5-75	52	250	215	125	645	2.50	3.770	1.360	0.000	185	Shear Compression
	225	MHB2.5-100	52	250	215	125	645	2.50	3.770	1.810	0.000	191	Shear Compression
	226	HB1.5-0	73	250	215	125	645	1.50	3.770	0.000	0.000	165	flexure failure
	227	HB1.5-25	73	250	215	125	645	1.50	3.770	0.450	0.000	249	Diagonal splitting
	228	HB1.5-50	73	250	215	125	645	1.50	3.770	0.910	0.000	286	Diagonal splitting
	229	HB1.5-75	73	250	215	125	645	1.50	3.770	1.360	0.000	309	Shear Compression
	230	HB1.5-100	73	250	215	125	645	1.50	3.770	1.810	0.000	326	Shear Compression
	231	HB2.0-0	73	250	215	125	645	2.00	3.770	0.000	0.000	116	flexure failure
	232	HB2.0-25	73	250	215	125	645	2.00	3.770	0.450	0.000	166	Diagonal splitting
	233	HB2.0-50	73	250	215	125	645	2.00	3.770	0.910	0.000	228	Diagonal splitting
	234	HB2.0-75	73	250	215	125	645	2.00	3.770	1.360	0.000	268	Shear Compression
	235	HB2.0-100	73	250	215	125	645	2.00	3.770	1.810	0.000	282	Shear Compression
	236	HB2.5-0	73	250	215	125	645	2.50	3.770	0.000	0.000	93	flexure failure
	237	HB2.5-25	73	250	215	125	645	2.50	3.770	0.450	0.000	134	Diagonal splitting
	238	HB2.5-50	73	250	215	125	645	2.50	3.770	0.910	0.000	173	Diagonal splitting
	239	HB2.5-75	73	250	215	125	645	2.50	3.770	1.360	0.000	194	Shear Compression
	240	HB2.5-100	73	250	215	125	645	2.50	3.770	1.810	0.000	214	Shear Compression
Yang et all	241	L5-40	31.4	400	355	160	1000	0.56	1.000	0.000	0.000	447	Crushing of strut
	242	L5-60	31.4	600	555	160	2100	0.54	0.980	0.000	0.000	535	Crushing of strut
	243	L5-60R	31.4	600	555	160	1500	0.54	0.980	0.000	0.000	479	Crushing of strut
	244	L5-75	31.4	750	685	160	1350	0.55	1.000	0.000	0.000	597	Crushing of strut
	245	L5-100	31.4	1000	935	160	1600	0.53	0.900	0.000	0.000	582	Crushing of strut
	246	L10-40	31.4	400	355	160	1400	1.13	1.000	0.000	0.000	192	Crushing of strut
	247	L10-40R	31.4	400	355	160	1400	1.13	1.000	0.000	0.000	312	Crushing of strut
	238	HB2.5-50	73	250	215	125	645	2.50	3.770	0.910	0.000	173	Diagonal splitting
	239	HB2.5-75	73	250	215	125	645	2.50	3.770	1.360	0.000	194	Shear Compression
	240	HB2.5-100	73	250	215	125	645	2.50	3.770	1.810	0.000	214	Shear Compression

Reference	No	deep beam ID	$f`_c$ (Mpa)	h (mm)	d (mm)	b (mm)	l_e (mm)	a/d	P (%)	ρ_{sv} (%)	ρ_{sh} (%)	V_u on each load	failure mode
Yang et all	241	L5-40	31.4	400	355	160	1000	0.56	1.000	0.000	0.000	447	Crushing of strut
	242	L5-60	31.4	600	555	160	2100	0.54	0.980	0.000	0.000	535	Crushing of strut
	243	L5-60R	31.4	600	555	160	1500	0.54	0.980	0.000	0.000	479	Crushing of strut
	244	L5-75	31.4	750	685	160	1350	0.55	1.000	0.000	0.000	597	Crushing of strut
	245	L5-100	31.4	1000	935	160	1600	0.53	0.900	0.000	0.000	582	Crushing of strut
	246	L10-40	31.4	400	355	160	1400	1.13	1.000	0.000	0.000	192	Crushing of strut
	247	L10-40R	31.4	400	355	160	1400	1.13	1.000	0.000	0.000	312	Crushing of strut
	238	HB2.5-50	73	250	215	125	645	2.50	3.770	0.910	0.000	173	Diagonal splitting
	239	HB2.5-75	73	250	215	125	645	2.50	3.770	1.360	0.000	194	Shear Compression
	240	HB2.5-100	73	250	215	125	645	2.50	3.770	1.810	0.000	214	Shear Compression
Yang et all	241	L5-40	31.4	400	355	160	1000	0.56	1.000	0.000	0.000	447	Crushing of strut
	242	L5-60	31.4	600	555	160	2100	0.54	0.980	0.000	0.000	535	Crushing of strut
	243	L5-60R	31.4	600	555	160	1500	0.54	0.980	0.000	0.000	479	Crushing of strut
	244	L5-75	31.4	750	685	160	1350	0.55	1.000	0.000	0.000	597	Crushing of strut
	245	L5-100	31.4	1000	935	160	1600	0.53	0.900	0.000	0.000	582	Crushing of strut
	246	L10-40	31.4	400	355	160	1400	1.13	1.000	0.000	0.000	192	Crushing of strut
	247	L10-40R	31.4	400	355	160	1400	1.13	1.000	0.000	0.000	312	Crushing of strut
	248	L10-60	31.4	600	555	160	2100	1.08	0.980	0.000	0.000	375	Crushing of strut
	249	L10-75	31.4	750	685	160	2100	1.09	1.000	0.000	0.000	272	Crushing of strut
	250	L10-75R	31.4	750	685	160	2100	1.09	1.000	0.000	0.000	330	Crushing of strut
	251	L10-100	31.4	1000	935	160	2600	1.07	0.900	0.000	0.000	544	Crushing of strut
	252	UH5-40	78.5	400	355	160	1000	0.56	1.000	0.000	0.000	733	Crushing of strut
	253	UH5-60	78.5	600	555	160	2100	0.54	0.980	0.000	0.000	823	Crushing of strut
	254	UH5-75	78.5	750	685	160	1350	0.55	1.000	0.000	0.000	1010	Crushing of strut
	255	UH5-100	78.5	1000	935	160	1600	0.53	0.900	0.000	0.000	1029	Crushing of strut
	256	UH10-40	78.5	400	355	160	1400	1.13	1.000	0.000	0.000	499	Crushing of strut
	257	UH10-40R	78.5	400	355	160	1400	1.13	1.000	0.000	0.000	385	Crushing of strut
	258	UH10-60	78.5	600	555	160	2100	1.08	0.980	0.000	0.000	573	Crushing of strut
	259	UH10-75	78.5	750	685	160	2100	1.09	1.000	0.000	0.000	338	Crushing of strut
	260	UH10-75R	78.5	750	685	160	2100	1.09	1.000	0.000	0.000	361	Crushing of strut
	261	UH10-100	78.5	1000	935	160	2600	1.07	0.900	0.000	0.000	769	Crushing of strut
Kong and Rangan	262	S1-1	63.6	350	292	250	1960	2.50	2.803	0.157	0.000	228	Crushing of strut
	263	S1-2	63.6	350	292	250	1960	2.50	2.803	0.157	0.000	208	Crushing of strut
	264	S1-3	63.6	350	292	250	1960	2.50	2.803	0.157	0.000	206	Crushing of strut
	265	S1-4	63.6	350	292	250	1960	2.50	2.803	0.157	0.000	278	Crushing of strut
	266	S1-5	63.6	350	292	250	1960	2.50	2.803	0.157	0.000	253	Crushing of strut
	267	S1-6	63.6	350	292	250	1960	2.50	2.803	0.157	0.000	224	Crushing of strut
	268	S2-1	72.5	350	292	250	1960	2.50	2.803	0.105	0.000	260	Crushing of strut
	269	S2-2	72.5	350	292	250	1960	2.50	2.803	0.126	0.000	233	Crushing of strut
	270	S2-3	72.5	350	292	250	1960	2.50	2.803	0.157	0.000	253	Crushing of strut
	271	S2-4	72.5	350	292	250	1960	2.50	2.803	0.157	0.000	219	Crushing of strut
	272	S2-5	72.5	350	292	250	1960	2.50	2.803	0.209	0.000	282	Crushing of strut
	273	S2-6	72.5	350	292	250	1960	2.50	2.803	0.262	0.000	359	flexure failure
	274	S3-1	67.4	350	297	250	1980	2.49	1.659	0.101	0.000	209	Crushing of strut
	275	S3-2	67.4	350	297	250	1980	2.49	1.659	0.101	0.000	178	Crushing of strut
	276	S3-3	67.4	350	293	250	1960	2.49	2.793	0.101	0.000	229	Crushing of strut
	277	S3-4	67.4	350	293	250	1960	2.49	2.793	0.101	0.000	175	Crushing of strut
	278	S3-5	67.4	350	299	250	1940	2.41	3.692	0.101	0.000	297	Crushing of strut
	279	S3-6	67.4	350	299	250	1940	2.41	3.692	0.101	0.000	283	Crushing of strut
	280	S4-1	87.3	600	542	250	3100	2.40	3.020	0.157	0.000	354	Crushing of strut
	281	S4-2	87.3	500	444	250	2640	2.41	2.959	0.157	0.000	573	Crushing of strut
	282	S4-3	87.3	400	346	250	2160	2.40	2.849	0.157	0.000	243	Crushing of strut
	283	S4-4	87.3	350	292	250	1960	2.50	2.803	0.157	0.000	258	Crushing of strut
	284	S4-5	87.3	300	248	250	1680	2.38	2.968	0.157	0.000	321	flexure failure

Reference	No	deep beam ID	$f`_c$ (Mpa)	h (mm)	d (mm)	b (mm)	l_e (mm)	a/d	P (%)	ρ_{sv} (%)	ρ_{sh} (%)	V_u on each load	failure mode
	285	S4-6	87.3	250	198	250	1500	2.53	2.788	0.157	0.000	203	Crushing of strut
	286	S5-1	89.4	350	292	250	2260	3.01	2.803	0.157	0.000	242	Crushing of strut
	287	S5-2	89.4	350	292	250	2100	2.74	2.803	0.157	0.000	260	Crushing of strut
	288	S5-3	89.4	350	292	250	1960	2.50	2.803	0.157	0.000	244	Crushing of strut
	289	S5-4	89.4	350	292	250	1660	1.99	2.803	0.157	0.000	477	Crushing of strut
	290	S5-5	89.4	350	292	250	1520	1.75	2.803	0.157	0.000	573	Crushing of strut
	291	S5-6	89.4	350	292	250	1380	1.51	2.803	0.157	0.000	648	flexure failure
	292	S7-1	74.8	350	294	250	2440	3.30	4.468	0.105	0.000	217	Crushing of strut
	293	S7-2	74.8	350	294	250	2440	3.30	4.468	0.126	0.000	205	Crushing of strut
	294	S7-3	74.8	350	294	250	2440	3.30	4.468	0.157	0.000	247	Crushing of strut
	295	S7-4	74.8	350	294	250	2440	3.30	4.468	0.196	0.000	274	Crushing of strut
	296	S7-5	74.8	350	294	250	2440	3.30	4.468	0.224	0.000	304	Crushing of strut
	297	S7-6	74.8	350	294	250	2440	3.30	4.468	0.262	0.000	311	Crushing of strut
	298	S8-1	74.6	350	292	250	1960	2.50	2.803	0.105	0.000	272	Crushing of strut
	299	S8-2	74.6	350	292	250	1960	2.50	2.803	0.126	0.000	251	Crushing of strut
	300	S8-3	74.6	350	292	250	1960	2.50	2.803	0.157	0.000	310	Crushing of strut
	301	S8-4	74.6	350	292	250	1960	2.50	2.803	0.157	0.000	266	Crushing of strut
	302	S8-5	74.6	350	292	250	1960	2.50	2.803	0.196	0.000	289	Crushing of strut
	303	S8-6	74.6	350	292	250	1960	2.50	2.803	0.224	0.000	284	Crushing of strut
Aguilar et all	304	ACI-I	28	915	791	305	4020	1.16	1.094	0.305	0.458	1357	flexure failure
	305	STM-I	28	915	719	305	4020	1.27	1.094	0.305	0.153	1134	flexure failure
	306	STM-H	28	915	801	305	4020	1.14	1.094	0.305	0.103	1285	Crushing of strut
	307	STM-M	28	915	801	305	4020	1.14	1.094	0.305	0.000	1277	Crushing of strut
Tan et all	308	A-0.27-2.15	58.84	500	463	110	1000	0.27	1.230	0.480	0.000	675	Crushing of strut
	309	A-0.27-3.23	51.62	500	463	110	1500	0.27	1.230	0.480	0.000	630	Crushing of strut
	310	A-0.27-4.30	53.85	500	463	110	2000	0.27	1.230	0.480	0.000	640	Crushing of strut
	311	A-0.27-5.38	57.31	500	463	110	2500	0.27	1.230	0.480	0.000	630	Crushing of strut
	312	B-0.54-2.15	55.98	500	463	110	1000	0.54	1.230	0.480	0.000	468	Crushing of strut
	313	B-0.54-3.23	45.68	500	463	110	1500	0.54	1.230	0.480	0.000	445	Crushing of strut
	314	B-0.54-4.30	53.85	500	463	110	2000	0.54	1.230	0.480	0.000	500	Crushing of strut
	315	B-0.54-5.38	52.99	500	463	110	2500	0.54	1.230	0.480	0.000	480	Crushing of strut
	316	C-0.81-2.15	51.15	500	463	110	1000	0.81	1.230	0.480	0.000	403	Crushing of strut
	317	C-0.81-3.23	43.96	500	463	110	1500	0.81	1.230	0.480	0.000	400	Crushing of strut
	318	D-1.08-2.15	48.2	500	463	110	1000	1.08	1.230	0.480	0.000	270	Crushing of strut
	319	D-1.08-3.23	44.12	500	463	110	1500	1.08	1.230	0.480	0.000	280	shear-flexure
	320	D-1.08-4.30	46.81	500	463	110	2000	1.08	1.230	0.480	0.000	290	shear-flexure
	321	D-1.08-5.38	48.03	500	463	110	2500	1.08	1.230	0.480	0.000	290	flexure failure
	322	E-1.62-3.23	50.56	500	463	110	1500	1.62	1.230	0.480	0.000	290	Crushing of strut
	323	E-1.62-4.30	44.6	500	463	110	2000	1.62	1.230	0.480	0.000	190	shear-flexure
	324	E-1.62-5.38	45.33	500	463	110	2500	1.62	1.230	0.480	0.000	173	flexure failure
	325	F-2.16-4.30	41.06	500	463	110	2000	2.16	1.230	0.480	0.000	150	shear-flexure
	326	G-2.70-5.38	42.8	500	463	110	2500	2.70	1.230	0.480	0.000	105	shear-flexure
Marco Rigotti	327	B150S6	28.9	356	305	95	1269	1.87	3.710	0.390	0.000	186	Crushing of strut
	328	B250S6	34.5	356	305	95	1269	1.87	3.710	0.390	0.000	248	Crushing of strut
	329	B350S6	28.9	356	305	95	1269	1.87	3.710	0.390	0.000	211	Crushing of strut
	330	B150S19	28.9	356	305	95	1269	1.87	3.710	0.000	0.000	178	Crushing of strut
	331	B250S19	28.9	356	305	95	1269	1.87	3.710	0.000	0.000	189	Crushing of strut
	332	B350S19	25.5	356	305	95	1269	1.87	3.710	0.000	0.000	156	Crushing of strut
	333	B160S6	28.9	356	305	95	1549	2.33	3.710	0.390	0.000	196	Crushing of strut
	334	B260S6	28.9	356	305	95	1549	2.33	3.710	0.390	0.000	186	Crushing of strut
	335	B360S6	34.5	356	305	95	1549	2.33	3.710	0.390	0.000	178	Crushing of strut
	336	B160S25	16.5	356	305	95	1549	2.33	3.710	0.000	0.000	85	Crushing of strut
	337	B260S25	34.5	356	305	95	1549	2.33	3.710	0.000	0.000	178	Crushing of strut

Reference	No	deep beam ID	$f`_c$ (Mpa)	h (mm)	d (mm)	b (mm)	l_e (mm)	a/d	P (%)	ρ_{sv} (%)	ρ_{sh} (%)	V_u on each load	failure mode
Garay & Lubell	338	MS1-1	46	607	501	300	1700	1.19	0.520	0.333	0.241	626	flexure failure
	339	MS1-2	44	607	503	300	1700	1.19	1.130	0.333	0.412	1071	flexure failure
	340	MS1-3	44	607	506	300	1700	1.19	2.290	0.333	0.237	1374	Diagonal splitting
	341	MS2-2	47	607	503	300	2300	1.79	1.130	0.333	0.412	716	flexure failure
	342	MS2-3	43	607	506	300	2300	1.79	2.290	0.333	0.403	1028	flexure-splitting strut
	343	MS3-2	48	607	503	300	2900	2.38	1.130	0.444	0.412	577	flexure failure
	344	NS1-4	23	607	507	300	1700	1.18	1.770	0.262	0.412	784	Diagonal splitting
	345	NS2-4	25	607	507	300	2300	1.80	1.770	0.430	0.412	206	Diagonal splitting
	346	MW1-2	39	607	503	300	1700	1.19	1.130	0.000	0.412	784	flexure-splitting strut
	347	MW3-2	43	607	503	300	2900	2.38	1.130	0.000	0.412	539	flexure failure

Appendix B:

An example for application of the STM provisions of the Canadian Code:

To illustrate the procedure of calculating the ultimate shear strength and prediction of failure location for specimen No II-5/1.00 in the experimental study Tan et al. [1997a] by the Canadian Code Fig.A-1.

After selecting the appropriate truss model according to the number of loading points, the height of bottom node can be calculated by

$$h_{bn} = 2 \times (H - d) \qquad \text{(A1.1)}$$

where H is the beam height and d is the effective depth

$$h_{bn} = 2 \times (500 - 442.5) = 115\ mm$$

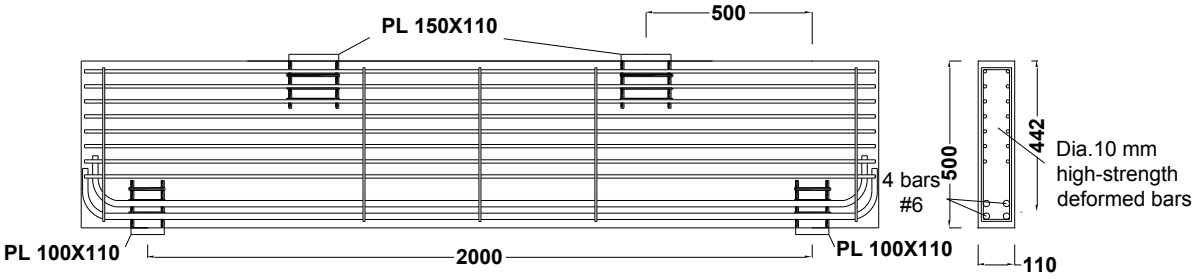

Fig. (A-1) The Detailing of Beam No II-5/1.00 (Tan et al. [1997a]).

Since $C=T$ and to limit stresses in the nodal zones the height of top node is produced

$$h_{tn} = \frac{0.75}{0.85} h_{bn}$$

$$h_{tn} = \frac{0.75}{0.85} 115 = 101.47\ mm$$

Due to those dimensions the strut angle α can be determined

$$\alpha = \tan^{-1}\ [(d - h_{tn}/2)\ /a]$$

$$\alpha = \tan^{-1}\ [(442.5 - 101.47/2)\ /500.025] = 38.07^{\circ}$$

which is not to exceed the minimum allowable angle which is $\theta = 29 + 7000\varepsilon_x = 27.6^{\circ}$.

According Equations (11-22) and (11-23) of Canadian code CSA A23.3-04, the limiting compressive stress in strut f_{cu} has been calculated as 31.14 N/mm^2

Also the width of the strut at the top and bottom nodes can be calculated as

$$w_{s\ Top} = (h_{tn} \times \cos\alpha) + (w_{tn} \times \sin\propto)$$

$$w_{s\ Top} = (101.47 \times \cos 38.07) + (150 \times \sin 38.07) = 172.37\ mm$$

$$w_{s\ Bottom} = (h_{bn} \times \cos\alpha) + (w_{bn} \times \sin\propto)$$

$$w_{s\ Bottom} = (115 \times \cos 38.07) + (100 \times \sin 38.07) = 152.20\ mm$$

The strut strength is governed by the least strut width $w_{s\ Bottom}$

$F_{strut} = f_{cu} \times w_{s\ Bottom}\ \times \mathrm{b}$

where b is beam width

$$F_{strut} = 31.14 \times 152.20\ \times 110/1000 = 521.35\ \mathrm{KN}$$

The maximum magnitude of the applied load predicted from the strut strength can be expressed as follows

$$P1 = F_{strut} \times \sin\propto$$

$$P1 = 521.35 \times \sin 38.07 = 321.48\ KN$$

The stresses at the top nod is calculated at both faces vertical and horizontal as follows

$F_{Top\ nV}\ = 0.85 \times \phi_c \times \acute{f}_c \times h_{n\ top\ V}\ \times \mathrm{b_{n\ top}}$

where ϕ_c is Material safety factor is 0.65

$F_{Top\ nV} = 0.85 \times 0.65 \times 86.3 \times 101.47 \times 110/1000 = 532.20$ KN

$F_{Top\ nH} = 0.85 \times \phi_c \times \acute{f_c} \times w_{n\ top} \times \mathrm{b_{n\ top}}$

$F_{Top\ nH} = 0.85 \times 0.65 \times 86.3 \times 150 \times 110/1000 = 786.73$ KN

The applied load predicted from the top node can be expressed as follows

$P2 = F_{Top\ nV} / \tan\alpha$

$$P2 = 532.20/\tan 38.07 = 679.47\ KN$$

$P3 = F_{Top\ nH} = 786.73$ KN

Also the stresses at bottom nod is calculated at both faces, vertical and horizontal, as follows

$F_{Bot\ nV} = 0.75 \times \phi_c \times \acute{f_c} \times h_{n\ bot\ V} \times \mathrm{b_{n\ bot}}$

$F_{Bot\ nV} = 0.75 \times 0.65 \times 86.3 \times 115 \times 110/1000 = 532.20$ KN

$F_{Bot\ nH} = 0.75 \times \phi_c \times \acute{f_c} \times w_{n\ bot} \times \mathrm{b_{n\ bot}}$

$F_{Bot\ nH} = 0.75 \times 0.65 \times 86.3 \times 100 \times 110/1000 = 462.78$ KN

The applied load predicted from the bottom node can be expressed as follows

$P4 = F_{Bot\ nV} / \tan\alpha$

$$P4 = 532.20/\tan 38.07 = 679.47\ KN$$

$P5 = F_{Bot\ nH} = 786.73$ KN

The tie strength equal to

$F_{Tie} = 0.85 \times A_s \times f_y$

where A_s is the area of longitudinal steel reinforcement and f_y is yield strength of steel

$F_{Tie} = 0.85 \times 1255 \times 498/1000 = 531.59\ KN$

$P6 = F_{Tie}\ /\tan\alpha$

$P6 = 531.59/\tan 38.07 = 678.69\ KN$

The ultimate load that can be applied to the beam is governed by P_1 which is the least value of the P that calculated from the strength of different elements of the truss in STM. Also the failure occurred at that location corresponding to the element with the least strength. In this case, the results indicate that the beam will fail by strut crushing at ultimate shear strength V_{calc} equal to 321.48 KN.

For calculating the nominal capacity, the resistance factors ϕ_c and ϕ_s are taken as 1.0 in the above procedure.